Universidade do Minho

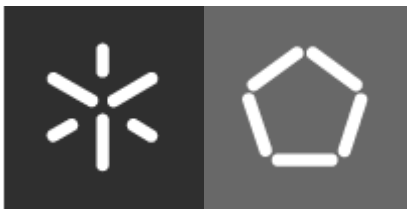

Escola de Engenharia

Institute for Sustainability and
Innovation in Structural Engineering

Rolando Salgado Estrada

Damage Detection Methods in Bridges through Vibration Monitoring: Evaluation and Application

Métodos de Detecção de Dano em Pontes mediante a utilização de Técnicas de Monitorização Dinâmica: Avaliação e Aplicação

Supervisors:
Professor Paulo J.S. Cruz, University of Minho
Professor Gustavo Ayala, UNAM

Doctoral Thesis
Department of Civil Engineering
ISISE-University of Minho
Guimarães

September 2008

To my wife Nora and my son Kevin for his patient and moral support during our stay in Portugal.

Acknowledgements

In this thesis, I received the important support of many people who motivated me to do my best effort.

First of all, I would like to express my sincere gratitude to my supervisor Prof. Paulo Cruz for inviting me to do my thesis in Portugal and for his support to develop this work.

I would like to thank to my co-supervisor Dr. Gustavo Ayala. He has been my academic tutor since my Master's studies. His comments and suggestions throughout this time have helped me in my training as a researcher.

I would also like to thank Prof. Elfgren Lennart, Ola Enochsson and their staff at Luleå University of Technology for their support during the execution of the dynamic tests on the Övik railway bridge.

I would like to acknowledge the people whose unconditional helped me during the realization of dynamic tests.

To begin, I would like to express my gratitude to Luis Ramos, for introducing me in the topic of dynamic analysis of structures. Moreover, his comments and suggestions helped me in improving my thesis.

Also, I would like to thank Jorge Branco for his dedication and collaboration during the dynamic tests on Góis footbridge. His comments and suggestions were very important in this part of my thesis.

Thanks to Everaldo Bonaldo who helped in the execution of the static failure tests on the concrete beams, and collaborated for the correct realization of the dynamic tests in these beams.

Matos, Marco and technicians at the Laboratory of Civil Engineering at the University of Minho for their unconditional help during the execution of the tests.

I would like to acknowledge Prof. Guido De Roeck for his suggestions given in the Góis footbridge research.

My special gratitude to my best friend Lukasz Topczewski for his moral support and for good times that we spent together.

It would not possible to forget Kesio Palacio, his good humour gave me the force to continue in this challenge.

Thanks to Maciej for his suggestions given to my thesis and his wife, Dagmara for his friendship not only to me, but also to my family.

To my colleagues at the University of Minho, Fernando, Abraham, Ismael, Gihad and his family, Claudio, Konrad, Milena, Asha, Cornelia and all the people that I had the opportunity to meet in Portugal.

To the Erasmus students Pawel, Dorota, Rafael, Jan, Mieszko who helped me in several topics and issues in this thesis.

I would like to dedicate this research work to my grandfather Chon who died during my stay in Portugal.

Finally but not less important, I appreciate the courage and support given by my wife, Nora and my son, Kevin. They left their lives in México to accompany me in this adventure in Portugal. I also appreciate the invaluable support given by my parents, Rolando and Lupe, my brother Erik and my sister-in law Magui.

The research work presented in this thesis was carried out at the Institute for Sustainability and Innovation in Structural Engineering (ISISE) of the University of Minho between May 2004 and October 2008. This research was financially supported by the Sustainable Bridges Project in the Sixth Framework Programme and by the Portuguese Foundation of Science and Technology (FCT) through the grant SRFH/BD/29317/2006, both are acknowledged.

Abstract

In this thesis, a detailed analysis of the most important vibration-based damage detection methods applied to bridge structures is addressed. Special attention is focused on those methods capable to detect damage only with information provided from a damage stage of the structure.

For that purpose, methods based on wavelet analysis, curvature of the mode shapes and changes in the flexibility and stiffness matrices of the structure methods are selected. These methods are easy to implement to bridge structures for its on-line structural evaluation or for its evaluation at different damage stages.

The selected damage detection methods are evaluated under three different cases: (1) damage scenarios are simulated on numerical methods for cracked beam structures; (2) experimental tests are carried out in the laboratory with metallic and concrete beams strengthened with CFRP laminates; (3) real-scale bridge structures are tested under different damage scenarios.

To do an accurate simulation of the dynamic behaviour of cracked bridges, some of these methods are investigated and evaluated on beams with rectangular cross sections. Later, the methods are generalized to be applicable to more complex structures, like bridges, and to other cross sections, as in composite bridges.

From the research done here, it is concluded that the performance of the damage detection methods depends of several factors, for example, the number of sensors located near the damage zones, level of noise present in the acquired dynamic response, location, extension and severity of the damage. Finally, it is recommended to do the process of damage identification in the bridge using the selected group of damage detection methods where successful damage detection is obtained when more than one method clearly indicates damage.

Resumo

Na presente dissertação é apresentada uma análise comparativa detalhada da eficácia de métodos de detecção de dano em pontes. Uma atenção especial é dada aos métodos baseados, exclusivamente, na resposta dinâmica da estrutura danificada.

Para este efeito são escolhidos os métodos baseados na análise de "wavelets", na curvatura das formas modais e na modificação da matriz de flexibilidade ou de rigidez da estrutura. Estes métodos são de fácil implementação em pontes, tanto nos cases em que ser requer uma monitorização contínua do comportamento da estrutura como nos que é suficiente a obtenção de valores em fases discretas da vida útil das mesmas.

Os métodos utilizados são avaliados em três situações distintas: (1) a introdução de cenários de dano em modelos numéricos de estruturas fissuradas; (2) a realização de ensaios experimentais em laboratório, em vigas metálicas e em vigas de betão armado reforçadas com lâminas de material compósito (CFRP); (3) a realização de ensaios dinâmicos em pontes de betão e madeira, sob diferentes cenários de dano.

Para uma simulação apropriada do comportamento dinâmico de pontes fissuradas, alguns dos métodos existentes são investigados e avaliados em vigas com secções transversais rectangulares. Posteriormente, estes métodos são generalizados para ser aplicáveis a estruturas com secções transversais mais complexas, nomeadamente pontes de secções mistas aço-betão.

Dos estudos realizados concluiu-se que a eficácia de detecção de dano dos métodos estudados depende de vários factores, como por exemplo: o número de sensores próximo da zona danificada; o nível de ruído da resposta dinâmica utilizada; a localização, extensão e intensidade do dano. Finalmente, recomenda-se fazer o processo de identificação de dano na ponte usando o grupo escolhido de métodos de detecção de dano onde uma detecção bem sucedida é obtida quando mais de um método detecta claramente o dano.

Resumen

En esta tesis se realiza un análisis detallado de la eficacia de los más importantes métodos de detección de daño aplicados a la respuesta dinámica de puentes. Una atención especial es considerada a los métodos capaces de detectar daño con únicamente la información obtenida de la estructura dañada.

Para el análisis de evaluación, son seleccionados los métodos basados en análisis de "wavelets", en la curvatura de las formas modales y en el cambio de las matrices de flexibilidades y rigideces de la estructura. Estos métodos son elegidos debido a que pueden ser fácilmente implementados en puentes, ya se requiera una monitorización continua ó a través de fases discretas durante la vida útil de las mismas.

Los métodos seleccionados son evaluados bajo tres diferentes casos: (1) la introducción de escenarios de daño en modelos numéricos de estructuras agrietadas; (2) la realización de ensayos experimentales en vigas metálicas y de concreto reforzadas con láminas de fibra de carbono (CFRP); (3) la realización de ensayos dinámicos en puentes ante diferentes escenarios de daño.

Para una simulación más precisa del comportamiento dinámico de puentes agrietados, se investigan y evalúan algunos de estos métodos en vigas de sección transversal rectangular. Más adelante, estos métodos se generalizan para ser aplicables a estructuras más complejas como puentes y a otro tipo secciones transversales, como en puentes de sección compuesta.

De estos estudios realizados, se concluye que la eficacia de los métodos de detección de daño evaluados depende de varios factores, por ejemplo: el número de sensores próximo de la zona dañada; el nivel de ruido de la respuesta dinámica adquirida; la localización, extensión e intensidad del daño. Finalmente, se recomienda hacer el proceso de identificación de daño del puente utilizando el grupo seleccionado de métodos de detección del daño donde una detección adecuada se obtiene cuando más de un método indica claramente el daño.

Contents

Acknowledgements ..... **v**
Abstract ..... **vii**
Resumo ..... **ix**
Resumen ..... **xi**
Contents ..... **xiii**
Nomenclature ..... **xvii**

1 Introduction **1**

1.1 Motivation **2**
1.2 Classification of damage detection methods **3**
1.3 Objectives and scope **7**
1.4 Outline of the thesis **8**

2 State of the art **11**

2.1 Vibration-based damage detection methods applied to bridges –State of the art **12**
2.2 Wavelet theory **13**
2.2.1 Properties of Wavelet functions 14
2.2.2 Continuous Wavelet Transform (CWT) 15
2.2.3 Discrete Wavelet Analysis (DWA) 16
2.2.4 Hoelder exponent 17
2.2.5 Wavelet Packet Transform (WPT) 19
2.2.6 Examples of the applicability of the wavelet theory for the detection of singularities related to damage 21

2.3 Wavelet analysis methods **28**
2.3.1 Wavelet based level I damage detection methods (Structural Health Monitoring) 30
2.3.2 Wavelet based level II damage detection methods 34
2.3.3 Wavelet based level III damage detection methods 38
2.3.4 Non Wavelet damage detection methods 43
2.3.5 Application to vibration-based damage detection methods to real-scale damaged bridges 49

2.4 General description of selected vibration-based damage detection methods 55

2.4.1 COMAC method 56
2.4.2 Curvature method 57
2.4.3 Damage Index (DI) Method 57
2.4.4 Flexibility change method 59
2.4.5 Stiffness change method 60
2.4.6 Wavelet analysis methods 61
2.4.7 Wavelet Packet Signature (WPS) method 61
2.4.8 Level I methods 63

3 Dynamic simulation methods 65

3.1 State of the art 66

3.2 Dynamic simulation methods 70

3.2.1 Modified Christides and Barr method 70
3.2.2 Shifrin and Ruotolo method 74
3.2.3 Zheng and Kessissoglou method 76

3.3 Adopted conditions for the evaluation of the methods 79

3.4 Comparison of modal parameters calculated from simulated Ambient Vibration Tests (AVTs) 81

3.5 Comparison of modal parameters calculated from the cracked beam methods 83

3.6 Conclusions 86

4 Damage detection using numerical models 87

4.1 Introduction 88

4.2 Single Degree Of Freedom (SDOF) systems 88

4.2.1 SDOF systems with harmonic excitation 90
4.2.2 SDOF systems with random excitation 93
4.2.3 SDOF systems with seismic excitation 95
4.2.4 SDOF systems with stiffness degradation 100

4.3 Damage evaluation on one-dimensional numerical models 101

4.3.1 Bridge characteristics 101
4.3.2 Damage Scenarios 101
4.3.3 Dynamic Simulations 103
4.3.4 Evaluation of damage detection methods 104

4.4 Damage evaluation on two-dimensional numerical models 107

4.4.1 Bridge characteristics 107
4.4.2 Dynamic simulation of the cracked bridge 108
4.4.3 Damage scenarios 110
4.4.4 Parameters adopted for the evaluation of damage detection methods 111
4.4.5 Performance of the evaluated methods 112
4.4.6 Conclusions and remarks 117

5 Damage detection in beam specimens 119

5.1 Introduction 120

5.2 Considerations adopted for the damage detection procedure 121

5.3 Damage identification in steel I beams 122

5.3.1 Description of the beam specimens 122
5.3.2 Description of the induced damage on the beams 123
5.3.3 Description of the dynamic tests 125
5.3.4 Modal identification 126
5.3.5 Damage detection 130

5.4 Damage detection in reinforced concrete beams Strengthened with Composite Laminates bonded into slits 143

5.4.1 Introduction 143
5.4.2 Description of the laboratory tests 144
5.4.3 Modal comparison 156
5.4.4 Detection and location of damage 158
5.4.5 Simulation of the dynamic behaviour of the beam specimens 163

5.5 Conclusions 171

6 Damage detection in bridges 175

6.1 Introduction 176

6.2 Considerations adopted for the dynamic tests and damage detection procedure 177

6.3 Damage detection in the Övik bridge 178

6.3.1 Bridge structure 178
6.3.2 Description of damage tests 180
6.3.3 Description of the dynamic tests 182
6.3.4 Modal identification after the damage tests 184
6.3.5 Damage detection in the Övik bridge 188

6.4 Dynamic analysis and structural evaluation of a timber arch footbridge 192

6.4.1 Introduction 192
6.4.2 Footbridge description 195
6.4.3 Finite element model 199
6.4.4 Static analysis 200
6.4.5 Dynamic analysis 200
6.4.6 Evaluation of the structural performance using damage detection methods 225
6.4.7 Summary and conclusions 232

7 Conclusions and suggestions for further research 237

7.1 Summary 238
7.2 Damage detection on numerical simulations 238
7.3 Damage detection on beam specimens 239
7.4 Real-scale bridges 240
7.5 General conclusions 240
7.6 Recommendations and suggestions for further research 241

References 245

Appendix A 259

Experimental modal analysis methods 259

Appendix B 263

Solutions for the Shifrin & Ruotolo method 263

Annex A 269

Damage detection graphs from beam specimens 269

Annex B 289

Damage detection graphs from bridges 289

Nomenclature

List of symbols

α	Normalized scale factor
α_{DI}	Damage index severity factor
α_{cr}	Decay rate exponent
β	Damage index
β_{FRF}	Damage index applied to FRF operational mode shapes
β_K	Kurtosis
β_s	Slope factor
γ_{cr}	Contact parameter
$\mathbf{\Delta C}$	Matrix representing the differences between the undamaged and damaged flexibility matrices
ΔK	Stiffness reduction
$\mathbf{\Delta M}$	Matrix of additional masses
Δ_f	Ratio between the undamaged and damaged frequencies
Δk	Stiffness reduction
Δ_ξ	Ratio between the undamaged and damaged damping ratios
δ	Crack depth ratio (a/h)
δc	Element of the $\mathbf{\Delta C}$ matrix
ϵ	Mode shape curvature
$\zeta(x, z)$	Function representing the modification of the displacement field due to the crack
θ	Mother wavelet
$\lambda^4 =$	$\omega^2 \rho A / (EI)$
μ	Mean value

$\eta(\omega)$	Frequency Response Function operational mode shape at circular frequency ω
ν	Poisson ratio
ξ	Damping ratio
ρ	Mass density
σ	Standard deviation
ϕ	Normalized mode shape
χ	Shearing factor
ψ	Non-normalized mode shape
ω	Circular natural frequency
ϱ	Gaussian function
ϑ	Scaling function
$\mathcal{L}$	Laplacian difference operator
A	Undamaged cross sectional area
A_{cr}	Cross sectional area at damage location
a_c	Acceleration
a_{pd}	Acceleration for certain pedestrian density
B	Unknown coefficient
b	Translations (Wavelet Analysis)
$\mathbf{C}$	Undamaged flexibility matrix
$\mathbf{C}^*$	Damaged flexibility matrix
$\mathbf{C_{ov}}$	Overall flexibility matrix
$\mathbf{C_{tot}}$	Total flexibility matrix
C_{cr}	$m_I - 1 = (I - I_{cj})/I_{cj}$
c_j	Flexibility of the *j*th rotational spring
E	Young's modulus

$E_j^i(n)$	Energy of the decomposed function $f_j^i(t)$ at measuring point n
EI	Flexural stiffness
f_n	Natural frequency of the *n*th mode shape
$f(x)$	Function representing mode shapes
$f(x,z)$	Cracked function
$f(t)$	Function representing dynamic response
$f_j^i(t)$	Element of the *i*th component function of the *j*th level of the WPT decomposition
g_m	Difference between the flexural stiffness of the first and second node of an element
$g(k)$	Quadrature mirror filter associated with the mother wavelet
h	Total depth of the cross section
$h(k)$	Quadrature mirror filter associated with the scaling function
he	Hoelder exponent
I	Inertia at the undamaged cross section
I_c	Inertia at damaged cross section
J	Polar moment of inertia at undamaged cross section
J_c	Polar moment of inertia at damaged cross section
K	Stress intensity factor
$\mathbf{K}$	Global stiffness matrix
$\mathbf{K_c}$	Stiffness matrix of the cracked element
k	Element of the stiffness matrix
L	Total length of the beam
L_e	Length of a discrete element
$\mathbf{M}$	Mass matrix
m	Element of the mass matrix
m_I	Ratio between the undamaged and damaged inertias I/I_c

$N =$	$\int_A z f(x)\, dA$
N_r	Number of pedestrians in the footbridge
n	Number of samples (cracks, measuring points, modes)
$\mathbf{P_r}$	Matrix of the selected structural parameters for the model updating process
P	Acting force in the discrete element
Q_p	Pulsating force for the load model DLM1
Q_g	Pulsating force for the load model DLM2
$Q(x)$	Function representing the modification of the geometrical properties of the element caused by cracks.
q_s	Pulsating force for the load model DLM3
$R =$	$\int_A f^2(x)\, dA$
$\mathbf{S}$	Normalized sensitivity matrix
S	Factor of synchronization
s	Scales (Wavelet Analysis)
t	Time
U_{ij}	Contribution of the *j*th member to the *i*th modal strain energy
x	Longitudinal coordinate
w	Harmonic transversal oscillation of the beam
z	Transversal coordinate

List of abbreviations

AM	Area Method
ASCE	American Society of Civil Engineers
AVT	Ambient Vibration Test
CB	Christides and Barr
CFRP	Composite Fibre Reinforced Polyester
COMAC	Co-ordinate Modal Assurance Criterion
COV	Coefficient Of Variation
CVA	Canonical Variate Analysis
CWT	Continuous Wavelet Transform
DAQ	Data AcQuisition system
DI	Damage Index method
DOF	Degree Of Freedom
DWA	Discrete Wavelet Analysis
DWT	Discrete Wavelet Transform
EFDD	Enhanced Frequency Domain Decomposition Method
FEM	Finite Element Model
FRF	Frequency Response Function
FT	Fourier Transform
HExp	Hoelder Exponent
IHT	Impact Hammer Test
LB	Loading Beam
LCL	Lower Control Limit
LDM	Logarithmic Decrement Method
MAC	Modal Assurance Criterion
MCP	Mass Change Procedure
MMM	Mass Matrix Method

NDT	Non-Destructive Technique
NMD	Normalized Modal Difference
NN	Neural Network
OMA	Operational Modal Analysis
PC	Principal Component
PGA	Peak Ground Acceleration
PSD	Power Spectral Density
SDOF	Single Degree Of Freedom
SHM	Structural Health Monitoring
SIF	Stress Intensity Factor
SLS	Serviceability Limit State
SSI	Stochastic Subspace Identification
STFT	Short Time Fourier Transform
SVD	Singular Value Decomposition
ULS	Ultimate Limit State
UPC	Unweigthed Principal Component
WPERI	Wavelet Packet Energy Rate Index
WPS	Wavelet Packet Signature
WPT	Wavelet Packet Transform
WT	Wavelet Transform
ZOM	*Zero*th Order Moment

1

Introduction

1.1 Motivation

The structural performance of bridges decreases progressively throughout their service life due to many deterioration processes (fatigue, carbonation, etc). Bridges are considered an important part of the overall infrastructure of a country. Their structural failure could cause significant economical losses and even loss of human lives. Around the world, innumerable bridges have already exceeded their estimated service life and many of them have approached this limit. In the USA, 13.1 % (77720) of the total inventory of bridges were catalogued as structurally deficient in 2004 (U.S. DOT, 2006). In Europe 66 % of the railway bridges are more than 50 years old (see Figure 1.1) [Bell, 2007]. Hence the identification, location and evaluation of damage in bridges have gained the interest of the scientific community.

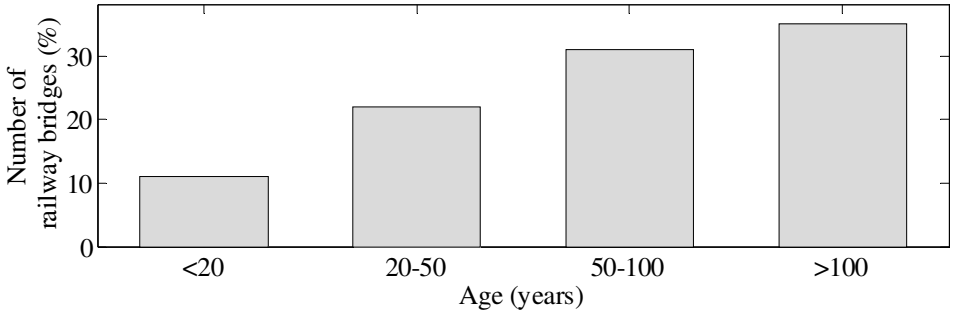

Figure 1.1. Railway bridge age profile in Europe.

The structural assessment of bridges has been traditionally performed using visual inspection. This method could detect damage in elements easy to access by the inspectors. Inner damage and/or damage located in inaccessible zones have big probability to be undetected (Chase, 2001). For these reasons, scientific community has been motivated to propose more rational methods for the evaluation of bridge structures. Furthermore, since the first decade of this century, modal parameters of bridges can be obtained easier and with lower costs than previously. Expensive shakers needed during the dynamic bridge tests are now not inevitable. Data acquisition during bridge dynamic tests can be performed with ambient vibration. The new modal analysis techniques called as Operational Modal Analysis (OMA) methods allow working just with the output data, not requiring details about the input force. An overview of the most famous OMA methods was given by Andersen *et al.* (1999).

Since the 1990s, several methods based on the vibration parameters of structures have been proposed, but any of them have successfully applied to all the

possible conditions in bridges. Moreover, the lack of dynamic tests obtained from these structures in their damage and undamaged conditions have not permitted the evaluation of these methods. For this reason, the numerical simulation of cracked structures plays an important role. However, these methods were proposed for simple beams and their application to more complex structures, like bridges, has not been fully investigated.

Due to these reasons, it was decided to study the detection of damage in bridges through their vibration parameters. It is desirable to have a damage detection method and/or methodology as simple as possible and applicable to the all possible conditions (damage, loading, ambient factors, etc.) in the bridge. Methods which can detect damage with only information obtained from the damage condition of the bridge are more appropriate for bridges since their condition before damage is rarely known. In this context, the application of the wavelet based methods can be useful. These methods detect the singularities present in the modal parameters caused by damage and therefore they do not require the condition of the structure before damage. It is also necessary to determine a numerical procedure for the simulation of the dynamic response of cracked bridges. In this way, evaluation of the damage detection methods can be practical.

1.2 Classification of damage detection methods

For the purpose of the evaluation of the structural condition of bridge structures, damage is defined as changes in the material and/or geometrical properties of the structures, *i.e.,* in their boundary conditions, connectivity between elements, geometrical cross sections, loading, material properties and any other factor capable to provoke a current or future unusual structural behaviour of the bridge (Doebling *et al.*, 1996).

Since the beginning of this century, a generation of Non-Destructive Techniques (NDTs) capable to get information from a bridge without disruption of its serviceability has been proposed. NDTs include those involving acoustics, dye penetrating, eddy current, emission spectroscopy, fibre-optic sensors, fibre-scope, hardness testing, isotope, leak testing, optics, magnetic particles, magnetic perturbation, X-ray, noise measurements, pattern recognition, pulse-echo, radiography, vibration-based damage detection and visual inspection, etc. More information about NDTs applied to bridge management can be found in Abudayyeh

et al. (2004) and SB-WP3 (2007). These NDTs can be classified as local and global methods. Local damage detection methods are more suitable to evaluate the structural performance in small localized areas of a bridge. For an efficient use of these local methods, it is necessary to know in advance the probable damage location. In this group can be included most of the non-destructive evaluation tools (ultrasonic tests, impact echo methods, radar, radiographic tests, etc.).

Global damage detection methods take advantages of the global structural changes of bridges caused by damage. Most of these methods are based on vibration monitoring. These methods are based on the assumption that structural damage causes variation in the structural parameters of the structure (mass, stiffness, flexibility) which provokes a change in the dynamic parameters of the structure (natural frequencies, mode shapes, damping ratio). However, these changes are too small for giving successful damage identification in all the cases. Furthermore, ambient factors as gradient of temperature between two dynamic tests may lead to differences of dynamic parameters of the same magnitude than those caused by damage. Consequently, more advanced techniques based on vibration monitoring have been proposed in order to amplify these small changes. These vibration-based damage detection methods have gained popularity due to the significant advances in modal analysis methods and in monitoring technologies.

An efficient strategy of bridge maintenance should be implemented in these structures in order to preserve them in good structural conditions. The implementation of a damage detection strategy for aerospace, mechanical engineering and civil engineering infrastructure is called Structural Health Monitoring (SHM) [Sohn *et al.*, 2003]. The SHM process involves the observation of a system periodically or continuously using a specific array of sensors. Acquired measurements are processed to detect unusual behaviour of the system that can be associated with damage. In this context, the process of damage detection in structures is classified as follows (Rytter, 1993):

I) Detection of damage;

II) Location of damage;

III) Evaluation of the severity of damage and

IV) Determination of the remaining service life of the bridge due to damage.

This classification increases in robustness according to the level of damage evaluation. In this way, level I methods consider only the determination whether the structure presents damage or not. Level II methods consider whether the structure is damaged and its location. In level III methods, the detected and located damage must be quantified in extension and severity, and finally in the last level IV, the remaining service life of the bridge needs to be determined considering the quantified damage. Actually, Rytter (1993) proposed another level of damage classification referring to the type of damage identified. To do that, information related to different kind of damage must be available for correlation. In general, most of the work done in damage detection has been focused in the levels II and III. Some methods have been found out to work better under certain conditions but their performance is not uniform for all possible scenarios. Therefore, more investigation needs to be done in order to determine a reliable method or methodology for the damage evaluation of bridges.

Vibration-based damage detection methods can also be classified as linear and non-linear methods (Doebling *et al.*, 1996). Linear damage detection methods suppose that the structure remains linear after damage occurs. Normally this condition is considered reasonable even though the structure exhibits non-linear behaviour after damage. This is the case of opening cracks and changes of the boundary conditions. On the other hand, non linear damage detection methods have to be used in the case of breathing cracks. These cracks open and close during normal operation of the bridge and an additional stiffness have to be considered when they close.

OMA methods have become a powerful tool for damage identification of bridges. The application of these methods to bridges with linear behaviour has given rise to model based and non-model based damage detection methods (Maeck, 2003). In former methods, the structural model of the bridge is done by the finite element method and their modal parameters are adjusted with those obtained from the dynamic tests. Model updating methods fall in this category. In the latter methods, modal parameters obtained at different damage bridge scenarios are compared. Vibration-based damage detection methods, like change in the Flexibility and Stiffness matrix and Damage Index methods among others are included in this last group. Finally, there are vibration-based damage detection methods able to locate damage in the structure just with the information provided from the damaged

structure. Wavelet analysis methods and mode shape curvature methods are into this last category.

The previously described classification of damage detection methods applied to structures is illustrated in Figure 1.2. This study is focused in methods which used the vibration parameters of the structures for finding indications of damage. Such methods commonly called as vibration-based damage detection methods will be briefly reviewed in Chapter 2.

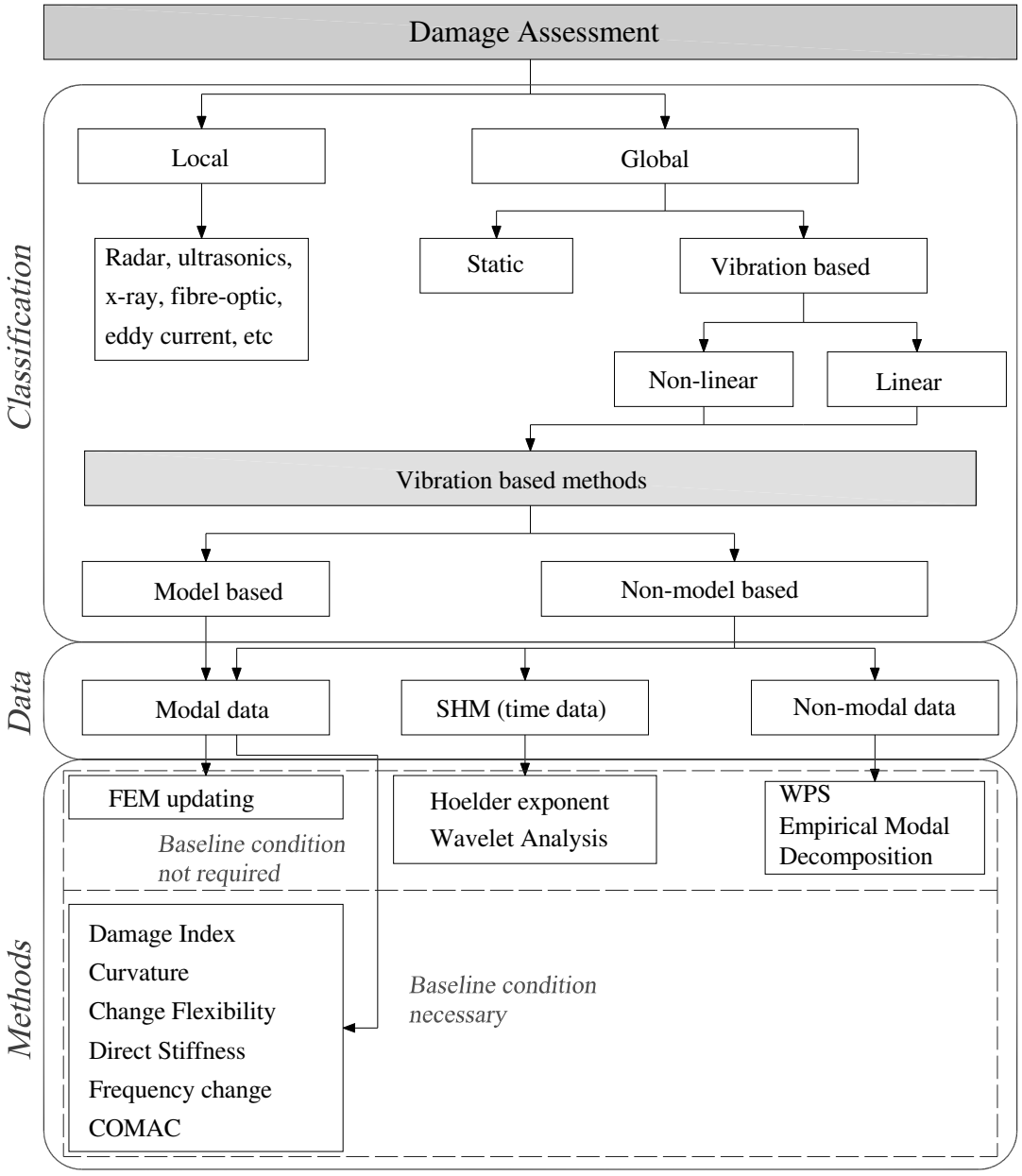

Figure 1.2. Diagram for the adopted classification of damage detection methods for bridges (taken and adapted from Ramos, 2007).

1.3 Objectives and scope

In this thesis is determined the applicability of several vibration-based damage detection methods applied to bridges. To accomplish this objective, the following activities were planned:

- Summarize the most important contributions related to the damage detection methods using vibration parameters, with a special attention to wavelet analysis methods. For a better understanding of the last methods, the mathematical background of the wavelet theory will be presented.
- Select a group of vibration-based damage detection methods. These methods must detect and locate damage in the structure and be easily implemented in bridges. Furthermore, they have to present good performance in other studies. A detailed description of these methods will be done as well as their implementation in a computer program for their further applicability to several defined cases.
- Develop a procedure for the simulation of the dynamic response of cracked bridges. Several methods for the dynamic simulations of cracked structures are compared. A description of the current state of the art of these methods and a comparison of several of them in a numerical example will be done.
- Simulate the dynamic behaviour of cracked bridges. Three examples are considered: in the first example, Single Degree Of Freedom (SDOF) systems are done to detect when the damage occurs; in the second example, one-span bridges are modelled as one dimensional Euler-Bernoulli beam. In the last example, one-span bridges are modelled as three-dimensional Finite Element Model (FEM).
- The selected damage detection methods are applied to the dynamic parameters obtained from the numerical models before and after the introduction of different damage scenarios. The performance of such methods is evaluated under different damage severity, location, damage extension and sensor layouts of simulated data acquisition.
- The evaluation of the selected damage detection methods is also conducted on beam specimens. Beams with different span length, material and

reinforcement are considered. These beams are purposely damaged and the efficiency of the selected damage detection methods is verified.

- Evaluate the performance of the selected damage detection methods in real-scale bridges. Dynamic tests are performed on this bridge for different structural conditions. Applications of the damage detection methods are used to locate the inflicted damage in the bridge. The damage detection and the vibration level of footbridges are also considered.
- Propose a methodology for the evaluation of damage in bridges.

In the objectives above described, the dynamic response (experimental and numerical) used for the damage evaluation is obtained using Ambient Vibration Tests (AVTs) and only the acceleration response is used for the damage detection procedure. In fact, these two situations are commonly found in the modal identification of bridges and therefore they are adopted.

1.4 Outline of the thesis

The content of the thesis is organized as follows (see Figure 1.3):

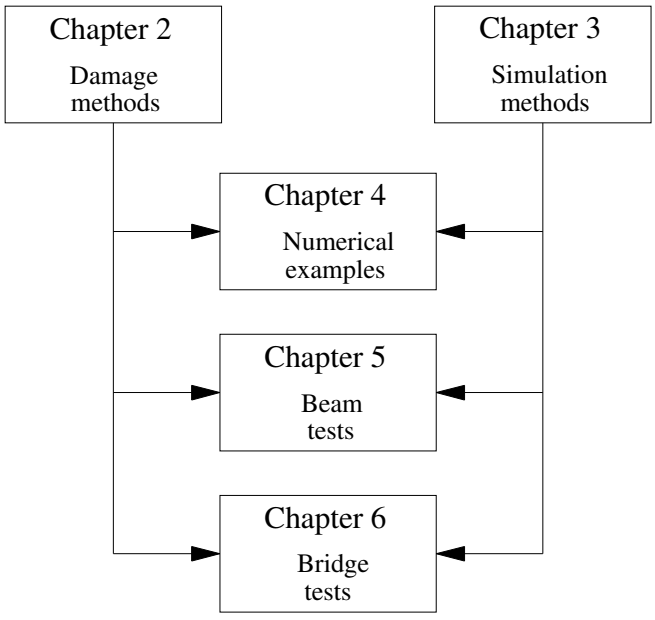

Figure 1.3. Diagram of the outline of the thesis.

Chapter 1 is the *Introduction* to this study. In this part is stated the damage definition as well as the damage classification. The *motivation* for doing the research

of this topic, the factors that influence the damage detection of bridges and the principal problems that needs to be tackled are discussed herein.

Chapter 2 presents the *state of the art* related to the most important contributions done in vibration-based damage detection methods. A special attention to wavelet analysis methods and the mathematical background of the wavelet theory is given. From the universe of vibration-based damage detection methods, some of them are chosen and they are explained in more detail.

Chapter 3 gives a review of the *dynamic simulation methods of cracked structures*. Selected methods are compared on a simulated example. In this chapter the importance of an adequate simulation of the dynamic behaviour of cracked structures is highlighted.

Chapter 4 shows *the application of the vibration-based damage detection methods to numerical examples*. SDOF systems are done where damage is simulated as a decrement of the total stiffness of the system. Later, the possibility to detect damage on-line using the time series of the dynamic response is evaluated. In a more complex numerical model, a one-span bridge modelled as an Euler Bernoulli beam is used to compare the performance of the vibration-based damage detection methods. The modelled bridge represents a typical highway composite cross section bridge. The input force, required for the simulation of the dynamic response, is simulated as concentrated forces moving with constant speed along the discrete nodes defined on the beam. In other example, a three dimensional numerical model of a one-span composite cross section bridge is done. In this model, six degrees of freedom per node are considered. Evaluation of the damage detection methods are carried out considering several crack locations, intensities and two layouts of sensors.

Chapter 5 presents *the evaluation of the damage methods on two beam specimens*. In the first part of this chapter, the results of applying the selected methods to steel I beams purposely damage with saw cuts in its transversal cross section is explained. These results are compared with those from a numerical model of the beam. In a second part of this chapter, the damage detection methods are applied to reinforced concrete beams strengthened with three different composite laminate contents. These beam specimens are severely damaged and results of the damage detection procedure are discussed and compared with numerical models of the beams.

Chapter 6 describes *the applicability of the damage detection methods on two real-scale bridges*. In the first case, damage detection methods are applied to the dynamic parameters obtained from the railway Övik bridge. This bridge was deliberately damaged as part of the experimental analysis carried out by the Sustainable Bridges project. The dynamic data acquisition on the bridge was performed after two different structural conditions. In the second case, a timber arch footbridge is analyzed. Damage detection methods are applied on the footbridge in order to detect delamination present in the arch and hanger elements. A FEM of the footbridge is done and updated with information provided from the experimental modal analysis. Besides to the application of the damage detection methods, the vibration level of the footbridge is determined from experimental and numerical studies. Moreover, the mass normalized mode shapes are calculated performing a second dynamic data acquisition, but now several additional masses are located in strategic points on the deck of the footbridge.

Chapter 7 discusses the *final conclusions* and gives suggestions for further work to do in this topic.

2

State of the art

2.1 Vibration-based damage detection methods applied to bridges – State of the art

The first study in vibration monitoring was carried out in 1940s. Kirmser (1944) reported the relationship between natural frequencies and the introduction of a crack in an iron beam. Since then and up to now, a vast number of vibration-based damage detection methods have been proposed. During this time, several researchers have compiled the most relevant work in damage detection methods. For instance, a comprehensive review of vibration-based damage detection methods was done by Doebling *et al.* (1996). The application of these methods to beams, large civil structures, space and composites structures were also summarized by the authors. Critical issues to be addressed in the damage detection field were also proposed.

Regarding the frequency based methods; Salawu (1997) reviewed the most important methods. He pointed out that frequency change methods which only rely on the measured data are more appropriate for large civil structures. Moreover, he recognized that natural frequencies may not be sufficient for a unique damage identification. Finally, he highlighted the importance of the ambient factors in the damage detection process.

Some time later, Sohn *et al.* (2003) presented a review of the Structural Health Monitoring studies done between 1996 and 2001. As opposed of the Doebling *et al.* review, the compiled studies were organized according to the statistical pattern recognition paradigm reported by Farrar *et al.* (2003). A review of the most important wavelet analysis methods applied to civil and mechanical structures was done by Kim and Melhem (2004). The advantages of these methods for the damage detection were highlighted. In recent years, Montalvão *et al.* (2006) did a revision of the vibration-based damage detection methods with emphasis in composite structures. The authors followed the damage classification proposed by Sohn *et al.* (2003) including the most recent method reported until 2006.

In this thesis, the literature review is focused on the evaluation of the most promising and well-known methods capable to be applied to bridge structures. A special attention will be paid to the Wavelet Analysis methods which are considered one of the most promising methods for the damage detection in bridge structures. Before summarizing the studies based on wavelet analysis, the mathematical background of such methods will be briefly explained.

2.2 Wavelet theory

Briefly, wavelets are functions that contain waves with zero mean value which drop to zero after some oscillations as represented in Equation (2.1).

$$\int_{-\infty}^{\infty} \theta(x)\, dx = 0 \tag{2.1}$$

in this last equation, x represents time or a space variable. These functions with only one independent variable should satisfy the admissibility condition, *i.e.,* they have finite energy (Mallat, 1989),

$$\int_{-\infty}^{\infty} |\theta(x)|^2\, dx < \infty \tag{2.2}$$

This condition implies that,

$$\int_{-\infty}^{\infty} \theta(x)\, dx = 0 \tag{2.3}$$

The function with these characteristics is called "mother wavelet" θ. Examples of mother wavelets are Morlet, Gaussian, Haar, Daubechies, Gabor, Mexican hat, Symlets and Shannon mother wavelets, among others (Poularikas, 1999). In the particular case of a Gaussian function, this is infinitely derivable and its derivative of order *n* may be a wavelet. For instance, the second derivative of the Gaussian function satisfying the admissibility condition is a mother wavelet expressed as:

$$\begin{aligned} \theta(t) &= \left(1 - x^2\right) \exp\left(-x^2/2\right) \\ \Theta(\omega) &= \sqrt{2\pi}\omega^2 \exp\left(-\omega^2/2\right) \end{aligned} \tag{2.4}$$

where $\Theta(\omega)$ is the Fourier Transform (FT) of $\theta(t)$. The graphical representation of this wavelet is given in Figure 2.1.

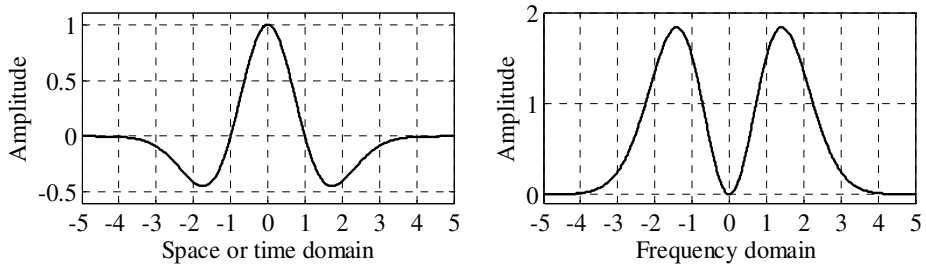

Figure 2.1. Gaussian 2 mother wavelet (left) and its wavelet transform (right).

2.2.1 Properties of Wavelet functions

The wavelet functions have different properties enabling them to be more suitable for certain purposes. The most relevant properties that a wavelet function needs for a damage detection process are:

Orthogonality and *biorthogonality:* These properties assure a fast calculation of their coefficients. Unfortunately, not all wavelet functions have these two properties.

Compact support: This property means that the wavelet function has not zero values for finite intervals. This property allows representing more efficiently signals that have localized features.

Vanishing moments: This property determines the degree of the polynomial that can be approximated. This property is used for selecting the mother wavelet more suitable for damage detection. A wavelet is said to have m vanishing moments when it fulfils:

$$\int_{-\infty}^{\infty} x^k \theta(x)\, dx = 0, \quad k=0,\ldots,m-1 \tag{2.5}$$

Regularity: It is the *r*-times that a function is differentiable at x_0. Singularities in a function can be detected for its regularity.

According to these properties, the most well-known mother wavelets are classified in (Ovanesova and Suarez, 2004):

- The Haar, the Daubechies of order *N*, Meyer, the Symlets of order *N* and the Coiflets of order *N* are examples of orthogonal mother wavelets;
- The Haar, the Daubechies of order *N*, the Symlets of order *N* and the Coiflets of order *N* mother wavelets have a compact support;
- The Daubechies of order *N*, the Symlets of order *N* and the Coiflets of order *N* mother wavelets have an arbitrary number of vanishing moments;
- The Morlet, Meyer and Gaussian mother wavelets are regular. On the other hand, the Daubechies of order *N*, the Symlets of order *N* and the Coiflets of order *N* mother wavelets have a poor regularity.

2.2.2 Continuous Wavelet Transform (CWT)

Different sets of mother wavelets can be generated dilating by *s* scales and translating in space by *b* translations the original function. In this way, Continuous Wavelet Transform (CWT) is defined as the integral over time of the wavelet convolution. Its mathematical representation is given by,

$$CWT_{\psi}^{f}(s,b) = \frac{1}{\sqrt{s}} \int_{-\infty}^{\infty} f(x)\, \theta\left(\frac{x-b}{s}\right) dx = \int_{-\infty}^{\infty} f(x)\, \theta_{s,b} dx \qquad (2.6)$$

The results of this transformation are called wavelet coefficients and show how well the function correlates with the signal. These wavelet coefficients are very sensitive to discontinuities and singularities present in the analyzed signal. Considering this property, it was found that damage due to a sudden loss of stiffness can be detected through mode shapes with wavelet coefficients which achieve large amplitudes like a spike or an impulse in the damage location. This perturbation of wavelet coefficients due to this damage is clearer in the finest scales of the CWT. This procedure is the basis of the CWT damage detection.

It is possible to recover the original signal $f(x)$ from its CWT if the used mother wavelet satisfies the admissibility condition [Equation (2.2)] defined in frequency domain as:

$$K_{\theta} = \int_{-\infty}^{\infty} \frac{|\Theta(\omega)|^2}{|\omega|} d\omega < \infty \qquad (2.7)$$

The original signal $f(x)$ is reconstructed from the CWT coefficients using the inverse CWT defined as:

$$f(x) = \frac{1}{K_{\theta}} \int_{s=-\infty}^{\infty} \int_{b=-\infty}^{\infty} CWT_{\psi}^{f}(s,b)\, \theta_{s,b}(x)\, db \frac{ds}{s^2} \qquad (2.8)$$

An alternative way to express the CWT is to consider a wavelet with *n* vanishing moments. For any integer $p < n$, a wavelet function can be expressed as:

$$\theta = \frac{d^p \theta^1(x)}{dx^p} \qquad (2.9)$$

If a function $f(x)$ is *p*-times differentiable, hence:

$$CWT_{\theta}^{f}(s,b) = f(x) \otimes \theta_s(x) = \frac{d^p}{dx^p}\left(f \otimes s^p \theta_a^1\right)(x) = s^p \left(\frac{d^p f}{dx^p} \otimes \theta_a^1\right)(x) \tag{2.10}$$

Where $\otimes$ denotes the convolution of the functions. To better understand the scope of Equation (2.10), the Gaussian function ϱ, and its second derivative are considered (Mallat and Hwang, 1992):

$$\varrho_s = \frac{1}{s}\varrho(x/s); \quad \theta_{G2} = \frac{d^2\varrho}{dx^2}; \quad CWT_{\theta}^{f}(s,b) = f(x) \otimes \theta_{G2}$$
$$CWT_{\theta}^{f}(s,b) = f \otimes \left(s\frac{d^2\varrho_s}{dx^2}\right)(x) = s^2 \frac{d^2}{dx^2}(f \otimes \varrho_s)(x) \tag{2.11}$$

Hence, the CWT is proportional to the second derivative of the function $f(x)$ smoothed by θ_s. This property becomes important when it has been recognized that the second derivative of mode shapes can be used to locate damage (Pandey *et al.*, 1991). Therefore CWT of mode shapes can be also used for damage location.

2.2.3 Discrete Wavelet Analysis (DWA)

Discrete Wavelet Analysis (DWA) can be deduced taking advantage of the redundant information contained in CWT. In this way, it is possible to use dyadic values of dilations *a* and translations *b* based on powers of two without loss of accuracy. This procedure reduces the computational effort in the calculations of the wavelet coefficients. For this purpose, dilation is defined as $s = 2^j$ and translation parameters as $b = k2^j$ where $(j,k) \in Z$ and Z is the set of integers. Using these discrete parameters, the Discrete Wavelet Transform (DWT) is given as:

$$DWT_{j,k} = 2^{-j/2}\int_{-\infty}^{\infty} f(x)\,\theta\left(2^{-j}x - k\right)dx = \int_{-\infty}^{\infty} f(x)\,\theta_{j,k}(x)\,dx \tag{2.12}$$

In the same way, the inverse of the DWT is:

$$f(x) = \sum_{j=-\infty}^{\infty}\sum_{k=-\infty}^{\infty} DWT_{j,k}2^{-j/2}\theta\left(2^{-j}x - k\right) \tag{2.13}$$

As opposed to the CWT, the DWT needs, for the reconstruction of the signal, another additional function $\vartheta(x)$ referred to as the scaling function.

A function is considered a scaling function if satisfies the following conditions:

$$\begin{aligned} \int_{-\infty}^{\infty} \vartheta(x)\, dx &= 1 \\ \int_{-\infty}^{\infty} |\vartheta(x)|^2\, dx &= 1 \\ \langle \vartheta(x), \vartheta(x-n) \rangle &= \delta(n) \end{aligned} \tag{2.14}$$

For the singularity detection purpose, it is better to represent the inverse DWT as follows:

$$f(x) = \sum_{j=-\infty}^{\infty} \left(\sum_{k=-\infty}^{\infty} cD_j(k)\, \theta_{j,k}(x) \right) + \sum_{k=-\infty}^{\infty} cA_J(k)\, \vartheta_{j,k}(x) \tag{2.15}$$

In the DWA, the analyzed signal is represented by approximations and details. Thus, the discrete reconstruction of the function can be expressed by,

$$\begin{aligned} cD_J(k) &= \int_{-\infty}^{\infty} f(x)\, \theta_{J,k}(x)\, dx \\ cA_J(k) &= \int_{-\infty}^{\infty} f(x)\, \vartheta_{J,k}(x)\, dx \\ D_J(x) &= \sum_{k=-\infty}^{\infty} cD_J(k)\, \theta_{J,k}(x)\, dx \\ A_J(x) &= \sum_{k=-\infty}^{\infty} cA_J(k)\, \vartheta_{J,k}(x)\, dx \\ f(x) &= A_J + \sum_{j \le J} D_j \end{aligned} \tag{2.16}$$

where cD_J and cA_J are the level J detail coefficients and the level J approximation coefficients, respectively. D_J is the level J detail function and A_J is the approximation at level J. In Equation (2.16) cD_J and cA_J define the DWT, while D_J and A_J are parts of the Inverse DWT. The DWA damage detection procedure consists of selecting a suitable mother wavelet for the analysis. Afterwards, first level details D_J of the analyzed mode shape are examined looking for disturbance that can indicate damage.

2.2.4 Hoelder exponent

The Hoelder exponent, also known as the Lipschitz exponent, is an important tool for measuring the regularity of a signal. As described in wavelet properties, regularity measures the order which a function is r-times differentiable. Damage in structures

may introduce a discontinuity in its dynamic parameters. This bounded discontinuity has a Hoelder exponent clearly below those of its vicinity. Hence, the regularity of the dynamic parameters of a structure in time or space can be used for detecting or locating damage. Nevertheless, the calculation of the Hoelder exponent of a signal has not been an easy task. Previously, the Fourier Transform (FT) was used for its calculation. With the FT approach a global measure of the regularity of the function could be found, but regularity of the function and specific time or space was not possible. The WT can analyse a function in frequency as well as time or space domain and its wavelet functions present suitable properties for the calculation of the Hoelder exponent (*e.g.,* regularity and vanishing moments). The Hoelder exponent of a function $f(x)$ can be deduced using WT as follows:

If it is assumed that the function $f(x)$ can be approximated at x_0 by a polynomial calculated with the form,

$$\begin{aligned} f(x) &= e_0 + e_1(x - x_0) + \cdots + e_n(x - x_0)^n + e_{he}|x - x_0|^{he} \\ &= P_n(x - x_0) + e_{he}|x - x_0|^{he} \end{aligned} \tag{2.17}$$

where P_n is a polynomial associated with the Taylor expansion of $f(x)$ at x_0 and e_{he} is the constant for the polynomial member rises to n. The term associated with he can be seen as the residual that remains after the function is fitted with a polynomial of order n. The function $f(x)$ has a local Hoelder exponent he at x_0 if, and only if, a polynomial of order $n < s$ and a constant e_{he} exists,

$$|f(x) - P_n(x - x_0)| \leq e_{he}|x - x_0|^{he} \tag{2.18}$$

Taking advantage that a WT with n vanishing moments can discard polynomials up to order n [see Equation (2.5)] and examining the decay of wavelet coefficients as s tends to zero, an isolated singularity can be measured as:

$$\left|CWT_\theta^f(s,b)\right| \leq e_{he}s^{he+1/2} \tag{2.19}$$

A more convenient form of Equation (2.19) for the calculation of the Hoelder exponent is:

$$\log_2\left|CWT_\theta^f(s,b)\right| \leq \log_2 e_{he} + \left(he + \frac{1}{2}\right)\log_2 s \tag{2.20}$$

The Hoelder exponent has been used for location of cracks on time and space domain. Moreover, the severity of the damage can also be estimated. In the state of the art related to wavelet methods, several studies using this technique are mentioned.

2.2.5 Wavelet Packet Transform (WPT)

This transform is considered as a generalization of the discrete wavelet transform and can be defined as the linear decomposition of the evaluated function. Thus, a set of wavelet packets can be determined from the wavelet mother sets, just by adding a modulation $i \in Z$,

$$\theta_{j,k}^{i} = 2^{j/2}\theta^{i}\left(2^{j}t - k\right) \tag{2.21}$$

ψ^{i} can be calculated from the following recursive relationships,

$$\begin{aligned} \theta^{2i}(t) &= \sqrt{2}\sum_{-\infty}^{\infty} h(k)\,\theta^{i}(2t-k), \\ \theta^{2i+1}(t) &= \sqrt{2}\sum_{-\infty}^{\infty} g(k)\,\theta^{i}(2t-k) \end{aligned} \tag{2.22}$$

where $h(k)$ and $g(k)$ are the quadrature mirror filters associated with the scaling function and the mother wavelet function.

The recursive relations between the $j\text{th}$ and the $j+1\text{th}$ level components are:

$$f_{j}^{i}(t) = f_{j+1}^{2i-1}(t) + f_{j+1}^{2i}(t), \tag{2.23}$$

$$f_{j+1}^{2i-1}(t) = Hf_{j}^{i}(t), \tag{2.24}$$

$$f_{j+1}^{2i}(t) = Gf_{j}^{i}(t) \tag{2.25}$$

where *H* and *G* are the filtering-decimation operators and they are related to the discrete filters $h(k)$ and $g(k)$ as follows:

$$\begin{aligned} H\{\cdot\} &= \sum_{k=-\infty}^{\infty} h(k-2t), \\ G\{\cdot\} &= \sum_{k=-\infty}^{\infty} g(k-2t) \end{aligned} \tag{2.26}$$

Any signal $f(t)$ like dynamic response functions can be represented as the combination of wavelet packet component functions,

$$f(t) = \sum_{i=1}^{2j} f_j^i(t) \tag{2.27}$$

where $f_j^i(t)$ is the linear combination of the wavelet packet functions $\theta_{j,k}^i$,

$$\begin{aligned} f_j^i(t) &= \sum_{k=-\infty}^{\infty} d_{j,k}^i \theta_{j,k}^i(t) \\ d_{j,k}^i &= \int_{-\infty}^{\infty} f(t)\, \theta_{j,k}^i(t)\, dt \end{aligned} \tag{2.28}$$

In WPT the signal is decomposed in approximations (A) and details (D) as defined in Equations (2.24) and (2.25), respectively, these two results are themselves decomposed into another level of decomposition. Then this process is repeated until the required level of accuracy is achieved (see Figure 2.2). At the bottom of the WPT tree, $f_j^i(t)$ presents good resolution in frequency and bad resolution in time, while at the top of the WPT tree, a bad resolution in frequency and a good resolution in time are obtained.

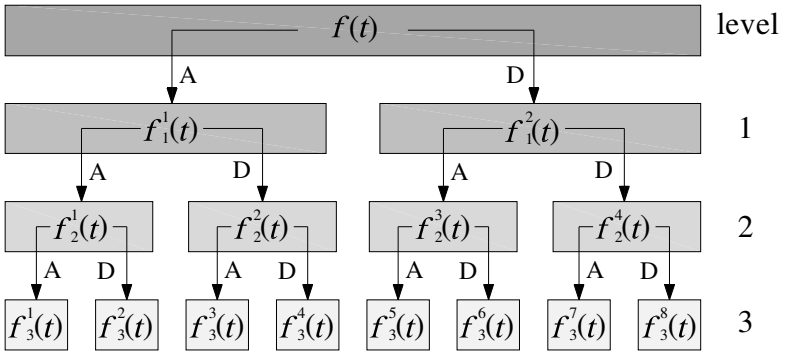

Figure 2.2. Wavelet Packet Transform at 3rd level of decomposition.

The damage detection methods based on the WPT calculate the energy associated with each component function $f_j^i(t)$. The comparison of this index parameter between the baseline and damaged structure can be used as damage indicator. In the state of the art of wavelet based damage detection methods, an explanation of such methods is given.

2.2.6 Examples of the applicability of the wavelet theory for the detection of singularities related to damage

The wavelet theory used for damage detection can be better understood with two academic examples. The wavelet analysis was done using the wavelab computer program (Buckheit *et al.*, 2005). The first example tries to simulate the dynamic response of a structure in a particular point and is represented by a sinusoidal function (referred here as time function), with three different characteristic frequencies (2, 8 and 18 Hz). A singularity in the function is simulated by a small change of its characteristic frequencies with a magnitude of 0.1 % after 10 s recorded as represented in Equation 2.29 and illustrated in Figure 2.3a.

$$f(t) = \begin{cases} \sin(4\pi t) + \sin(16\pi t) + \sin(36\pi t) & \text{for } (0 \leq t \leq 10 \text{ s}) \\ \sin(3.996\pi t) + \sin(15.984\pi t) + & \\ \sin(35.964\pi t) & \text{for } (10 \leq t \leq 20 \text{ s}) \end{cases} \tag{2.29}$$

A close up of the sinusoidal function at two different times, before and after frequency change, did not indicate any visible difference. The Power Spectral Density (PSD) Function for the first and last 10 s determined using FT is shown in Figure 2.3b. As expected, change in frequencies could not be determined from the PSD function. A more robust technique able to detect small changes in the dynamic response is required. The application of the wavelet theory for detection of singularities could be a solution to identify these small changes in the function.

The second example simulates the first mode shape of a simply supported beam in which the ordinate at the mid-length of the beam was increased by 0.1%. The function, referred as mode function, for a 20 m span, unit-normalized and divided in 101 nodes can be represented by:

$$\begin{aligned} f(x) &= \sin\left(\frac{\pi x}{20}\right) \quad \text{for } (0 \leq x \leq 20 \text{ and } x \neq 10 \text{ m }) \\ f(x) &= 1.001 \qquad \text{for } (x = 10 \text{ m}) \end{aligned} \tag{2.30}$$

A visual inspection of the function of Equation (2.30) did not detect this small change until a close up of the function shows the change introduced (see Figure 2.4).

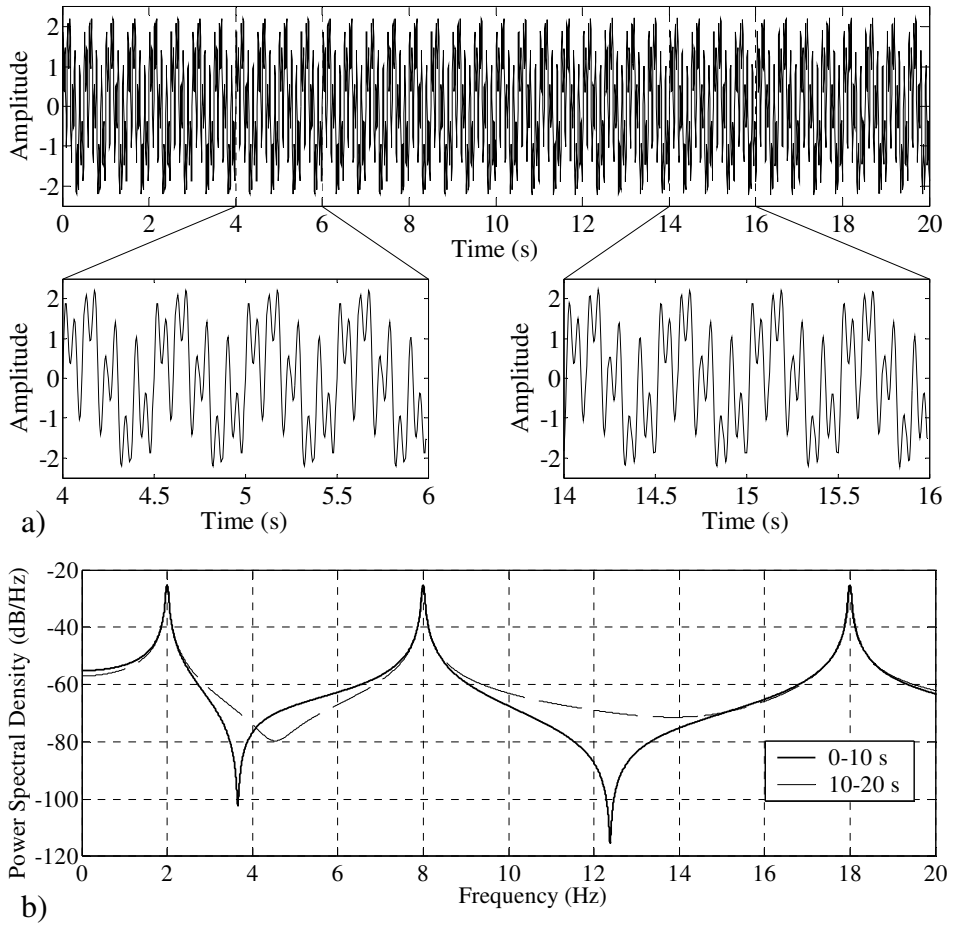

Figure 2.3. Sinusoidal function representing the a) dynamic response of a structure and b) its PSD function.

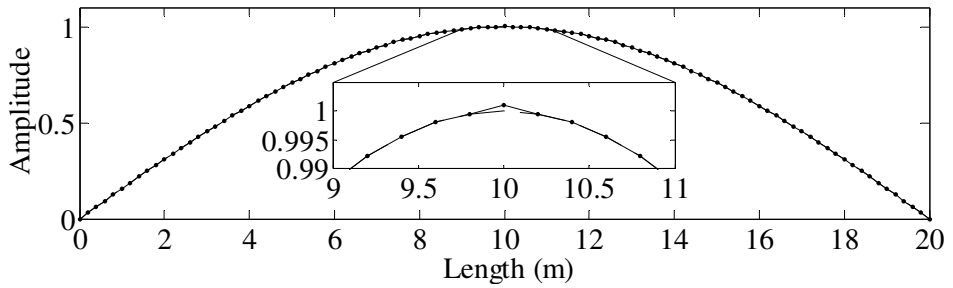

Figure 2.4. Function represented a mode shape with a singularity added to the mid-length of the span.

The DWA, the CWT, the Hoelder exponent and the WPT will be applied to the sinusoidal functions to try to detect the introduced discontinuities. As explained in the wavelet theory these methods need to define a mother wavelet. A trial and error analysis leads that a good candidate for singularity detection using DWA and WPT can be Daubechies 4 mother wavelet. In the case of the CWT and the Hoelder

exponent methods, the Gauss 4 mother wavelet demonstrated good performance for the detection of singularities. These mother wavelets have both four vanishing moments. If it is considered that the second derivative of the mode shapes can be used for damage detection purposes, an equivalent procedure can be done with wavelet analysis methods with a mother wavelet with at least two vanishing moments. For these two sinusoidal functions with this frequency content, four vanishing moments are enough for a clear detection. However, for a noisy function with higher frequency content, a mother wavelet with more vanishing moments may be required.

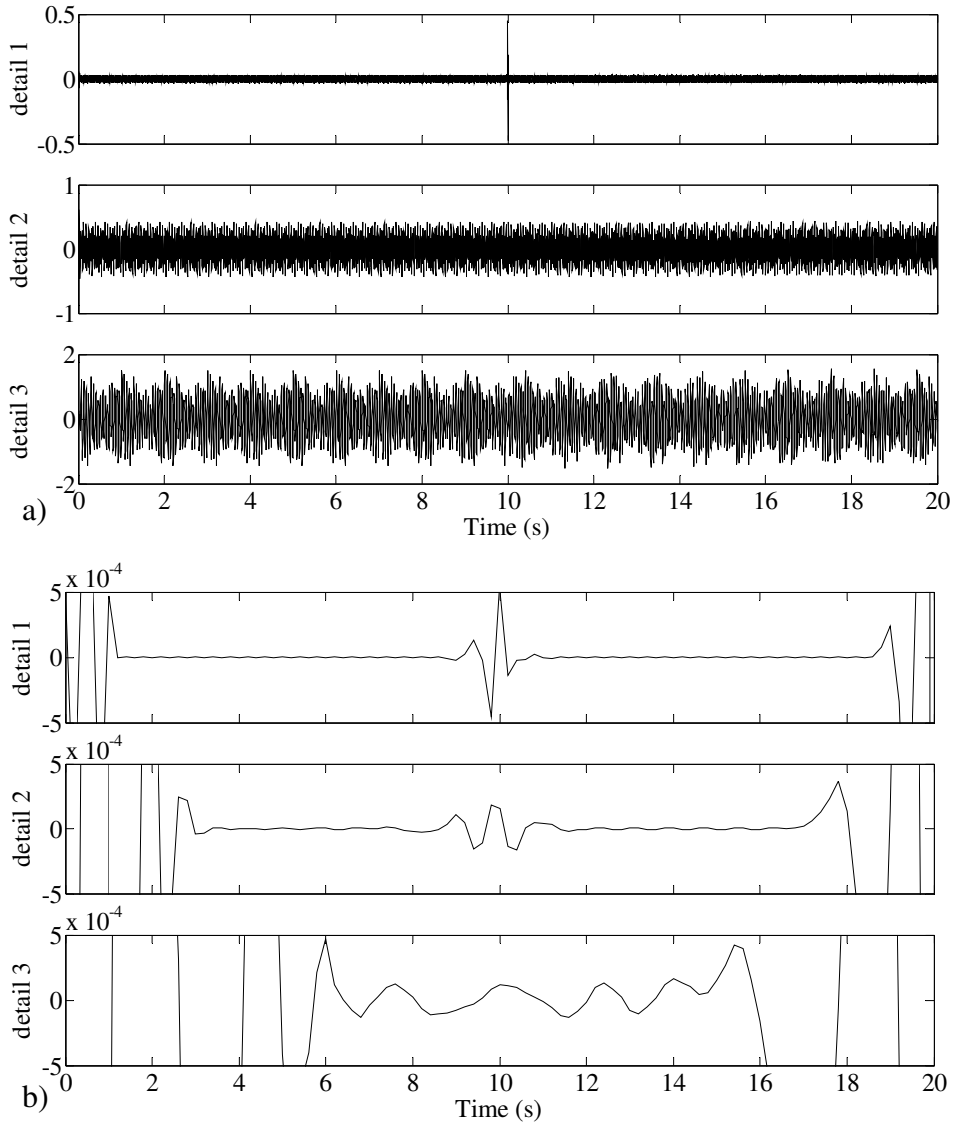

Figure 2.5. DWA method applied to: a) the time function and b) the mode function.

The detection of singularities using the DWA method is done in its first details. In fact, singularities are clearer detected in the first two details as shown in Figure 2.5a for the time function and Figure 2.5b for the mode function.

The singularity is detected by one or more spikes or a disturbance in the DWA coefficients clearly above than those of its close neighbourhood. Considering this definition, singularity was detected for the detail 1 in both cases. However, there are some differences between the evaluated examples. Firstly, more points were considered for the time function than for the mode function. This caused a clearer detection for the first example. The performance of singularity detection increases when more points are included in the wavelet analysis. This fact can be extended for all the wavelet analysis methods. Moreover, a disturbance is present in the beginning and end of the function. The DWA method interprets a discontinuity at these zones. The extent of this effect can be reduced considering more points in the analysis as shown in Figure 2.5a.

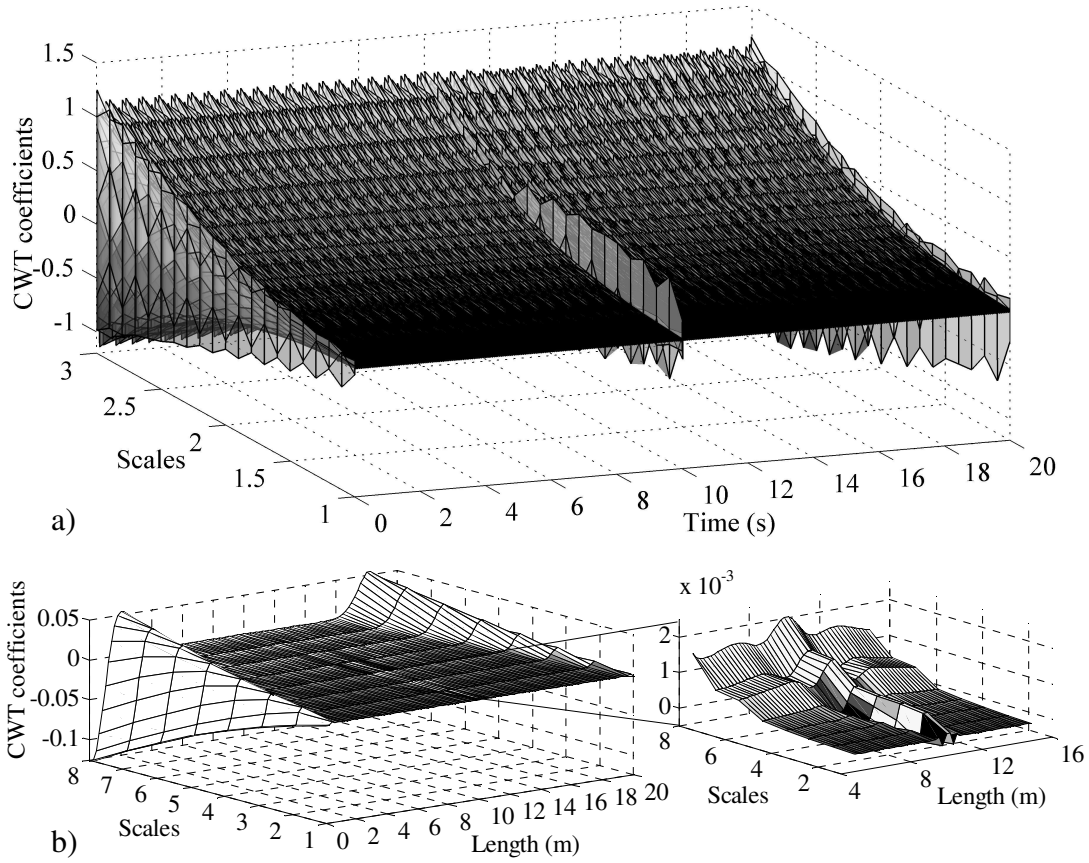

Figure 2.6. 3D representation of CWT for singularity detection; a) time function and b) mode function.

Even when the singularity location was clearly detected by the detail 1, other factors present in dynamic parameters like noisy data, and influence of ambient factors may decrease the quality of this detection. Hence, in some circumstances, the detail 2 with less noise content may be used for damage detection.

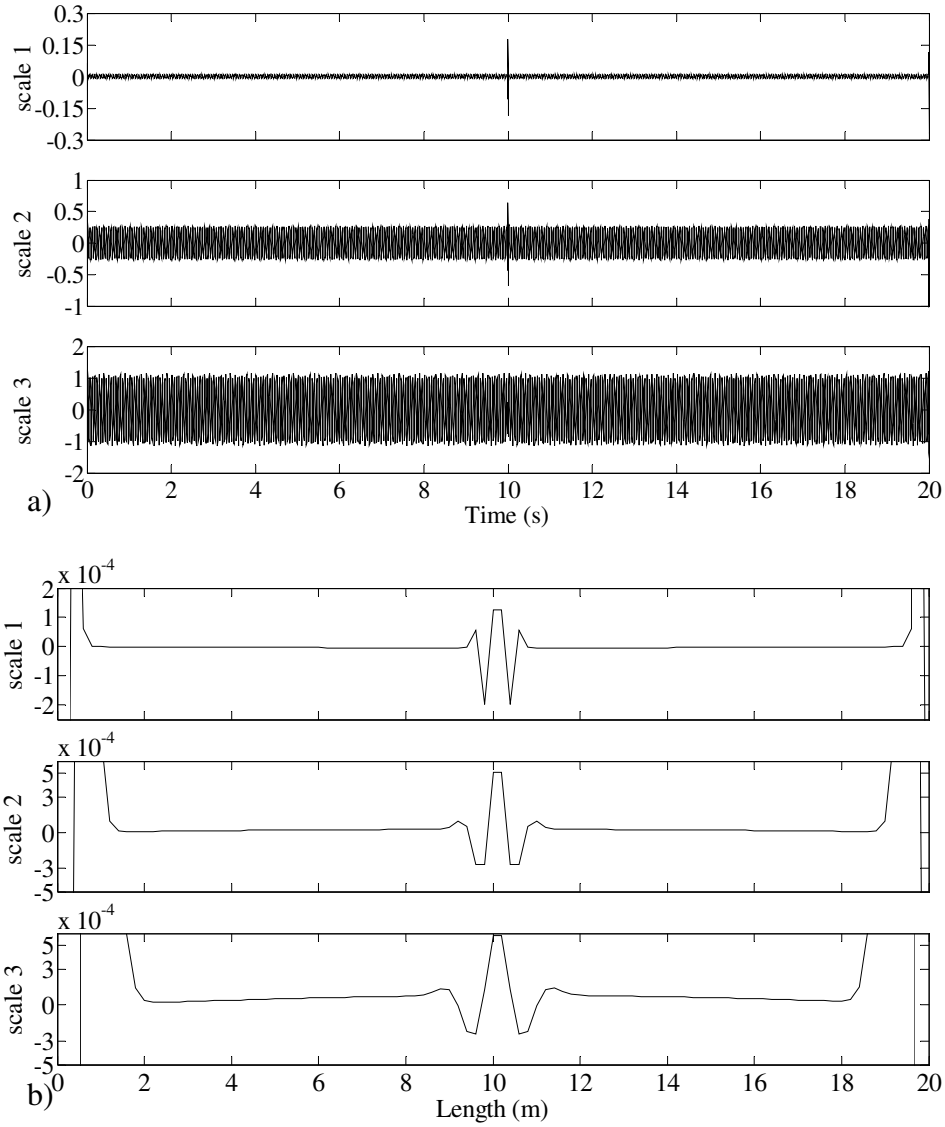

Figure 2.7. CWT for the first three scales; a) time function and b) mode function.

In the CWT method, the 3D representation of the time and scales (frequency) representation is possible as shown for the evaluated cases in Figure 2.6. In this figure, singularity is located in the finest scales and hidden for the effect of the high coefficient amplitude at the beginning and at the end of the mode function. A close view of the CWT coefficients at the singularity location shows the disturbance that indicates damage. A better way to represent CWT coefficients for damage detection

consists of 2D representation at the finest scales. In this way, and ignoring the high coefficient amplitudes at the beginning and the end of the functions, the CWT method applied to these two examples is shown in Figure 2.7.

As well as indicated for DWA method, the CWT can better detect singularities for the first scales with the best performance for the scale 1. At scales higher than 1, the amplitude of the spikes decreases and the disturbance caused by the singularity increases. Nevertheless, as shown for the mode function (Figure 2.7b), the detection of the singularity can still be done with good accuracy for the scale 3. When noisy data is being analyzed, the scale 1 could contain several spikes associated with noise which can hide the disturbance caused by the singularities. As an alternative, the scales 2 and 3 with less noise could give better detection of these singularities.

In the Hoelder exponent method, the determination of the degree of differentiability of the function can detect singularities related to damage. In the point of this singularity, the Hoelder exponent achieves a value clearly below than its close vicinity. The Hoelder exponent method applied to the evaluated examples are shown in Figure 2.8.

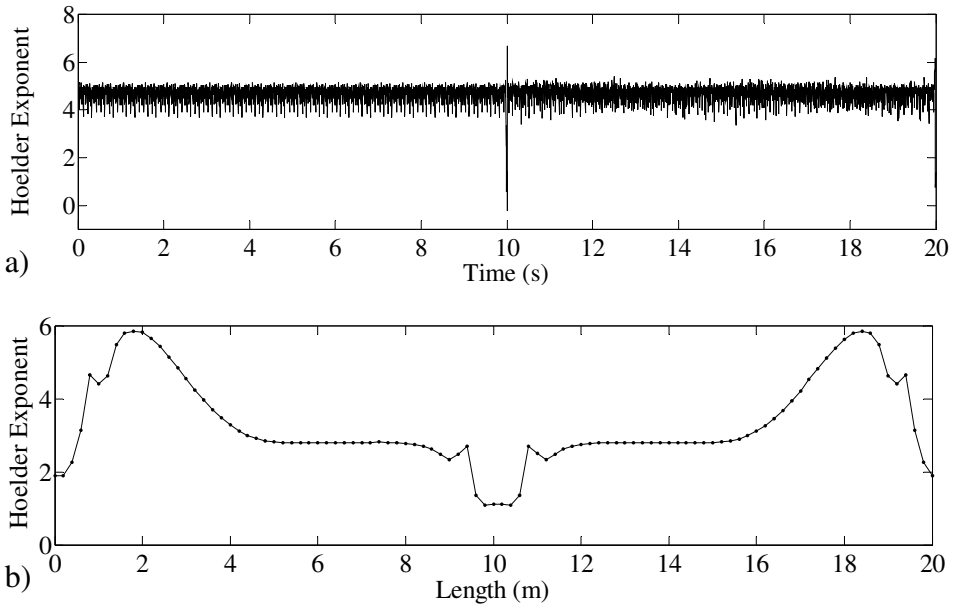

Figure 2.8. Hoelder exponent method applied to: a) time function and b) mode function.

The detection of the singularity is clearly detected from the first example than for the second one. According to the calculation of the Hoelder exponent using wavelet transform, the slope defining the Hoelder exponent at this time or space

point of the function should be calculated along the scales with the maximum local values. This requirement is fulfilled by the time function but not by the mode function where the local maximum is less clear as scales increase (see Figure 2.6) leading to a disturbance zone somewhat larger than the damage zone.

In the last described wavelet analysis method, the WPT was used to locate singularities. An inspection of the WPT coefficients for different levels indicated that high level functions keep the information related to this singularity. However, high levels contain fewer points due to the number of points of the decomposed function decreases to the half from one level to the next one. As a result, less accuracy to detect singularities may be expected. For the two selected examples, the 3rd and 2nd WPT levels of decomposition were selected for the time and mode functions, respectively. The WPT coefficients obtained from the decomposition of the evaluated functions are shown in Figure 2.9.

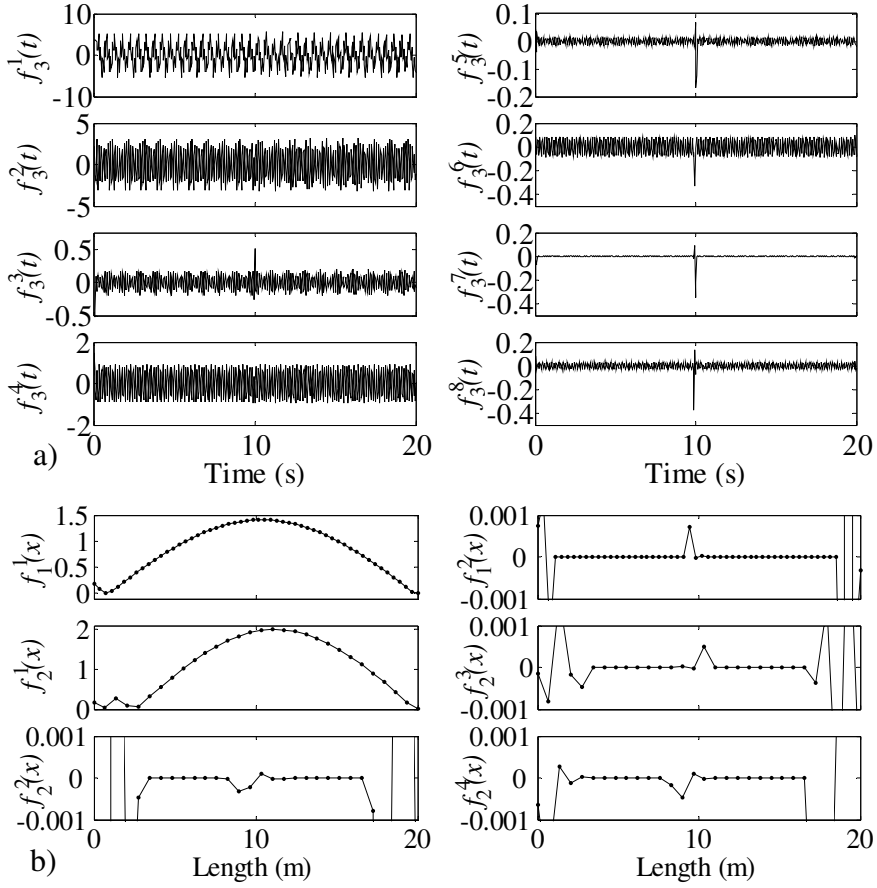

Figure 2.9. WPT decomposition a) at the 3rd level for the time function and b) at the 1st and 2nd levels for the mode function.

The left side graphs showed the decomposed functions obtained from the *approximation* decompositions of the previous level, while the right side graphs showed the decomposed functions obtained from the *detail* decompositions of the previous level. The information related to the singularity is mainly contained in the right side functions.

The examples showed in this part of the thesis are only academic and tried to illustrate the potential of this technique for the location and detection of damage which causes singularities in the dynamic parameters of the structures. Other important factors as noise which commonly pollutes the dynamic parameters and ambient factors could diminish the performance of the methods before described.

These methods based on Wavelet Analysis have become popular because they do not require differentiation of the measured data and it is possible to detect damage only with the existing damage information. Unfortunately, the singularities detected with these methods in the finest scales of CWT and the first details are prone to high frequency disturbances related to noise. Several variants of wavelet analysis methods seem to be less sensitive to this factor.

An exhaustive description of the mathematical background of the Wavelet Theory has been done by several authors (*e.g.,* Mallat, 1999 and Chan, 1995).

2.3 Wavelet analysis methods

The FT is the most used tool for finding the frequency components of a signal. However, the frequency components can only be extracted from the complete duration of the signal. In practical cases, instead of that, frequency components are obtained from an average of time windows over the finite length of the signal. Hence, it is not suitable tool for non-stationary signals such as the impulse response of cracked structures. Moreover, time or space information which enables to detect when or where a particular event took place is lost after Fourier Transformation. For dealing with these problems, the short time Fourier transform (STFT) was implemented for determining the time and frequency components of the analyzed signal. However, in the STFT the time-frequency resolution is fixed and high resolution in time or space and frequency domain is not possible since once the windows size is chosen (according to the uncertainty principle). Then, this method may not be suitable to find singularities in the signals related to damage.

The Wavelet Transform (WT) with adjustable window location and size could satisfactory overcome the shortcomings of the FT methods. Unlike FT where the signal is broken up into sinusoidal waves of different frequencies and phases, the WT decomposes the signal in wave functions. Mathematicians started the development of the Wavelet Theory since the beginning of the last century. Haar (1909) studied the wavelet theory trying to find a basis in space similar to Fourier's basis in frequency space. Much of the work in wavelet analysis was done in the 1930s; however the contributions done at that time did not result in a coherent theory.

The current mathematical background of the Wavelet Analysis used in applied fields was introduced by Grossmann and Morlet (1984). Some time later, Mallat (1989) established the wavelet theory for signal decomposition, which has been considered as the basis of the discrete wavelet transform. Based on Mallat's work, Daubechies (1988) presented the formal mathematical formulation of the WT using a set of wavelet orthonormal basis functions. Mallat and Hwang (1992) proposed a method for the detection of singularities in a signal using wavelets. The modern wavelet theory was applied for the first time during 1990s in geophysics to analyze data from seismic surveys, information used for obtaining the layer composition in surface rock. Newland (1994) was the first to apply this method to vibration analysis. He analyzed the level of vibration of buildings caused by underground trains and road traffic to determine similarities between response signals in each floor.

Other applied fields that are making use of wavelets include astronomy, acoustics, nuclear engineering, sub-band coding, signal and image processing, neurophysiology, music, magnetic resonance imaging, speech discrimination, optics, fractals, turbulence, earthquake-prediction, radar, human vision, and pure mathematics applications such as solving partial differential equations.

In its short life, wavelet analysis methods have suffered a constant evolution seeking for more reliable damage detection methods. Hence, wavelet based damage detection methods are classified according to the damage detection classification proposed by Rytter (1993) and presented here in the introduction, *i.e.,* level I, II and III wavelet methods. Level IV methods are not included in the wavelet classification as they need the participation of different fields, like fracture mechanics, fatigue life analysis, and/or structural design assessment. A study of the current state of the damage prognosis, related to level IV methods, was done by Farrar *et al.* (2003).

2.3.1 Wavelet based level I damage detection methods (Structural Health Monitoring)

The detection of damage in level I methods is commonly done by comparison of the wavelet coefficients. In this way, Surace and Ruotolo (1994) detected damage applying WT to the dynamic response signal from a single accelerometer located in a cantilever beam before and after the introduction of a single crack.

Hou *et al.* (2000) examined the potential of the discrete wavelet transform (DWT) for detecting the precise time when damage occurs. They proved that damage caused by change of stiffness in structures may be detected by spikes in the first details of the wavelet decomposition of the response data. For that purpose they used a simple numerical model with three parallel breakable springs as shown in Figure 2.10 .

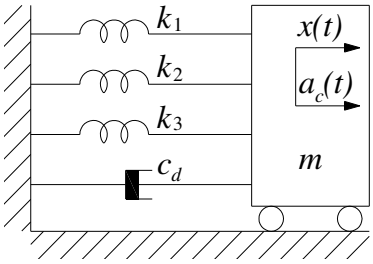

Figure 2.10. Structural model with three paralleled breakable springs.

This model was excited first with a harmonic load and later with real earthquake response data recorded during the 1971 San Francisco Earthquake. Each spring breaks when the structural response exceeds a corresponding threshold value. Results obtained with the harmonic excitation after breaking two springs, which significantly reduced the total stiffness of each one in 20%, did not indicate any disturbance that could be associated with damage from the corresponded history of accelerations. On the other hand, a clear detection of damage was obtained using the detail 1 wavelet decomposition of the acceleration response.

A cumulative fatigue effect was also simulated with the same model using a repetitive step reduction of the stiffness (4% each step). At that time, smaller spikes were present at the time that the reduction of stiffness occurred. In the case of the *detail* wavelet decomposition applied to the acceleration response at the roof of the Bank of California for the 1971 California Earthquake, no dominant spikes were identified even when the structure suffered cracks and spalling of columns and girder stubs. Finally, the severity of damage and noise intensity were evaluated using the

detail wavelet decomposition of the acceleration response obtained from the numerical model with harmonic excitation by means of a detectability map. It was concluded that damage was easier to be detected for the lowest noise levels and the most severe damage intensities.

Melhem and Kim (2003) detected damage due to fatigue in a Portland cement concrete pavement on grade and in a simply supported prestressed concrete beam. In the concrete pavement, damage was not detected by the frequency decomposition using the Fast Fourier Transform. However, the WT contour map determined from the deflection response indicated an increment of the number of ridges when the number of applied cycles increased. In the damage analysis of the prestressed concrete beam, a reduction of the frequencies of the beam during the fatigue tests was clearly detected (*e.g.,* 25% for the first natural frequency after 2 million cycles). Moreover, the WT contour map determined from the acceleration response of the beam indicated that the number of ridges decreased when the number of applied cycles increased.

Robertson *et al.* (2003) investigated the possibility to apply the Hoelder exponent, a measure of the differentiable degree of a signal, for detecting when the damage occurs. Presence of damage in time histories caused singularities which are not differentiable and therefore presents a Hoelder exponent close to zero. The authors determined the Hoelder exponent of a signal based on the calculation of its CWT. The slope of the logarithmic Wavelet function at the logarithmic scales domain corresponds to the Hoelder exponent for the selected time. They applied the proposed method to an earthquake acceleration response where damage was added as two impulses at predefined time of the acceleration response in a first case, and with a step function on the same signal in a second case. An example of the damage detection methodology proposed by the authors when two impulses were added to the Borah Earthquake at times t=7.47 s and t=20 s with magnitudes equal twice the acceleration response at these times is shown in Figure 2.11.

Using statistical process control, lower control limits (LCLs) were determined. Hoelder exponents below these limits were identified as singularities at this time. Results showed that damage was detected for the first case with impulses added to the acceleration response but damage was undetected for the second case with the step function. As a result, a new lower control limit was defined as 1.5 times the maximum drop of the Hoelder exponent calculated from the side of the signal

without singularities. Finally, a system with a loose internal part which caused a harmonic response was analyzed. Hoelder exponent values below the LCL were determined for the cases analyzed with the CWT. They concluded that the Hoelder exponent procedure is highly dependent on the magnitude of the jump and the regularity of the overall signal.

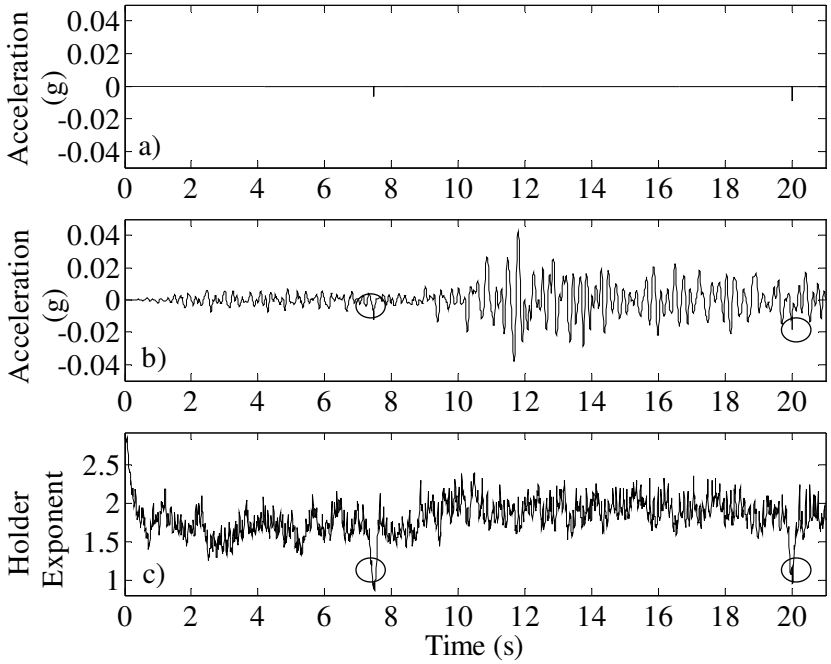

Figure 2.11. Typical example of the application of Hoelder Exponent method using Robertson *et al.* (2003) method; a) Impulses at times t=7.46 s and t=20 s; b) Borah accelerogram with impulses added; c) Hoelder exponent graph where impulses were detected.

Hera and Hou (2004) applied the *detail* wavelet decomposition method to detect damage in a benchmark study problem which consisted of a four storey scale steel frame scale building braced in all its bays and subjected to simulated lateral wind at each floor as shown in Figure 2.12.

Damage scenarios were simulated removing braces in the numerical model at a predefined time. Damage was detected from the *detail* wavelet decomposition (DWA) of the acceleration response in the nodes closer to the braces removed. Furthermore, the authors noticed the possibility to determine the location of damage observing that spikes were clearer in the nodes closer to the braces removed. However, spikes at the fourth floor were found to be of the same amplitude as those determined in the first floor, where damage was simulated. Moreover, artificial noise added to the dynamic response significantly decreased the performance of the

applied method. The damage detection procedure applied by these authors is shown in Figure 2.13.

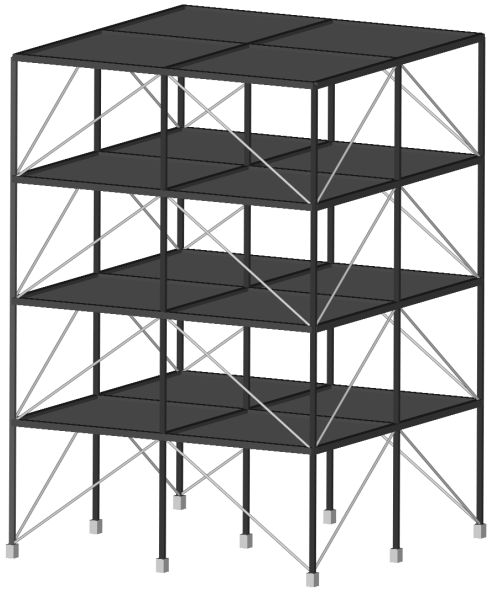

Figure 2.12. Benchmark study problem proposed by the ASCE SHM group (Johnson *et al.*, 2004).

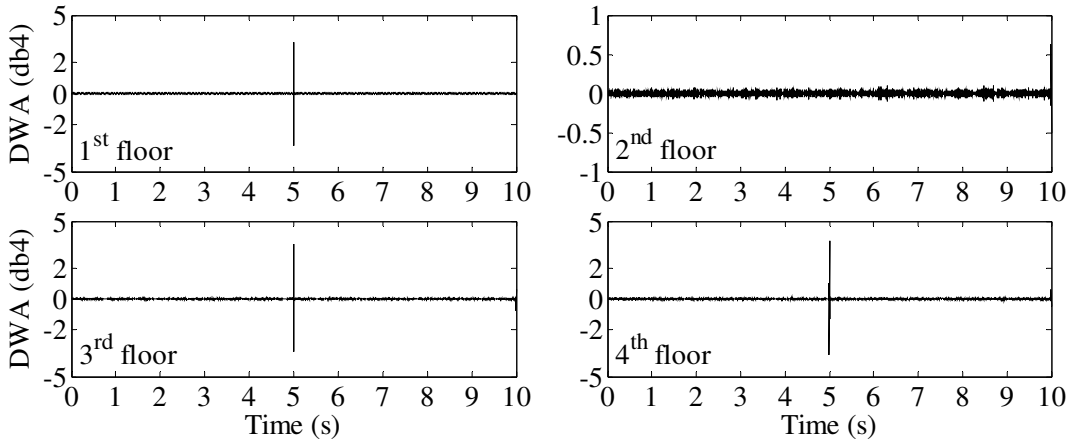

Figure 2.13. Typical example of the damage detection procedure adopted by Hera and Hou (2004). Results obtained from the ASCE benchmark study using the Daubechies 4.

The identification of stiffness degradation in structures using wavelet analysis was addressed by Basu (2005). Two Single Degree Of Freedom (SDOF) numerical models with two parallel springs were used for illustrating the potential of this method. The first model was a bi-linear non-hysteretic model excited with an accelerogram.

Comparison between the linear and non-linear responses of the model did not lead to significant differences. However, comparison of the energies calculated from the WT at different bands (scales) showed noticeable differences. The second model is a continuous hysteretic model excited with white noise. Two different cases were simulated with this model, namely the WT of the acceleration response for a linear behaviour case (defined as the undamaged case) and the non-linear behaviour case (defined as the damaged case). Moreover, the wavelet coefficients of the input force were determined. Comparison of the two cases indicated differences between the undamaged and damaged cases. Moreover, a similitude between the undamaged case and the input force wavelet coefficients were determined. Basu (2005) pointed out that this finding may be used for indicating the presence of damage in the structure just with the dynamic response from the damaged structure.

2.3.2 Wavelet based level II damage detection methods

Wavelet analysis can also be used for determining the location of damage in a structure. One of the first approaches for locating damage using wavelet analysis was proposed by Liew and Wang (1998). They developed a numerical model of a simply supported beam with a transversal open non-propagating crack, modifying its stiffness matrix. The displacement response of the beam was determined using the traditional eigen theory and a wavelet approach proposed by the authors. According to the authors, the displacement response $u\left(x,t^{*}\right)$ of the system at time t^{*} can be expressed as:

$$\begin{aligned} u\left(x,t^{*}\right) &= a_{0}+\sum_{j=0}^{\infty}\sum_{k=0}^{2^{j}-1} e_{2^{j}+k} W\left(2^{j}-k\right) \text{ for } 0\leq x\leq 1; \\ W\left(x\right) &= \sin\frac{2\pi x}{L}+i\cos\frac{2\pi x}{L}; \\ e_{2^{j}+k} &= 2^{j}\int_{0}^{1} u\left(x,t^{*}\right) W\left(2^{j}x-k\right) dx \end{aligned} \tag{2.31}$$

where $W\left(x\right)$ is the adopted mother wavelet and $e_{2^{j}+k}$ are coefficients which contain local information of the space domain of the structure and were used by damage detection purposes.

Comparison of the first 5 modes and frequencies did not show noticeable changes. However, their wavelet counterparts were able to detect the location of damage for the higher levels of displacement wavelet coefficients.

Wang and Deng (1999) took advantage of the multiresolution ability of the WT for determining the location of damage in two numerical examples. In the first one, the displacement response of a simply supported beam with an open vertical crack subject to static and impact loading was analyzed. In the second case, the dynamic displacement response of a plate with a through-thickness crack was analyzed. Displacements of the beam were calculated using a finite difference scheme, while displacement response for the plate was determined using a crack-tip solution for an elastic body. Haar and Gabor mother wavelets were used for calculating the wavelet coefficients of the deflections of the beam and plate. Results indicated that simulated damage was detected for the higher levels of displacement wavelet coefficients with better performance for the Gabor mother wavelet. A sensitivity analysis of the number of evenly distributed signal points was also done. Damage was not detected when the number of signal points in the beam was less than 15 compared with the original 1024 using during the previous analyses.

Hong *et al.* (2002) applied the CWT and the Lipschitz exponent to locate damage in structures. They found out that the Lipschitz exponent in the location when damage appears in the structure must lie between one and two. In consequence, the minimum number of vanishing moments of the selected mother wavelet used during the analysis should be at least two. The Lipschitz exponent, in the location of damage, is calculated from the local maximum along the scales of the CWT. Damage caused a singularity in the mode shapes which are detected as a disturbance in the CWT. This disturbance consists of coefficients with local maximums at this location. The slope of the logarithmic distribution of these local maximums and the scales defined the value of this exponent.

A simply supported plane beam was simulated and tested in order to verify the assumptions before stated. It was found out that damage can be determined with more accuracy for the lower mode shapes. The number of sampling points and noise had an important influence in the value of the Lipschitz exponent. A correlation between exponent value and crack depth was found and it preserves even for large sampling distance.

Gentile and Messina (2003) explained, in a more rational manner, the potential of the WT for detecting damage in structures. They highlighted the ability of the CWT to detect damage by means of performing an equivalent derivative of the signal. A certain derivative of the signal can be approached chosen the number of

vanishing moments of a mother wavelet. For proving this fact, a numerical model of an Euler-Bernoulli beam where damage was simulated with a sub-beam having a decrement in its Young's modulus was done. The decrement of the Young's modulus at the crack location was determined according to the next expression:

$$\frac{E_{eq}}{E} = \left[(1-\delta)^3 + \frac{4.41}{12} \frac{(1-\delta)}{d/h} \left[(1-\delta)^6 - 3(1-\delta)^2 + 2 \right] \right]^{-1} \tag{2.32}$$

where δ is the crack depth ratio (*a/h*) and *d* represent the half-width of the notch.

Damage location was performed applying the CWT to the mode shapes at certain scales. The Haar and Gaussian mother wavelet were used during the wavelet analysis. Damage detection was clearly better for mother wavelet with large vanishing moments. Moreover, damage detection was clearer at finest scales when the signal was not contaminated with noise. Large scales performed better with signal contaminated with noise; nevertheless, they lost definition for the damage location. Furthermore, a smoothing function was proposed for reducing the disturbance present in the wavelet coefficients near the boundary conditions. However, this effect smoothes the CWT coefficients as well reducing the disturbance related to damage.

Chang and Chen (2003) developed a damage detection method based on spatial wavelet analysis. A cantilever Timoshenko beam with a transversal crack modelled as a rotational spring was done for calculating its mode shapes. Damage was located through the wavelet coefficients of the mode shapes determined with the Gabor mother wavelet. Different crack locations were proved including two cracks in the beam with different separation between them. Damage was successfully detected in all the cases especially for the finest scales. Errors during the data acquisition were also simulated in the mode shapes. The moving average method was used for denoising the modes. By definition, a moving average $\bar{F}$ at position *x* of a discretized signal *f* is given by:

$$\bar{F} = \frac{1}{T} \sum_{i=0}^{T-1} f(x-i) \tag{2.33}$$

Damage location was detected for the simulated cases when the smoothing method was applied. They finally proposed that the magnitude of the wavelet coefficients can be used as parameter to determine the crack depth of the beam.

Chang and Sun (2005) proposed a method based on the Wavelet Packet Transform (WPT) for located damage in beam structures. The dynamic response of the structure between the baseline condition and the current state are required for the damage location procedure. Then the dynamic responses along several measuring points in the structure are decomposed using the WPT. In a next step, the entropy energies of the components of the decomposed signal are determined. Differences between the component energies between the healthy and damaged structure along the measuring points are calculated. An appropriate energy component is selected for all the measuring points and the curvatures of these WPT energy shapes are calculated. This process, called as Wavelet Packet Signature (WPS), seems to be highly sensitive to damage present in the structure.

Two numerical studies, one on a 15-storey shear-beam building frame and another in a simply supported beam, and an experimental case on a simply supported reinforced concrete beam were performed for validating the proposed method. Damage was numerically simulated reducing the stiffness of either one or several of the elements in the model. Successful damage location, indicated a disturbance at the damaged elements, was detected for all the evaluated cases even when noise was numerically introduced in the models. Moreover, the intensity of the damage may be determined from the magnitude of this disturbance. In the experimental study, where only seven accelerometers were located in the beam, damage was successfully identified for all evaluated damage scenarios. Therefore, this method was able to give good results for most of the practical cases when few measuring points were acquired in the dynamic test.

Another method based on the WPT was proposed by Han *et al.* (2005). This method uses a procedure similar to that proposed by Chang and Sun (2005) but now a new damage detection index and procedure for locating damage was proposed. This method determines the energies of several components of the decomposed dynamic response of the structure using WPT. The proposed damage index referred as Wavelet Packet Energy Rate Index (WPERI) calculates the summation of the absolute differences between the energy of the WPT components $E_{f_j^i}$ of level *j* at two different time ranges *a* and *b*. The WPERI can be expressed as follows:

$$\Delta\left(E_{f_j}\right) = \sum_{i=1}^{2^j} \frac{\left|\left(E_{f_j^i}\right)_b - \left(E_{f_j^i}\right)_a\right|}{\left(E_{f_j^i}\right)_a} \tag{2.34}$$

The damage detection procedure consists of determining by trial and error the minimum level of WPT decomposition sensitive to damage. The proposed index is calculated for the dynamic response in all the measuring points in the structure. Finally, threshold values are calculated based on statistical process control. In this way, an upper limit (UL) defined as the statistical confidence level was obtained from

$$UL_{WPERI}^{Pr} = \mu_{WPERI} + Z_{Pr}\left(\frac{\sigma_{WPERI}}{\sqrt{n}}\right) \tag{2.35}$$

where μ_{WPERI} and σ_{WPERI} are the mean and standard deviation of the *n* determined WPERIs, respectively; Z_{Pr} is the value of a standard normal distribution with zero mean and unit variance such that the cumulative probability is $100\,(1-Pr)\,\%$.

For validating the applicability of the proposed method, simply supported beams with different damage scenarios were simulated. 30 elements were considered in the model subject to an impulse rectangular force applied at one node of the beam. Damage was introduced as reduction of the stiffness (10% and 20%) in two or several predefined beam elements. It was demonstrated that damage was correctly located in the evaluated damage scenarios when the UL was defined as 98% of confidence level. The proposed method was also experimentally verified in a simply supported steel I beam. Three damage scenarios consisted of severe reduction of its cross section (half of the total depth) was introduced to the beam. 26 accelerometers acquired the dynamic response on the beam under impulse force excitation. Results indicated that damage could be correctly located. This method, as well as that proposed by Chang and Sun (2005), needs reliable information of the healthy structure. Moreover, the same force must be applied in both evaluated structural conditions.

2.3.3 Wavelet based level III damage detection methods

The ability of the WT to calculate the severity of the damage in a structure has been done mainly proposing a factor which compares the wavelet coefficients of the dynamic parameters of the structures under different known damage scenarios. The simplest level III damage methods relate the wavelet coefficient magnitudes with the intensity of damage. Several of these methods have been already described into level

II methods because their main objective was to locate damage in the structure and not to quantify it.

A more rational method for calculating the severity of damage was proposed by Douka *et al.* (2003). In this method, the location of damage is determined by the sudden change in the spatial variation of the CWT applied to the mode shapes of a beam. The size of the single open crack is calculated by an intensity factor related to the Lipschitz exponent of the CWT at the crack location. A numerical and experimental model of a cantilever beam was done for testing the proposed method. Damage was introduced in the numerical model as a rotational spring in the location of damage. The CWT applied to the fundamental mode shapes was calculated with the Symlet mother wavelet with four vanishing moments from scales 1 to 25 with unit increments. Correlations between different crack depths and the intensity factor were determined from the numerical model when noise was not taken into account. In a next step, fundamental mode shape of the cantilever beam was corrupted with noise. Under this condition, the Lipschitz exponent could be accurately calculated for crack depths larger than 50% of the total depth. Moreover, it was pointed out that noise introduced to the fundamental mode shape of the cantilever beam was present in the finest scales and does not increase regularly with the scales. In this way, a careful observation of the CWT can discriminate those singularities related to noise. In the last step, the proposed procedure was applied to an experimental cantilever beam.

Results showed the induced vertical crack was correctly located; however the crack depth was overestimated. The proposed method is clearly influenced by the number of measuring points located in the structure, noise present in the modal parameters and accuracy of the used response signal.

One year later, Loutridis *et al.* (2004) proposed the same previous procedure but now applied to a numerical and experimental example of a cantilever beam with two open vertical cracks. The results found in this study were similar to those obtained by Douka *et al.* (2003). An important point found for these authors relies on the dependence of the wavelet coefficients to the damage location. Two cracks located in the cantilever beam with the same crack depth can have different wavelet coefficients. This is caused by the slope of the fundamental mode shape which is different for the two crack positions. This problem should be taken into account during the evaluation of the damage severity of several cracks present in the beam.

Sun and Chang (2002) proposed a combined method between the WPT and the Neural Network (NN) for detecting, locating and quantifying damage in a structure. The method consists in decomposing the acceleration response of the structure in different components using WPT and calculates the energy of each component. This is equivalent to decompose the total energy of the signal into a summation of wavelet packet component energies corresponding to different frequency bands. A shift in the component energies between the healthy and damage structure is more evident for high levels of decomposition. For selecting the best component energies for the damage evaluation, a sensitivity analysis of the component energies with respect to the flexibility of the undamaged structure was done.

This procedure was verified with a numerical example of a three-span continuous bridge made of steel and with span lengths of 15-20-15 m. A simple finite element model with 10 elements subject to an impact force in the middle of the second span was considered. Acceleration response was calculated in the same position where the force was applied. For the damage detection procedure, two NN models were done. The first one was capable to detect damage as small as 4% of reduction of the stiffness in one of the elements of the beam. The second NN model was able to locate and quantify the severity of damage for a moderate damage (10-20% stiffness reduction in one of the elements) with reasonable accuracy. The main disadvantages of this method lies in that the same force must be applied in the same position with the same magnitude. Moreover, a training of the NN models is needed before the damage detection procedure can be implemented on-line.

Law *et al.* (2005) proposed also a method based on the WPT component energies of the dynamic response of structures. The authors carried out a sensitivity analysis of the acceleration, strain response and WPT energy components. They found that acceleration response is more sensitive to change in the stiffness of the structure than strain response. They derived a formulation for calculating the sensitivity of the WPT component energies with respect to the change of stiffness of one element in the structure. This equation was proposed for evaluating the damage in structures.

A numerical and experimental study of a simply supported beam was done to validate the assumptions before mentioned. Several damage scenarios were considered for the numerical model. Damage was simulated as reduction of the bending stiffness (between 5 to 15%) of one of the elements of the beam. Impulse

and sinusoidal excitation were considered as the force excitation for the numerical example. A correct location and magnitude of the reduction of bending stiffness were detected for all the damage scenarios including when dynamic response was contaminated with noise. Only damage detection was not satisfactory detected for one scenario determined from the strain response of the beam which confirms the lower sensitivity of this parameter compared with the acceleration response.

In the experimental analysis, damage was introduced as a cut in the top and bottom of the cross section of the beam over a predefined length. Strain gauges were used for acquiring the dynamic response of the beam in seven locations evenly distributed along the length of the beam. Results of the proposed methods showed that damage was located in the zone where it was induced in the beam; however other points showed significant reduction in their stiffness. In opinion of the author, this false damage detection may be caused by the fact that damage affects its close neighbourhood and as a result the elements closer to the location of damage.

Zhu and Law (2006) proposed a method for damage identification of bridge structures based on CWT. For that purpose, they developed a model for calculating the dynamic deflections of a cracked simply supported bridge and subject to a moving load. Damage was simulated in the model as a rotational spring with a compliance value for a rectangular cross section given by:

$$c = \frac{1}{k} = \frac{2h}{EI}\left(\frac{\delta}{1-\delta}\right)^2 \left[5.93 - 16.69\delta + 37.14\delta^2 - 35.84\delta^3 + 13.12\delta^4\right] \quad (2.36)$$

where δ is the crack depth ratio (*a/h*), *k* is the stiffness of the spring, *EI* is the bending stiffness of the cross section and *h* is the depth of the beam.

Damage was detected applying the CWT to the dynamic displacement influence lines calculated at one selected point in the bridge beam. The method seemed not to be sensitive to the speed and weight of the moving load. Moreover, several cracks were successfully detected with this method. The detection was done using the Gauss 2 mother wavelet from scales one to 512 with unit increments. The larger scales contained the information necessary to perform the damage location. In this case, the scale 64 was adopted for the damage detection. The ratio of the logarithmic of the wavelet coefficients with and without damage at specified scale was the damage index proposed for estimating the damage extent. Noise was

numerically introduced in the numerical model but its influence was not relevant for the damage location procedure and determination of the damage indexes.

An experimental test carried out on a T concrete beam with two crack patterns showed that damage could be located better when it was delimited to a small zone. The damage severity could not be estimated from the experimental tests due to the fact that the CWT of the influence lines were contaminated with several peaks associated with the entry and exit of the vehicle.

Pakrashi *et al.* (2007) used the CWT for detecting and locating damage in a beam. As opposed to other studies which also used the CWT to detect damage, they improved the efficiency of this technique applying a partial windowing to the deflected (static or dynamic) shapes. Moreover, they proposed to measure the severity (crack depth) of the damage using the kurtosis of the transformed wavelet deflected shape. The kurtosis β_K of a mode shape $\phi(x)$ is represented as the ratio of the fourth central moment of the mode shapes to its squared variance, *i.e.,*

$$\beta_K = \frac{\int_0^L (x-\bar{\mu})^4 \phi(x)\, dx}{\left[\int_0^L (x-\bar{\mu})^2 \phi(x)\, dx\right]^2} \tag{2.37}$$

The methodology for damage detection was proved in a simulated and experimental simply supported beam. The simulated dynamic parameters of the beam were obtained with three different damage models, namely lumped cracked model, continuous cracked model and smeared cracked model. Damage was simulated as a single open crack with different depths. This damage was tried to be detected using Coiflet 4 mother wavelet with 8 vanishing moments. Clearer detection was obtained when partial windowing of the deflected shape was applied compared with the CWT procedure alone. Calibration of the CWT coefficients and kurtosis values were done for different crack depths and noise levels. Results indicated that the kurtosis of the transformed wavelet deflected shapes is more robust and stable parameter to indicate the severity of damage under high levels of noise.

Finally, the proposed method was verified with an experimental specimen where the deflected shapes were obtained from snapshots taken with a video camera when the beam was oscillating. The application of the CWT method after partial windowing of the deflected shape identified the location of the crack with a depth (5 mm) equal to half the total depth of the beam (10 mm). The kurtosis value

determined from this experiment (34.37) was closed to the value obtained from the calibration of the numerical model of the same beam (38.77).

2.3.4 Non Wavelet damage detection methods

As indicated for several authors, one of the most important characteristics of the wavelet analysis methods relies on the calculation of an equivalent function as the second derivative of the analyzed signal. The second derivative of the mode shapes was proposed by Pandey *et al.* (1991) as a candidate parameter for damage location. They called curvature mode shape to the second derivative of the mode shape. This parameter is proportional to the bending moment at a specific section and inverse proportional to the stiffness at the evaluated point. Therefore a decrement of the stiffness of the structure will cause an increment in its curvature mode shape.

The proposed method was proved with a numerical example of a beam with 20 nodes and two different boundary conditions, namely simply supported and cantilever. Damage was introduced to the numerical model as a reduction of the initial Young's Modulus. As comparison with the proposed method, Modal assurance criterion (MAC) method and Co-ordinate Modal Assurance Criterion (COMAC) method were calculated as well. Damage detection procedure was done calculating the differences between the curvatures of the beam before and after damage. As an example of the applicability of the method, the value of Young's Modulus was reduced in 50% in one of the elements of the beam. An increment in the curvature mode shapes for the evaluated cases was detected near the damaged element. As opposed to curvature method, MAC and COMAC method did not indicate any damage to the same evaluated cases.

The authors pointed out that damage is more evident for larger decrements of Young's Modulus. They also proposed that the damage detection procedure should be combined with the frequency change method which can be implemented with few sensors in the structure. After damage is located with the frequency change method, a full modal identification can be performed and the curvature mode shape method can be applied to locate the damage in the structure.

Three years later, Pandey and Biswas (1994) proposed another parameter for the detection and location of damage in structures, but at this time, variation caused by damage was measured through the flexibility matrix of the structure calculated from its modal parameters. A good approximation of the flexibility matrix can be

obtained from a few of the lower mode frequencies and corresponding mode shapes. The maximum absolute values of the differences between the flexibility matrix of a structure before and after damage can determine the probable location of damage.

The effect of the change of the flexibility matrix on a steel I beam was studied. For this purpose, a numerical finite element model of the beam with 32 elements was done. Three different boundary conditions were considered, namely simply supported, free-free and cantilever. Moreover, a simply supported beam with the same cross section as in the numerical model was experimentally tested to verify the results found in the numerical examples. Damage was simulated as a decrement in the Young's modulus at selected elements in the numerical model. In the experimental example, damage was simulated with a splice at the mid-span of the beam. Removing bolts from the splice led to two different damage scenarios.

Results indicated good detection of damage for the evaluated cases. Furthermore, damage was better detected in the points were the bending moment was higher. Fortunately, this point coincides with the most probable place of occurrence of damage. The authors also proposed to use the magnitude of the flexibility changes as an indicator of the severity of the damage.

Ratcliffe (1997) proposed a method which determines the second derivative of the mode shapes using the Laplacian difference operator. The one-dimensional Laplacian $\mathcal{L}$ of a mode shape ϕ is given by:

$$\mathcal{L} = (\phi_{i+1} + \phi_{i-1}) - 2\phi_i \tag{2.38}$$

For evaluating this method, simple numerical models of a cantilever and free-free steel beam were done. Damage was simulated reducing the total depth of the rectangular cross section at the damage locations. In addition to the numerical examples, a flat steel beam was tested to prove the numerical results. Damage in the experimental steel beam consisted of a saw cut 10% of the total depth. In the numerical examples, damage was detected for crack depths as low as 10% of the total depth. An alternative method was also proposed for detecting and locating damage as low as 0.5% of the total depth. This method calculates the differences between the Laplacian of the mode shape and a cubic polynomial fitting the same function. Spite of detecting less severe damage than the Laplacian method, the

alternative method was less efficient locating the damage. Moreover, both methods were less efficient when they were applied to high mode shapes.

Kim and Stubbs (2002) derived a new algorithm for the prediction of the damage location and damage severity of structures. This new method is an enhancement on the two previous versions of the damage index (DI) method proposed by the same authors. The updated damage index method β_j for n vibration modes, at *j*th location can be expressed as follows:

$$\beta_j = \frac{\sum_{i=1}^{n} \gamma_{ij}^*}{\sum_{i=0}^{n} \left[\gamma_i g_i\left(\lambda, \phi\right) + \gamma_{ij}\right]} \tag{2.39}$$

$$\begin{aligned} \gamma_{ij} &= \Phi_i^T C_{j0} \Phi_i; \\ \gamma_{ij}^* &= \Phi_i^{*T} C_{j0} \Phi_i^* \end{aligned} \tag{2.40}$$

where $g_i\left(\lambda, \phi\right)$ is a dimensionless factor representing the systematic change in modal parameters or the *i*th mode due to the damage; λ is the eigenfrequency of the system and the matrix C_{j0} involves only geometrical properties.

A similar damage severity factor was also proposed following the same formulation adopted in the previous two algorithms. This damage severity factor can be represented as:

$$\alpha_{\mathrm{DI}_j} = \frac{\sum_{i=1}^{n} \gamma_{ij} K_i^*}{\sum_{i=0}^{n} \gamma_{ij}^* K_i} - 1, \ \alpha_{\mathrm{DI}} \geq -1 \tag{2.41}$$

where K_i is the modal stiffness at the *i*th mode and the asterisk indicates damage parameter.

For testing the efficiency of the new method, the three versions of the DI methods were compared on a numerical example of a two span continuous beam modelled with 50 elements using the Euler-Bernoulli theory. Ten damage scenarios were considered in this example reducing the Young's modulus in one or two elements at the same time. Young's modulus decrements had a magnitude of 10% and did not caused an important change in natural frequencies and mode shapes. A statistical approach was established for the damage location criteria. Damage was successfully identified when the damage index value, considered as normally distributed, exceeded 98% of confidence level (two standard deviations).

Results of this analysis showed that the use of the new DI method resulted in a correct damage location and the estimated severities showed an average 7.7% error while other two methods had more than 70% errors and damage was not located in all the evaluated damage scenarios. The evaluation of the three methods clearly showed that the proposed new DI method had the best results while the previous two DI methods overestimated and underestimated the severity of the evaluated damage.

Barroso and Rodriguez (2004) applied the damage index (DI) method, proposed by Kim and Stubbs (1995), in the benchmark study developed by the ASCE task group of Structural Health Monitoring. The benchmark study consisted of a numerical model of a four storey steel building of 2 × 2 bays with diagonal bracing elements. In the DI method, the required baseline modal parameters of the structure delimited the application of this method. Trying to overcome this problem, the authors proposed a method for calculating the baseline modal parameters of the structures from the dynamic data of the damaged structure. For doing that, they used the stiffness-mass ratio approach which determines the undamaged modal parameters from the assumption that stiffness of the structure before and after damage did not vary significantly. Several damage scenarios were considered for the benchmark study consisted of eliminating all braces of one or more stories or just single brace at each time.

To determine the severity of the induced damage, a factor which expressed the fractional change of stiffness of the analyzed element was proposed. The application of this method to the analyzed example gave as a result that damage was successfully identified for the most severe cases when all braces of one or more stories were removed.

Wang and Zong (2002) developed a new damage detection method and damage index (the Energy Transfer Ratios (ETR) index) utilizing static parameter identification and energy based modal parameter identification. The authors also conducted a state of the art of structural health monitoring literature including signal treatment, damage detection methods, model bridge testing and finite element calculation. To verify the proposed methodology, they built a 1:6 scaled composite cross section highway bridge following the similitude laws for static and dynamic modelling. Damage was simulated as vertical open saw cuts at the bottom of the steel I beams. Damage was also introduced to the bearings of the bridge.

Comparison of different damage indexes indicated that different damage indexes have different sensitiveness to different types of damage and their extensions. Natural frequencies and damping ratios were not sensitive to the damage introduced to the bridge. Results indicated that the ETR index is highly affected by noise and relies on the large amount of measured data.

Maia *et al.* (2003) proposed to use the Frequency Response Functions (FRFs) as base for the application of several damage detection methods previously applied to the mode shapes. They indicated that obtaining the natural frequencies and corresponding mode shapes can be a time-consuming task and that the mathematical procedure used could add some unavoidable errors. Furthermore, much information is lost by using only the mode shapes. They pointed out that several methods applied to the mode shapes of structures can be generalized and made them applicable to operational mode shapes calculated from the FRFs. In this way, they evaluated the performance of five methods which compared the FRF mode shapes and their first and second derivatives before and after damage. A modified version of the well-known damage index (DI) method, now applied to the FRF operational mode shapes, was also proposed and is represented in Equation (2.42).

$$\beta_{\mathrm{FRF}_{ik}} = \frac{\eta''^{*2}_{ik}(\omega) + \sum_{i=1}^{N} \eta''^{*2}_{ik}(\omega)}{\eta''^{2}_{ik}(\omega) + \sum_{i=1}^{N} \eta''^{2}_{ik}(\omega)} \frac{\sum_{i=1}^{N} \eta''^{2}_{ik}(\omega)}{\sum_{i=1}^{N} \eta''^{*2}_{ik}(\omega)} \tag{2.42}$$

where $\beta_{\mathrm{FRF}_{ik}}$ is the damage indicator at segment *i* of the beam and force excitation *k*, $\eta_{ik}(\omega)$ is the FRF operational mode shape at circular frequency ω and *N* is the total number of segments of the structure.

The damage detection procedure consists in selecting an appropriate frequency range in the FRF. Later, at each frequency, the location where the difference between the damaged and the undamaged cases is a maximum is determined and that location is counted as an occurrence of damage. This way is followed along all the frequency range. The sum of differences found along all the frequency range is also calculated for determining the location of damage. The proposed method was verified with a numerical example of a free-free beam with 99 elements subjected to an impact force. Damage was simulated as a reduction (from 25% to 75%) of the Young's Modulus in one of its elements.

Results indicated that damage was correctly located for the methods based on the first and second derivative of the operational mode shape and the FRF DI

method. An experimental example done in a free-free beam was tested to verify the results from the numerical model. The same damage scenarios and location of the damage adopted for the numerical examples were also considered for this experimental case. At that time, damage was correctly located in the cases when the second derivative of the FRF operational mode shapes and the FRF DI methods were applied.

The authors highlighted that some improvements are needed to the proposed methods, for instance, the interpolation process needs to be enhanced, a noise level above which results cannot be reliable should be defined, a statistical process needs to be applied in order to determine the location of damage and improvements in the experimental dynamic test of structures are also required.

Alvandi and Cremona (2006) reviewed the performance of four vibration-based damage detection methods with the simulated dynamic behaviour of a simply supported beam. These methods were chosen by the authors as they do not require a numerical model of the structure, only the natural frequencies and mode shapes before and after damage: the mode shape curvature method, the change in flexibility method, the change in flexibility curvature method and the DI method were the chosen methods. The numerical model consisted of a simply supported beam, 5 m long, modelled with 20 elements where damage was introduced as reduction of the bending stiffness in one or more elements (from 1 to 10% stiffness reduction). Then, simulated dynamic response was contaminated with noise from 0.1% to 3.0 %. The successful damage location was studied in a probabilistic way counting the number of positive detections under different damage scenarios.

Results indicated that the DI methods had the better stability when noisy signals were considered. Damage simulated close the boundary conditions were difficult to detect by all the methods. The same behaviour was detected when two or more damage zones were simulated in the beam. The mode shape curvature, change of flexibility and change in flexibility curvature are able to detect localized damage in the structure but for complex and simultaneously damage cases are less efficient.

Choi *et al.* (2008) proposed, for calculating the damage severity of timber beam structures, a combined method between the flexibility method, proposed by Pandey and Biswas (1994), and a modification of the DI method, originally proposed by Kim and Stubbs (1995). The modified DI method consists of mass normalization of mode shapes as well as unit normalization of mode shape curvatures during the

calculation of the DI method. The modified DI method tries to improve the location of damage when more than one damage zone is present in the structure.

The proposed damage methodology was verified in timber beams trying to represent typical timber bridges in Australia. Damage in this study simulated timber decay caused by rot. This damage was induced to the beams as open windows in the rectangular cross section of the beams with three different depths representing the light, medium and severe damage scenario. The numerical simulations of the damage cases on the timber beams using noiseless data indicated that the modified DI method performed better for damage location than the original DI, especially when multiple damage locations were present in the beam. The proposed hybrid algorithm for calculating the damage severity performed well for single damage scenarios and reasonably estimated the severity of multiple damage scenarios. An experimental damage detection analysis was carried out on timber beam specimens with the same characteristics adopted for the numerical examples. At that time, the same results for damage location and severity estimation were found. Nevertheless, less accuracy for the damage location, due to multiple false detections, and less precision for the severity estimation when several multiple damage cases were evaluated, reduced the performance of the two proposed methods. In conclusion, the proposed methods can be considered accurate tools for damage location and severity estimation of medium and severe damage.

2.3.5 Application to vibration-based damage detection methods to real-scale damaged bridges

Few real-scale experiments have been done in deliberately damaged bridges with the objective to validate several vibration-based damage detection methods. In what follow, the most well-known experiments of this kind will be commented.

Farrar and Jauregui (1996) carried out a comparison of five damage detection methods with dynamic parameters provided from the deliberately damage I-40 highway bridge. Actually, this bridge had two independent sections, one in each traffic direction, each one made with a concrete deck supported on two plate girders. Each bridge section had three spans, 40 m long for the end spans and 50 m long for the middle span. A schematic representation of the I-40 bridge is shown in Figure 2.14.

Figure 2.14. Schematic representation of I-40 highway bridge (taken from Farrar and Jauregui, 1996).

The bridge, located in Albuquerque, New Mexico, USA, was replaced by new one and experimental modal analysis was performed on that bridge before removing it.

Four damage scenarios trying to represent typical fatigue cracks presented in this type of bridges were simulated by notch cuts on one of the steel plate girders. In addition to experimental dynamic parameters, a numerical model of the bridge simulated the introduced damage scenarios and another simulated damages located at other positions was done. The five damage detection methods selected for the analyses were: the DI method proposed by Kim and Stubbs (1995), the curvature method proposed by Pandey *et al.* (1991), the change in flexibility method proposed by Pandey and Biswas (1994), the Change in Uniform Flexibility Shape Curvature Method proposed by Zhang and Aktan (1995) and the Change in stiffness method proposed by Zimmerman and Kaouk (1994).

Results of the comparison of the performance of these damage detection methods led to the conclusion that the DI method was the best to detect and locate damage from the numerical and experimental data. The mode shape curvature method showed also a good performance. The remaining three methods failed several times to detect the different damage scenarios.

The authors pointed out that the simple comparison of the natural frequencies and mode shapes were poor indicators of damage and more sophisticated methods such the DI and the curvature methods improved the detectability of damage.

Other damage detection methods have also been applied to the experimental data acquired in the I-40 bridge. For instance, Mayes (1995) applied the Structural Translation and Rotation Error Checking (STRECH) algorithm to modal parameters from the I-40 bridge. This method searches for changes in displacements to locate areas where the stiffness of the structure has been reduced.

Sampaio *et al.* (1999) extended the applicability of the curvature mode shape and DI methods. These methods were initially proposed to be applied to the mode shapes of the structures. However, modal identification of large structures like bridges is a very time-consuming task and much useful information for damage detection may be lost after this process. Trying to solve this inconvenience, the authors proposed to apply the curvature of damage index methods to the operational mode shapes determined from the Frequency Response Function (FRF). For proving this fact, they applied this method to a numerical model of a 10 Degrees Of Freedom (DOFs) system connected with springs. Several damage scenarios were considered reducing the stiffness in one selected spring. Results showed that damage was clearly detected when stiffness were reduced from 20-80% with the FRF curvature and FRF DI methods. It was found that for a better performance of these methods, the range of the frequency selected for the analysis should be before the first anti-resonance or resonance FRF frequency. In addition to this numerical example, the methods were verified with experimental data acquired from the different damage scenarios introduced to the I-40 bridge.

Results demonstrated that damage can be clearly identified for the most severe damage scenarios by the proposed methods. However, several false-detection locations were present when less severe damage scenarios were considered.

Bayissa *et al.* (2008) developed a wavelet analysis method based on the statistical moments of the energy density function of the vibration responses in the time-scale domain. The *zero*th order moment (ZOM) of the CWT of a dynamic response along the DOFs of the structure is determined as follows:

$$\left(\mu^0\right)_{t,f} = \int_{-\infty}^{\infty}\int_{-\infty}^{\infty} \left|CWT\left(a,b\right)\right|^2 dtdf \tag{2.43}$$

where $CWT\left(a,b\right)$ contains the coefficients of the CWT and a, b, t and f are the scale and translation parameters, the time and space domain, respectively.

Later, DI and curvature methods are applied to the ZOM values in order to locate the damage. The proposed method was applied to a simulated plate and to the damaged span of the I-40 bridge. In the latter example, damage cases consisted in severe damage was included. The time series of the experimental analysis of the I-40 bridge were determined from their modal parameters using the theory of random vibrations. Application of the proposed methodology resulted in clear damage detection when the ZOM-DI method was applied. In the case of the ZOM-Curvature method, several peaks outside the damage zone diminished the performance of this method. The proposed method demonstrated to be stable and gave good results under the present of noise contamination of the dynamic responses.

Abdel Wahab and De Roeck (1999) applied the modal curvature method proposed by Pandey *et al.* (1991) to the modal parameters obtained from the Z24 bridge before and after introducing artificial settlement in one of its piers. The first five mode shapes of the bridge of the undamaged conditions are shown in Figure 2.15 (IMAC XIX, 2001).

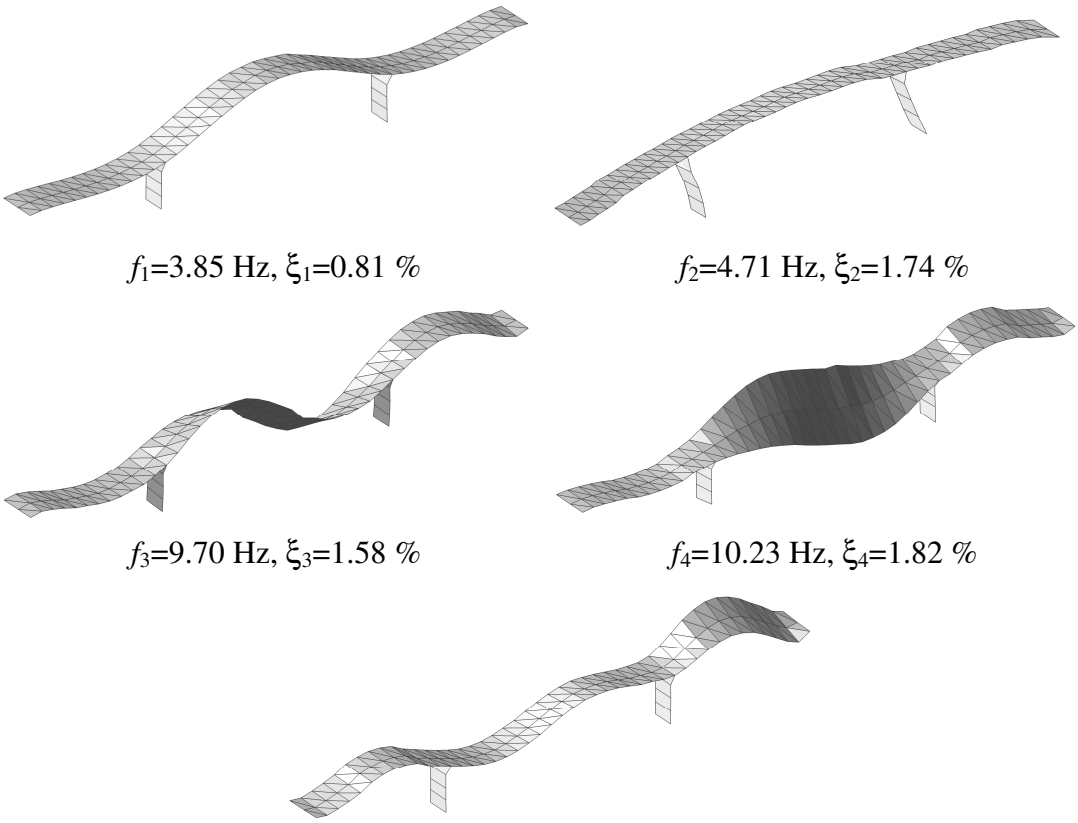

f_1=3.85 Hz, ξ_1=0.81 % f_2=4.71 Hz, ξ_2=1.74 %

f_3=9.70 Hz, ξ_3=1.58 % f_4=10.23 Hz, ξ_4=1.82 %

f_5=11.68 Hz, ξ_5=2.11 %

Figure 2.15. First mode shape of Z24 bridge before damage (determined from raw acceleration histories obtained from IMAC XIX Benchmark problem, 2001).

This kind of damage caused cracking in the main beams of the bridge near this pier. Application of the curvature method and a proposed curvature damaged factor which is the summation of the curvature differences along the considered mode shapes indicated that: 1) damage is clearly detected with the lower mode shapes, 2) for a correct damage location, damage should be looked for in several modes, 3) a denser grid of sensors is required for calculating the curvature of higher mode shapes, 4) mode shapes from experimental dynamic tests frequently present irregularities which introduce noise to the curvature method, therefore a smoothing techniques was recommended to be applied to the mode shapes to reduce this effect and 5) damage was successfully detected for the severe scenarios considering settlements of 80 mm and 95 mm, however other peaks, smaller in magnitude, were present in the curvature graphs which can be confused for the analyst who will not known a priori the location of the damage. In all these analyses, the central difference method was used for calculating the mode shape curvatures. It is clear that a better method for calculating the second derivative of a function capable to deal with noisy data will have better performance than the evaluated method.

Teughels and De Roeck (2004) carried out a model updating analysis of the Z24 bridge. 95 mm settlement of the middle pier was the damage scenario chosen for the analysis. This damage scenario caused cracking of the prestressed concrete girders in the vicinity of the pier. The numerical model used consisted of 82 beam elements for the prestressed concrete girders. The chosen variables to be updated were the Young´s modulus and the shear modulus of the girders. Moreover, the stiffness values of the springs modelling the soil stiffness were also updated.

Results of the model updating procedure indicated a good correlation between the experimental and numerical results. Moreover, a decrement of the Young's modulus at the damage zone was calculated, which indicated possible damage there. The results were compared with the Direct Stiffness Calculation, proposed by Maeck (2003), given a good agreement.

Kullaa (2003) used statistical process control to monitor, off and on-line, the dynamic parameters of the Z24 bridge under three damage scenarios. This technique was applied to the modal parameters (natural frequencies, mode shapes and damping ratios) of the bridge.

In addition to the above-mentioned vibration-based damage detection methods, there are other important methods. For instance, methods based on Genetic

Algorithms (Gomes and Silva, 2007 and Au *et al.*, 2003), Neural Network methods (Yeung and Smith, 2005 and Lee *et al.*, 2005), empirical modes decomposition methods (Xu and Chen, 2004 and Li *et al.*, 2007), methods based on statistical information (Fugate *et al.*, 2001 and Zhang, 2007), among others.

The vibration-based damage detection is a topic in constant development and new and innovative methods are proposed all the time. In fact, an improvement of these discussed methods is needed to be functional for detecting small damage in all the possible conditions and structural configurations. The research work in this active area should be focused in the near future in the next activities (Yan *et al.*, 2007 and Doebling *et al.*, 1996):

1. Dynamic simulation of structural damage. Gathered information from dynamic tests performed in damage bridges is always insufficient and limited, time consuming and costly. More accurate numerical models of damaged bridges would help to verify the performance of damage detection methods under different scenarios.
2. Proposal of feature indices for detecting small structural damage from the vibration response of the bridge. These indices should not only detect, locate and evaluate the severity of the damage, but also identify the type of damage in the bridge.
3. Proposal of more accurate feature indexes independent of complex finite element models of the structure and/or requiring information related to its baseline conditions. Finite element models may introduce more uncertainty in the damage detection process. Moreover, baseline conditions of the structure are rarely available.
4. Evaluation of the effect of environmental conditions in the damage detection procedure. It is recognized that environmental conditions may hide damage present in the structure. Even when several sensors are available for measuring different environmental conditions, this gathered information is rarely included in the damage detection procedure.
5. Consideration of multiple disciplines for the development of the vibration-based damage detection methods. These disciplines can be sensor technology, mathematics, finite element modelling, optimisation techniques, and experimental modal analysis.

6. Optimisation of the position of sensors for damage detection. This topic has been developed mainly for the extraction of modal parameters of structures; its application to damage detection is still a topic to be developed.

7. Non-linear factors in structural damage detection. Most of the proposed damage detection methods consider that the structure behaves as linear after damage occurs. This assumption may not be valid in all the cases. Therefore, the research in this topic needs to be enhanced for being applied to complex structures like bridges.

8. Evaluate the most promising damage detection methods in real full scale structures. Only few cases of deliberately damage structures with the purpose of evaluating vibration-based damage detection methods have been carried out. It has been widely proved that such experiments, like those done in the I-40 and the Z24 bridges, have improved the advance in this topic.

All this review in the vibration-based damage detection methods leads to consider the overall process of damage detection a very complex issue. Much work has been done in this field; however there are still several problems that need to be addressed for the practical application of several of the discussed methods. For instance, the uncertainty introduced to the damage detection procedure caused by ambient factors.

2.4 General description of selected vibration-based damage detection methods

From the previous described vibration-based damage detection methods, ten of them were selected for a detailed evaluation of their applicability to bridge structures. These methods were selected because they do not require a mathematical model of the bridge in order to detect damage. Furthermore, some of these methods have already been applied to real-scale bridge dynamic data or dynamic simulations of bridge structures with good performance. Other methods, like wavelet based methods have shown promising characteristics for the detection of damage in other structures, and they can detect damage with only information of the damaged structure which can be considered an important advantage when the baseline conditions of many damage bridges is unknown. The selected damage detection methods are:

- **Comparison of several sets of mode shapes**: COMAC method;
- **Curvature methods**: mode shape curvature and Damage Index methods;
- **Change in structural properties**: change in flexibility matrix and change in stiffness matrix;
- **Wavelet analysis methods**: the CWT, the DWA, the WPS, the Hoelder exponent and the combined CWT-DI methods;
- In addition, **level I methods**, like MAC and frequency change methods were as well evaluated.

2.4.1 COMAC method

One of the simplest mode shape damage detection methods is the Co-ordinate Modal Assurance Criterion (COMAC) method. This method measures the correlation between several vectors. If the modal displacements at node *i* of sets of mode shapes are identical, the COMAC value is one for this node. In contrast, disturbance in the damaged mode shape location may give less than one COMAC values (Ndambi *et al.*, 2002). Its mathematical interpretation is given in Equation (2.44).

$$COMAC_j = \frac{\left[\sum_{i=1}^{N} \left|\psi_{ij}\psi_{ij}^*\right|\right]^2}{\sum_{i=1}^{N} \psi_{ij}^2 \sum_{i=1}^{N} \psi_{ij}^{*2}}, \tag{2.44}$$

where $\psi_{ij}$and ψ_{ij}^* are the non scale mode shapes for the *j*th node of the *i*th mode for the baseline and damaged condition, respectively.

In the COMAC method, an offset was introduced to the mode shapes for avoiding numerical errors when mode shapes are close to zero.

Previous evaluations of this method found out that COMAC values do not present enough variation to clearly detect damage for all the conditions. Furthermore, false damage location can appear in undamaged zones restricting the applicability of this method. Successful detection may be obtained with this method if severe damage is present in the bridge. (Salgado *et al.*, 2006; Carrión, 2002).

2.4.2 Curvature method

Some time ago, it was discovered that mode shape curvature is a good parameter for damage detection. This method, proposed for the first time by Pandey *et al.* (1991), is based on the fact that mode shape curvature is related to the bending stiffness of the structure as follows

$$\epsilon = \frac{d^2y}{dx^2} = \frac{d^2 \sum_{i=1}^{\infty} \psi_i}{dx^2} = \frac{M}{EI} \tag{2.45}$$

where ν is the mode shape curvature of the cross section, *M* the bending moment at the cross section, *E* the modulus of elasticity, *y* is the total deflection, *I* the moment of inertia at that section and $d^2 \sum_{i=1}^{\infty} \psi_i / dx^2$ the second derivative of the summation of the mode shapes with respect to the longitudinal distance, *x*.

In this way, if a crack appears, the bending stiffness of the beam (*EI*) will decrease causing an increment in the magnitude of the curvature.

This method has been tested on some bridges with good results (Farrar and Jauregui, 1996 and Abdel Wahab and De Roeck, 1999). The best performance of this method was obtained with severe damage and smooth mode shapes. Under these conditions, location of the damage is identified with a sharp peak. In this method, damage can be detected only with information of the damage mode shape. Better results can be obtained comparing two different structural conditions of the bridge. The main disadvantages of this method are related to the technique used for obtaining the second derivatives of the mode shapes. The central difference method is commonly used in these cases. With this technique, small irregularities in the mode shapes not related to damage are also magnified, contaminating the results with several peaks. Other methods for obtaining second derivates have been tried. However, none of them so far have solved this problem, Maeck, (2003).

2.4.3 Damage Index (DI) Method

This method proposed by Kim and Stubbs (1995) calculates the change in the strain energy stored in the beam when it deforms in a particular mode shape.

Considering an Euler-Bernoulli beam of length *L* in which only the flexural stiffness about the vertical axis is allowed, the strain energy of the beam for a mode shape ϕ_i can be expressed as:

$$U_i = \frac{1}{2}\int_0^L EI\,(x)\left(\frac{\partial^2\phi_i^2}{\partial x^2}\right)^2 dx \tag{2.46}$$

If the beam is divided in *NE* elements with *N* nodes, the contribution of the *j*th member to the *i*th modal strain energy is given by:

$$U_{ij} = \frac{1}{2}EI_j\int_a^b\left(\frac{\partial^2\phi_i^2}{\partial x^2}\right)^2 dx \tag{2.47}$$

where $[a, b]$ are the limits of the member *j* and EI_j is the *j*th member stiffness assumed as constant over the defined interval. The contribution of the *j*th member to the total strain energy of the ϕ_i mode can be expressed by:

$$F_{ij} = U_{ij}/U_i \tag{2.48}$$

Similar expressions can be deduced for a damaged case:

$$\begin{aligned} F_{ij}^* &= U_{ij}^*/U_i^*, & f_{ij}^* &= F_{ij} + \text{higher order terms} \\ U_i^* &= \frac{1}{2}\int_0^L EI^*\,(x)\left(\frac{\partial^2\phi_i^*}{\partial x^2}\right)^2 dx, & U_{ij}^* &= \frac{1}{2}EI_j^*\int_a^b\left(\frac{\partial^2\phi_i^*}{\partial x^2}\right)^2 dx \end{aligned} \tag{2.49}$$

where the asterisk denotes parameters determined from the damaged case. In presence of small damage, the higher order terms can be discarded leading to:

$$1 = \frac{F_{ij}^*}{F_{ij}} = \frac{U_{ij}^* U_i}{U_{ij} U_i^*} = \frac{EI_j^*\int_a^b\left(\partial^2\phi_i^*/\partial x^2\right)^2 dx}{EI_j\int_a^b\left(\partial^2\phi_i/\partial x^2\right)^2 dx}\,\frac{EI\int_0^L\left(\partial^2\phi_i/\partial x^2\right)^2 dx}{EI^*\int_0^L\left(\partial^2\phi_i^*/\partial x^2\right)^2 dx} \tag{2.50}$$

It was assumed in Equation (2.50) that the stiffness over the length of the beam was constant for the damaged and undamaged cases. Furthermore, if it is considered that damage will be located in small number of elements, the stiffness from the damaged case will not significantly change over the entire beam, *i.e.,* $EI \cong EI^*$ and Equation (2.50) becomes:

$$\frac{EI_j}{EI_j^*} = \frac{\int_a^b\left(\partial^2\phi_i^*/\partial x^2\right)^2 dx}{\int_0^L\left(\partial\phi_i/\partial x^2\right)^2 dx}\,\frac{\int_a^b\left(\partial^2\phi_i'\partial x^2\right)^2 dx}{\int_0^L\left(\partial\phi_i^*/\partial x^2\right)^2 dx} \tag{2.51}$$

To avoid numerical problems, resulting of dividing by very small numbers, the damage index, β_{ij} is defined giving an offset to Equation (2.51) as follows:

$$\beta_{ij} = \frac{\int_a^b \left(\partial^2 \phi_i^* / \partial x^2\right)^2 dx \int_0^L \left(\partial^2 \phi_i / \partial x^2\right)^2 dx + 1}{\int_a^b \left(\partial^2 \phi_i / \partial x^2\right)^2 dx \int_0^L \left(\partial^2 \phi_i^* / \partial x^2\right)^2 dx + 1} \tag{2.52}$$

The DI formulation for discrete structural elements can be expressed as:

$$\begin{aligned} \beta_{ij} &= \frac{\left(\epsilon_{i,j}^*\right)^2 + \sum_1^{N_t} \left(\epsilon_{i,j}^*\right)^2 \sum_1^{N_t} \left(\epsilon_{i,j}\right)^2}{\left(\epsilon_{i,j}\right)^2 + \sum_1^{N_t} \left(\epsilon_{i,j}\right)^2 \sum_1^{N_t} \left(\epsilon_{i,j}^*\right)^2}; \\ \epsilon_{i,j} &= \left[\frac{\partial^2 \phi_i}{\partial x^2}\right]_{x=x_j}, \quad \epsilon_{i,j}^* = \left[\frac{\partial^2 \phi_i^*}{\partial x^2}\right]_{x=x_j} \end{aligned} \tag{2.53}$$

where N_t is the total number of nodes in the beam and ϵ is the mode shape curvature.

The DI method performed very well in previous evaluations (Farrar and Jauregui, 1996 and Alvandi and Cremona, 2006). Nevertheless, its performance depends on the accuracy of the mode shape curvatures. Therefore, it suffers from the same problems as those discussed for the curvature method.

2.4.4 Flexibility change method

Pandey and Biswas (1994) proposed to detect damage from the changes of the flexibility matrix calculated using the modal parameters of the structure as follows:

$$\begin{aligned} \mathbf{C} &= \mathbf{\Phi \Omega^{-1} \Phi^T} = \sum_{i=1}^{N} \frac{1}{\omega_i^2} \phi_i \phi_i^T; \\ \mathbf{C}^* &= \mathbf{\Phi}^* \mathbf{\Omega}^{*^{-1}} \mathbf{\Phi}^{*^T} = \sum_{i=1}^{N} \frac{1}{\omega_i^{*^2}} \phi_i^* \phi_i^{*^T}, \end{aligned} \tag{2.54}$$

where $\mathbf{C}$ is the flexibility matrix of the structure, $\mathbf{\Phi} = [\phi_i, \phi_2, \ldots, \phi_N]$ is the mode shape matrix, $\mathbf{\Omega} = diag\left(\omega_i^2\right)$ is the modal stiffness matrix, ω_i is the *i*th circular frequency, ϕ_i is the *i*th mode shape and the asterisk superscript denotes damage parameter.

The change in the flexibility matrix of the structure is obtained by the differences calculated from the undamaged and damaged flexibility matrix,

$$\mathbf{\Delta C} = \mathbf{C}^* - \mathbf{C} \tag{2.55}$$

A more appropriate index parameter can be determined from the maximum absolute value of the elements in the *j*th column of $\mathbf{\Delta C}$ as given by:

$$\bar{\delta c_j} = max\left|\delta c_{ij}\right| \tag{2.56}$$

where δc_{ij} are the elements of $\mathbf{\Delta C}$ and represent the flexibility variation at each degree of freedom. The largest $\bar{\delta c_j}$ indicates the degree of freedom when the maximum variation of flexibility has occurred that indicates the location of damage.

In the application of the Flexibility Change method, it was assumed that units, for vertical and transversal DOFs considered here, were m/kN.

In the application of this method to numerical and real cases, the largest value of $\bar{\delta_j}$ may not coincide with the location of damage (Pandey and Biswas, 1994). Moreover, extended damage is difficult to locate with this method and mass-normalized mode shapes are recommended for a better performance of the method. On the other hand, as shown in further chapters, the flexibility change method has low sensitivity to noise present in the modal parameters.

2.4.5 Stiffness change method

Zimmerman and Kaouk (1994) developed a damage detection methods based on the changes of the stiffness matrix of a structure. The proposed index parameter is deduced from the eigenvalue problem of an undamaged and undamped structure:

$$\left(-\mathbf{\Omega M} + \mathbf{K}\right)\mathbf{\Phi} = \mathbf{0} \tag{2.57}$$

where **M** and **K** are the mass and stiffness matrices of the undamaged structure.

Let $\mathbf{\Delta M}$ and $\mathbf{\Delta K}$ be the perturbations to the original mass and stiffness matrices, respectively, the eigenvalue problem of a damaged and undamped structure can be given by:

$$\left[-\mathbf{\Omega}^*\left(\mathbf{M} - \mathbf{\Delta M}\right) + \left(\mathbf{K} - \mathbf{\Delta K}\right)\right]\mathbf{\Phi}^* = 0 \tag{2.58}$$

where the asterisk denotes parameters from the damaged structure. Separating the perturbations and the original parameters, the index parameter D_i is defined as:

$$D_i = \left(\omega_i^{2^*}\mathbf{M} + \mathbf{K}\right)\phi_i^* = \left(\omega_i^{2^*}\mathbf{\Delta M} + \mathbf{\Delta K}\right)\phi_i^* \tag{2.59}$$

In bridge structures, damage frequently does not cause a significant change of their mass. Hence, without loss of accuracy the mass perturbation DM is neglected leading to:

$$D_i = \mathbf{\Delta K}\phi_i^* \tag{2.60}$$

The stiffness matrix of the undamaged and damaged structure can be obtained from its modal parameters in a similar way that was done for the flexibility matrix:

$$\begin{aligned} \mathbf{K} &= \mathbf{\Phi\Omega\Phi^T} = \sum_{i=1}^{N} \omega_i^2 \phi_i \phi_i^T; \\ \mathbf{K}^* &= \mathbf{\Phi}^*\mathbf{\Omega}^*\mathbf{\Phi}^{*\mathbf{T}} = \sum_{i=1}^{N} \omega_i^{*^2} \phi_i^* \phi_i^{*^T}; \\ \mathbf{\Delta K} &= \mathbf{K}^* - \mathbf{K} \end{aligned} \tag{2.61}$$

In the application of the Stiffness Change method, it was implicit assumed that units, for vertical and transversal DOFs, were kN/m.

The stiffness change method as well as the flexibility change method requires for a better performance, mass normalized mode shapes. Moreover, the accuracy of the calculation of the stiffness matrix increases when more modes are included in the analysis.

2.4.6 Wavelet analysis methods

The description of the wavelet analysis methods was already discussed in the section 2.2. Here, two variants of the wavelet based methods, namely the WPS and the combined CWT-DI methods will be discussed.

2.4.7 Wavelet Packet Signature (WPS) method

This method proposed by Chang and Sun (2005) calculates the operating energy shape of the analyzed structure. The method is based on The Wavelet Packet Transform (WPT). The energy of the dynamic response at measured points is obtained and normalized as follows:

$$
\begin{aligned}
E_j^i(n) &= -\sum_t f_j^i(t)^2 \log\left[f_j^i(t)\right], \\
E_f(n) &= -\sum_t f(t)^2 \log\left[f(t)\right] = \sum_{i=1}^{2j} E_j^i, \\
WPS_j^i(n) &= \frac{E_j^i(n)}{\max\left(E_j^i\right)}
\end{aligned}
\tag{2.62}
$$

where $f_j^i(t)$ is the linear combination of wavelet packet functions $\theta_{j,k}^i$ calculated according to Equation (2.28); E_f and $E_j^i(n)$ are the energies of the original function and decomposed functions $f_j^i(t)$ at measuring point *n*, respectively, $WPS_j^i(n)$ is the normalized WPS energy coefficients. For calculating the energy of the decomposed functions, the Shannon method was used in this thesis (Coifman and Wickerhauser, 1992).

The WPS method has been proved to be more tolerant to noise than the previous Wavelet Analysis methods. However, the procedure for calculating the WPT demands important computational effort at high levels of decomposition where energy WPS components are more sensitive to damage.

2.4.7.1 CWT-DI method

The Damage Index (DI) method proposed by Kim and Stubbs (1995) calculates the modal energy stored in the beam using the curvatures of the mode shapes. As explained in the wavelet theory, the CWT can be considered an equivalent function of the second derivative of the analyzed function smoothed with the mother wavelet. Taking advantages of this property of the CWT, a new variant of the DI method can be determined as follows:

$$
\begin{aligned}
(CWT-DI)_{ij} &= \frac{\int_a^b \left(CWT_\psi^{\phi_i^*}\right)^2 dx \int_0^L \left(CWT_\psi^{\phi_i}\right)^2 dx + 1}{\int_a^b \left(CWT_{\psi_i}^{\phi_i}\right)^2 dx \int_0^L \left(CWT_\psi^{\phi_i^*}\right)^2 dx + 1} \\
CWT &= CWT(a=s,x) \text{ and s=finest scales}
\end{aligned}
\tag{2.63}
$$

For a discrete evaluation of the CWT-DI method, it is more appropriate the next expression:

$$(CWT-DI)_{ij}=\frac{\left(CWT_{\psi,j}^{\phi_i^*}\right)^2+\sum_1^N\left(CWT_{\psi,j}^{\phi_i^*}\right)^2\sum_1^N\left(CWT_{\psi,j}^{\phi_i}\right)^2}{\left(CWT_{\psi,j}^{\phi_i}\right)^2+\sum_1^N\left(CWT_{\psi,j}^{\phi_i}\right)^2\sum_1^N\left(CWT_{\psi,j}^{\phi_i^*}\right)^2} \tag{2.64}$$

where the subscript *j* is the CWT coefficient at the *j*th node for the *s* scale.

The performance of this method seems to be influenced by the type of mother wavelet used.

2.4.8 Level I methods

2.4.8.1 MAC method

One of the most well-known methods to determine the correlation between two set of vectors is the Modal Assurance Criterion (MAC) method. This method determines the projection of one vector onto another in such way that both vectors are the same when MAC achieved a value equal to one while a MAC value close to zero indicates that both vectors are uncorrelated. The MAC method between two modal vectors is defined as (Allemang, 2003):

$$MAC\left(\phi_i,\phi_i^*\right)=\frac{\left|\phi_i^T\phi_i^*\right|^2}{\left(\phi_i^T\phi_i\right)\left(\phi_i^{*T}\phi_i^*\right)} \tag{2.65}$$

where ϕ_i and ϕ_i^* are the *i*th mode shape for the undamaged and damaged conditions, respectively, and the superscript *T* denotes transpose of the vector.

The MAC procedure averages the differences over all the involved nodes. Hence, damage that caused changes in few nodes of the mode shapes may not cause MAC values significantly different than one.

A variant of the MAC method is the Normalized Modal Difference (NMD). This method is related to MAC method as follows:

$$NMD\left(\phi_i,\phi_i^*\right)=\sqrt{\frac{1-MAC\left(\phi_i\phi_j^*\right)}{MAC\left(\phi_i\phi_i^*\right)}} \tag{2.66}$$

NMD is more sensitive than MAC method particularly for values near one commonly found for the comparison between undamaged and damaged modes.

2.4.8.2 Frequency change method

Long ago, it was known that damage affects the modal parameters of structures. For instance, damage which causes a loss of stiffness will increase the natural frequencies of the structure. Therefore, a measure of the frequency change can indicate if the structure is damaged or not. The frequency change method is given here as the rate of undamaged and damaged natural frequencies.

To know how a local change in stiffness can affect the modal parameters, a sensitivity analysis was carried out. For instance, the sensitivity of the resonant frequencies in a linear undamped dynamic system with multiple degrees of freedoms can be determined as (Zhao and Dewolf, 1999):

$$\frac{\partial \omega_r}{\partial k_{ij}} = \begin{cases} \frac{1}{\omega_r}\phi_{ir}\phi_{jr} & \text{for i} \neq \text{j} \\ \frac{1}{2\omega_r}\phi_{ir}^2 & \text{for i}= \text{j} \end{cases} \tag{2.67}$$

where ω_r is the natural frequency of the *r*th mode shape; k_{ij} is the element stiffness matrix located in the *i*th row and *j*th column and ϕ_{ir} is the amplitude of the normalized mode shape in the *i*th location and the *r*th mode.

In Equation (2.67) is evident that the frequency sensitivity to change of stiffness is inversely proportional to the same frequency. Stiff bridges with high frequencies are less sensitive to damage than flexible bridges with low frequencies. On the other hand, frequency sensitivity is proportional to the amplitude of the normalized mode shape. This implies that sensitivity is highly dependent of the damage location. Damage located near to supports, piers, bears and near to any node point have low frequency sensitivity. In fact, even when severe damage is present in the bridge, the frequency change hardly achieves 5%. Moreover, ambient factors can have an influence in the natural frequencies of the same magnitude as damage caused. For this reasons, vibration-based damage detection methods using just the comparison of resonant frequencies were not as successful as expected. In this study, the frequency change method is used in combination with two or more damage detection methods. A review of frequency change methods can be found in Salawu (1997).

3

Dynamic simulation methods

3.1 State of the art

It is a known fact that cracks in structures cause changes in their modal parameters. Based on this fact, the recent past has witnessed the development of several methods to detect, locate and quantify the extent of damage in existing structures. However, these methods are not fully developed up to now and a reliable damage detection method applied to all structural conditions does not exist. For this sake it is thought that the vibration analysis of cracked beam structures can help in the development and validation of these methods.

The presence of a crack in a structural element provokes a local flexibility change near the crack tip. The introduction of damage in structural elements has been traditionally effectuated by means of ad hoc mathematical models at the location of damage. Up till now, several models based on this principle have been proposed.

One procedure for obtaining the dynamic response of beams with open transversal cracks consists in dividing the beam into several elements separated from each other by a crack represented by a rotational spring without mass (referred here as local flexibility method). Based on this procedure, Rizos *et al.* (1990) determined in a cantilever beam with a crack located at an arbitrary location, the local flexibility introduced by a crack using the fracture mechanics theory. The three first mode shapes and frequencies of the numerical model of a cantilever beam were compared with those obtained from beam specimens with fatigue cracks. Agreement of the modal parameters was evident, especially for the first two mode shapes and frequencies. Bamnios and Trochides (1995) determined the dynamic behaviour of a cantilever beam with a single crack at an arbitrary location. The prediction of the frequency decay caused by cracks with different depths was in agreement with measurements taken from experiments where cracks were represented by sawing cuts. Fernández-Sáez and Navarro (2002) proposed closed-form expressions (lower bounds) for the approximated values of the fundamental frequency of cracked beams in bending vibration. A comparison of the variation of the fundamental frequency of a beam with various boundary conditions and crack depths, determined with this procedure and obtained by numerical simulations using a refined finite element model, were done. An inspection of this comparison showed that the second lower bound is a good approximation to the fundamental frequencies obtained with the finite element model, taken as a reference.

Other local flexibility methods applied to beams with open vertical cracks have been proposed by many authors, *e.g.,* Chondros and Dimarogonas (1980) modelled a welded joint as cantilever beam with lumped mass at the free end and rotational spring represented the crack at the root; Lin (2004) obtained the dynamic behaviour of a simply supported beam with a single and double sided crack using the Timoshenko beam and Fracture Mechanics Theory; and Shifrin and Ruotolo (1999) who developed a local flexibility method to be explained in section 3.2.2.

Other solution to determine the dynamic behaviour of beams with open vertical cracks was proposed by Christides and Barr (1984), who developed the cracked Euler-Bernoulli beam theory from the Hu-Washizu variational principle. They derived the differential equation of equilibrium and the associated boundary conditions for a uniform Euler-Bernoulli beam with one or more pairs of symmetric cracks (double sided cracks). The modification of the stress field caused by the crack was considered by a local experimental function that includes a parameter that have to be evaluated by experiments. This theory was considered an important step in the development of more rigorous cracked beam vibration theories. In this context, Chondros *et al.* (1997), Chondros *et al.* (1998) and Chondros and Dimarogonas (1998) proposed a more consistent method based on the Christides and Barr theory. In these works, the function representing the modification of the stress field was obtained based on well-established Fracture Mechanics Theory. The first natural frequency of a bar (cantilever with longitudinal vibration, cantilever with lateral vibration and simply supported with lateral vibration) with a single crack at mid-span was calculated for different crack depth ratios using the proposed (continuous) method, a local flexibility solution proposed by the same authors, and the Christides and Barr method. These numerical frequencies were compared with those determined from experiments done in aluminium cracked beams. The numerical frequencies determined with the continuous cracked beam model fell closer than the remaining two compared methods.

SaMartín *et al.* (2004) proposed a variant of the Christides and Barr method for a one-sided crack beams using the Hu-Washizu variational principle and the Navier-Bernoulli beam theory. In this method, the crack function, which determines the change of the stress field caused by the crack, was proposed in the similar form as done by Christides and Barr, but at that time, the change of gravity centre due to the crack was considered. Furthermore, this method takes into account the difference in behaviour caused between upper and bottom sided cracks.

A simplified procedure of the Christides and Barr method was proposed by Sinha *et al.* (2002). This method considers that the local flexibility in the vicinity of the crack determines with the Christides and Barr method can be approximated with a triangular reduction function. Afterwards, the stiffness matrix of the element of the beam with the crack is obtained considering the triangular variation of the flexural stiffness. The authors determined that the effective length of the flexibility reduction is 1.5 times the total depth of the beam. For slender beams, as usually considered in bridge structures, this method leads to a long discrete crack element, *i.e.,* the crack element must be, at least as long as the effective length of the flexibility reduction. This effect may lead to a large element in the crack location which does not allow having valuable information related to the mode shapes and their derivatives near the crack. Therefore, this method is more suitable for shallow cross sections.

Other solutions for the dynamic behaviour of beams with open vertical cracks have been based on the finite element method. Calculating the stiffness matrix for the cracked elements has been the main objective of the methods using the finite element model, *e.g.,* Zheng and Kessissoglou (2004) proposed a method based on the calculation of the flexibility matrix of a cracked element.

Even when it has been recognized that cracks do not remain always open, the dynamic behaviour of beams with cracks that open and close, referred as breathing cracks, has not been extensively studied. If the static deflection due to some component loading (like self-weight or dead loads) is larger than the vibration amplitudes, then the crack remains open all the time, or opens and closes regularly and the problem is linear. If the static deflection is small compared with the vibration amplitude, the crack will open and close in time and the problem is non-linear.

A formulation for calculating the dynamic response of beams with breathing cracks was proposed by Shen and Chu (1992). This method introduced a contact parameter γ_{cr} into the assumed stress, strain and displacement expressions of the cracked beam theory proposed by Shen and Pierre (1990). When the crack faces are open and under tension, $\gamma_{cr} = 1$, and a cracked function is introduced in the stress and strain expressions. Besides the crack function, the cracked beam theory proposed by Shen and Pierre (1990) includes another function $\zeta(x, z)$ to model the modification of the displacement field due to the crack. On the other hand, when the crack faces are closed and under compression, $\gamma_{cr} = 0$, and the introduced functions vanish, leading to the classical Euler-Bernoulli beam. Regarding the cracked beam

theory proposed by Shen and Pierre, Carneiro and Inman (2001) proposed a modification to their formulation in order to avoid yielding complex eigenvalues and eigenvectors, inconsistent with the physical solution of the problem. Moreover, they determined that the function $\zeta(x,z)$ can be omitted from the proposed model without diminishing the numerical accuracy.

Chondros *et al.* (2001) proposed a method for calculating the dynamic behaviour of beams with breathing cracks using a bi-linear type model where cracks have only two states, either fully open or fully closed. In this method, the frequency of the crack does not depend on amplitude. It was assumed that crack transits from open to closed at times when the beam comes back to its undeformed shape. According to the authors, the ratio between the frequency of the breathing crack ω_b and the closed crack ω_1 may be given by:

$$\frac{\omega_b}{\omega_1} = 2\frac{\omega_1^*/\omega_1}{1+\omega_1^*/\omega_1} \tag{3.1}$$

where ω_1^* is the circular frequency obtained from the open crack model.

The decay of the first natural frequency caused by a crack at mid-span with different depths was obtained for a simply supported beam using the breathing crack and open crack methods proposed by the authors and experimental results. The comparison of the numerical and experimental results indicated closer agreement between the experimental results and the breathing crack model than with the numerical solution obtained with the open crack model. It is important to highlight that the breathing crack solution results in a smaller frequency decay than the open crack model predicts. This finding can also be determined from Equation (3.1) where the ratio ω_b/ω_1 is always bigger than $\omega_1^*/\omega_1 \in [0,1)$. A more detailed description of the methods for obtaining the vibration of cracked beams may be found in Dimarogonas (1996).

From the vast number of publications done in this field, it is important to point out, according to Dimarogonas (1996), that there is confusion in the literature in discerning between a notch and a crack. Several authors have treated a crack as a notch, numerically, experimentally or both. Due to fatigue cracks in structures are experimentally difficult to obtain with the assumption done in the numerical models (single, open, perpendicular, across the width, etc), many authors have tried to represent them as notches. Nevertheless, it must be understood that no matter how

thin a saw cut is, it will never behave as a crack. According to Silva and Gómez (1990), cracks of small depth result in about twice the change in natural frequencies caused by notch of the same depth. For higher depths (more than half of the total depth) the change in natural frequencies between a crack and a notch is about the same.

In the literature related to the dynamic behaviour of cracked beam structures, there are some unanswered questions that can be considered topics of interest for further research (Dimarogonas, 1996):

- Development of a rigorous cracked beam vibration theory,
- Dynamic behaviour of breathing cracks,
- The evaluation of crack beam methods under the same case study,
- Determination of the damping change due to cracking.

In this thesis, three methods for the dynamic simulation of cracked beam structures were selected, compared and evaluated. These methods were: i) Modified Christides and Barr method based on the Hu-Washizu variational principle; ii) Shifrin and Ruotolo method based on the use of rotational massless springs to represent cracks; iii) Zheng and Kessissoglou method based on the finite element model.

3.2 Dynamic simulation methods

All three considered methods were evaluated by introducing open vertical cracks with uniform depth across the width of the beam. During the analyses, three Degrees Of Freedom (DOFs) were considered for each node (see Figure 3.3) assuming that the introduced cracks did not modify considerably the initial mass of the element.

3.2.1 Modified Christides and Barr method

This approach, based on the Christides and Barr theory, calculates the flexibility along the structural element, according to a procedure proposed here, for its straightforward implementation in a computer program.

Christides and Barr (1984) developed a cracked Euler-Bernoulli theory by deriving the differential equation and boundary conditions for a uniform Euler-Bernoulli beam with one or more pairs of symmetric cracks. The problem was

reduced to one dimension integrating over the cross section after certain stress, strain, displacement and momentum fields of interest were selected. According to the authors, in many cases where analytical solutions related to St. Venant´s Principle are known the decay rates are found to be exponential. In a similar way, they proposed a local empirical function which assumed an exponential decay with the distance from the crack for the modification of the stress field induced by the crack. Application of the proposed procedure to the extended Hu-Washizu variational principle led to the following equation of motion for the cracked Euler-Bernoulli beam:

$$\begin{aligned} &E\left(I-N\right)Qw^{iv}+2E\left[Q'\left(I-N\right)-N'Q\right]w''' \\ &+E\left[Q''\left(I-N\right)-2K'Q'-N'\right]w''+\rho A\ddot{w}=0 \end{aligned} \tag{3.2}$$

where *E* is the Young's modulus of the beam, ρ the mass density of the beam, w is the harmonic transversal oscillation of the beam and A is the cross sectional area. Differentiation with respect to time is shown by a dot while commas in the subscripts indicate differentiation with respect to the longitudinal coordinate, x. The other variables are defined as:

$$\begin{aligned} &I=\int_A f^2\left(x\right)dA, \qquad N=\int_A zf\left(x\right)dA, \qquad R=\int_A f^2\left(x\right)dA, \\ &Q\left(x\right)=\frac{I-N}{I-2N+R}, \\ &f\left(x,z\right)=\left[z-m_I zH\left(h-\left|z\right|\right)\right]\exp\left(-\alpha_{cr}\left|x-x_j\right|/h\right), \quad m_I=I/I_c \end{aligned} \tag{3.3}$$

where A_c is the cross sectional area at the crack location, $f\left(x,z\right)$ is the crack function, and $H\left(h-\left|z\right|\right)$ is a unit step function at $z=h$. Equation (3.2) can be expressed in a more convenient way as follows:

$$\left[E\left(I-N\right)Qw''\right]''+\rho A\ddot{w}=0 \tag{3.4}$$

Equation (3.4) can be solved for different boundary conditions, for instance in the case of a simply supported beam with rectangular cross section (*b* x *h*) and symmetric pair of cracks (of depth *a*), Equation (3.4) takes the following form:

$$\begin{aligned} &\left[EIQw''\right]''+\rho A\ddot{w}=0 \\ &Q=\frac{1}{1+C_{cr}\exp\left(-2\alpha_{cr}\left|x-x_j\right|/h\right)}, \quad C_{cr}=m_I-1 \end{aligned} \tag{3.5}$$

where x_j determines the location of the crack and x is the coordinate where the mode shape of the beam is determined.

This procedure requires that the decay rate exponent α_{cr} must be determined experimentally for every different geometry and boundary condition, although the stress exponent has been reported not to change very much (Chondros *et al.*, 1998).

Christides and Barr (1984) determined the decay rate exponent to be equal to 0.67 for a simply supported beam with a pair of surface cracks located at mid-span. However, this value was obtained from a specimen where the crack was simulated as a notch. According to Dimarogonas (1996) there is a difference between the flexibility of a beam with a crack and with a notch. A thin cut results in a local flexibility substantially less than the local flexibility associated with a fatigue crack. The procedure proposed by Christides and Barr considered a pair of symmetric cracks, while in bridge structures, which are the elements to be analyzed, damage is commonly characterized by one sided surface cracks. The deficiencies of this method can be compensated with the determination of α_{cr} from experimental tests carried out on specimens with real one sided fatigue cracks.

In this context, Chondros *et al.* (1998) reported the first natural frequency of a simply supported cracked aluminium beam of length 0.235 m, cross section width 0.006 m and height 0.0254 m with a Young's modulus equal to 7.2x10^7 kN/m^2 and material density equal to 2.8 t/m^3. In this way, the value of the decay rate exponent that best fit these experimental results is 2.267. The comparison between the first natural frequency reduction of the experimental and numerical cases *versus* the crack depth ratio (*a/h*) is shown in Figure 3.1.

From Equation (3.5), when no cracks are considered $I_c = I \because C_{cr} = 0$ and $Q = 1$, substituting these values in Equation (3.5) gives:

$$EIw^{iv} + \rho A\ddot{w} = 0 \tag{3.6}$$

By comparing Equations (3.5) and (3.6) it is realized that the behaviour of the cracked beam at a specific location is similar to the behaviour of an uncracked beam of longitudinally variable flexural bending stiffness. The local effect of the cracks over the flexural bending stiffness, EI, can be given, according to Equation (3.5), in the following form:

$$EI\left(x\right)=\frac{EI}{1+C_{cr}\exp\left(-2\alpha_{cr}\left|x-x_{j}\right|/h\right)} \tag{3.7}$$

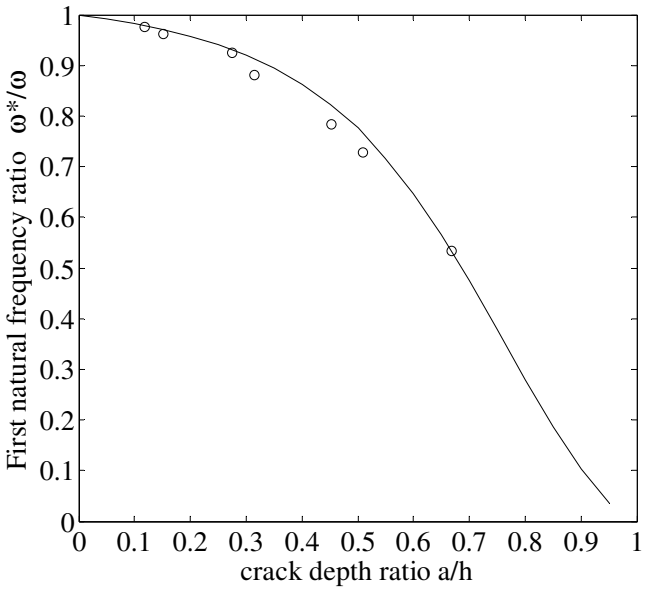

Figure 3.1. First natural frequency ratio for a simply supported beam with a surface crack at mid-span *versus* the crack depth ratio *a/h*. Keys: — numerical results determined with the modified Christides and Barr method using α_{cr}=2.267; ◦ experimental results (Chondros *et al.*, 1998).

As a simplification, a linear variation of flexural bending stiffness along the elements was proposed here as indicated in Figure 3.2. Under each condition, the stiffness matrix of each Euler-Bernoulli element found using the finite element model may be expressed as:

$$\mathbf{K_{e,i}}=\frac{EI_{1}}{L_{e}^{3}}\begin{bmatrix}12 & 6L_{e} & -12 & 6L_{e}\\ & 4L_{e}^{2} & -6L_{e}^{2} & 2L_{e}^{2}\\ & & 12 & -6L_{e}\\ \text{symmetrical} & & & 4L_{e}^{2}\end{bmatrix}+\frac{Eg_{m}}{L_{e}^{3}}\begin{bmatrix}6 & 2L_{e} & -6 & 4L_{e}\\ & L_{e}^{2} & -2L_{e} & L_{e}^{2}\\ & & 6 & -4L_{e}\\ \text{symmetrical} & & & 3L_{e}^{2}\end{bmatrix} \tag{3.8}$$

where EI_1 is the flexural bending stiffness evaluated with Equation (3.7) in the first node of the element; L_e is the length of the element; *i* is the element to be evaluated and g_m is the difference between the flexural bending stiffness of the first and second node of the element.

In principle, the flexibility variation caused by cracks is very local and they do not have a significant influence in the flexibility of locations out of the vicinity of the cracks. Therefore, several cracks can be taken into account in the modified Christides

and Barr method calculating the minimum value of the flexibilities at each location along the beam.

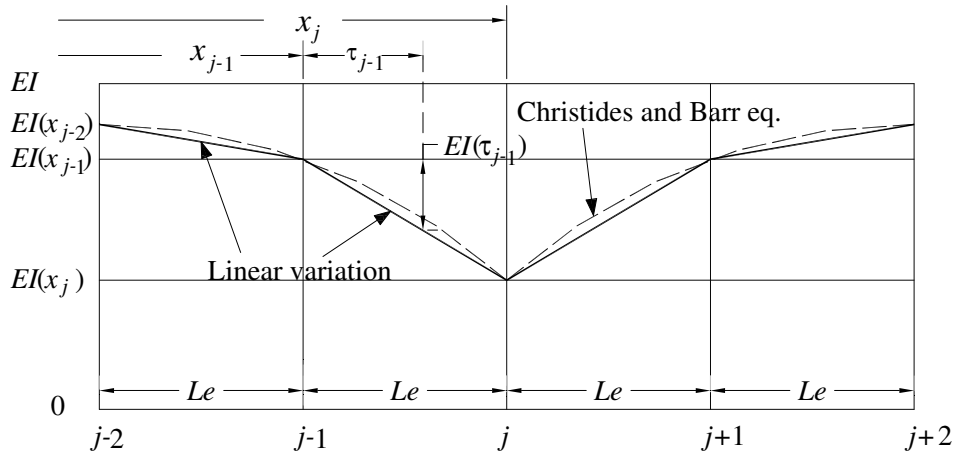

Figure 3.2. Variation of the flexibility of a beam caused by a crack located at x_j; ——proposed linear variation and - - - Christides and Barr Equation (3.7).

The global stiffness matrix of the beam $\mathbf{K}$ was formed by assembling the individual stiffness matrices of the elements $\mathbf{K}_{\mathbf{e,i}}$. Mode shapes and their corresponding natural frequencies were obtained from the solution of the eigenvalue problem for the undamped dynamic system in free vibration. It is evident from Figure 3.2 that the assumption of linear variation of the flexibility of the beam can be considered valid when a sufficient number of finite elements is considered in the vicinity of the crack.

3.2.2 Shifrin and Ruotolo method

In this method, the natural frequencies and corresponding mode shapes are obtained using massless rotational springs to simulate the presence of cracks. The method leads to a system of $(n+2)$ linear equations for a beam with *n* cracks with a determinant order smaller than those of other similar methods. As a result, the computational effort required for finding the natural frequencies is reduced considerably.

In this approach the beam is divided into $(n+1)$ beams connected by massless springs representing the *n* cracks. For a uniform cross section of the beam, the equation of harmonic transverse oscillations of each sub-beam can be represented by:

$$EIy_j^{iv}(x) - \omega^2 \rho A y_j(x) \quad j = 1, \ldots, n+1, \quad x_{j-1} < x < x_j \tag{3.9}$$

where ω is a natural circular frequency.

This method calculates the natural frequencies introducing between two elements conditions for displacement, bending moment and shear forces. The discontinuities in the rotation of the beam axis at the locations of the cracks are also taken into account. This condition is necessary for guarantying the equilibrium between transmitting bending moment and rotation of the spring simulating the crack.

$$\begin{aligned} y_j(x_j) &= y_{j+1}(x_j), \\ y_j''(x_j) &= y_{j+1}''(x_j), \\ y_j'''(x_j) &= y_{j+1}'''(x_j), \\ y_{j+1}'(x_j) - y_j'(x_j) &= \Delta_j = c_j y_j''(x_j) \quad j = 1, 2, \ldots, n \end{aligned} \tag{3.10}$$

where c_j are the flexibilities of the rotational springs. According to Rizos *et al.* (1990), for one sided cracks, these flexibilities can be expressed as:

$$\begin{aligned} c_j &= 5.436\, h f_{cr}(\delta_j), \\ f_{cr}(\delta_j) &= 1.86\delta_j^2 - 3.95\delta_j^3 + 16.38\delta_j^4 - 37.23\delta_j^5 + 76.81\delta_j^6 - 126.90\delta_j^7 \\ &\quad + 172.00\delta_j^8 - 143.94\delta_j^9 + 66.56\delta_j^{10} \end{aligned} \tag{3.11}$$

Considering these assumptions, the solution to the problem is obtained from Equations (3.12) to (3.14):

$$y(x) = y_o(x) + \sum_{j=1}^{n} \frac{\Delta_j}{2} |x - x_j| \tag{3.12}$$

$$\begin{aligned} y_o(x) =& B_1^* \cos(\lambda x) + B_2 \sin(\lambda x) + B_3 \cosh(\lambda x) + B_4 \sinh(\lambda x) \\ &+ \frac{\lambda}{4} \sum_{j=1}^{n} \Delta_j \int_0^x (\sinh(\lambda(x-s)) - \sin(\lambda(x-s))) |s - x_j| \, ds \end{aligned} \tag{3.13}$$

$$\begin{aligned} \Delta_i =& - B_1^* c_i \lambda^2 \cos(\lambda x_i) - B_2 c_i \lambda^2 \sin(\lambda x_i) + B_3 c_i \lambda^2 \cosh(\lambda x_i) \\ &+ B_4 c_i \lambda^2 \sinh(\lambda x_i) + \frac{c_i \lambda^3}{4} \sum_{j=1}^{n} \Delta_j M_{ij} \qquad i, j = 1, 2, \ldots, n \end{aligned} \tag{3.14}$$

where B_1 to B_4 are unknown coefficients; *n* is the number of cracks; x is the distance measured from the left end of the beam; y is the displacement amplitude of

the beam at position x; and y' and y'' denote first and second derivative of y with respect to the distance x, respectively. The other variables are defined as:

$$\lambda^4 = \omega^2 \rho A / (EI) \tag{3.15}$$

$$M_{ij}(\lambda) = \int_0^{x_i} (\sinh(\lambda(x_i - v)) + \sin(\lambda(x_i - v))) |v - x_j| \, dv \tag{3.16}$$

where ω is the circular frequency; *A* is the cross sectional area and v is a transformation variable.

The solution of the linear system of *n+4* equations given by Equation (3.14) for B_1 to B_4 and Δ_j needs the introduction of four more equations, which are obtained from the boundary conditions of the analyzed beams, Equation (3.12) for $y_0(x = 0, L)$ and its second derivative $y_0''(x = 0, L)$ in the case of simply supported beam; and $y_0(x = 0, L)$ and its first derivative $y_0''(x = 0, L)$ in the case of doubly clamped beam. Finally, the natural frequencies of the cracked beam are calculated from the roots of the polynomial (λ_1,…modes) result of the determinant of the linear system of equations **U** [four equations from Equation (3.12) plus *n* equations from Equation (3.14)] equal to nil, *i.e.*,:

$$det([U(\lambda)]) = 0 \tag{3.17}$$

where the matrix $\mathbf{U}(\lambda)$ can be expressed as follows:

$$\mathbf{U}(\lambda) = \begin{bmatrix} U_{1,1}(\lambda) & U_{1,2}(\lambda) & U_{1,j+2}(\lambda) \\ U_{2,1}(\lambda) & U_{2,2}(\lambda) & U_{2,j+2}(\lambda) \\ U_{i+2,1}(\lambda) & U_{i+2,2}(\lambda) & U_{i+2,j+2}(\lambda) \end{bmatrix} \tag{3.18}$$

The mathematical solution for a clamped-free beam was obtained by Shifrin and Ruotolo (1999). Solutions for simply supported, free-free, doubly clamped and clamped-hinged boundary conditions were obtained in this thesis and they are shown together with the clamped-free solution in the Appendix B.

3.2.3 Zheng and Kessissoglou method

Zheng and Kessissoglou (2004) proposed a finite element method to calculate the dynamic behaviour of cracked structures. In this procedure they incorporated the effect of the distance between the right hand side end node of the element and the crack location. This effect had been neglected in previous methods based on the

finite element method leading to less accurate results. This method overcomes this problem by adding an overall flexibility matrix $\mathbf{C_{ovl}}$ to the undamaged flexibility matrix $\mathbf{C}$ as indicated in Equation (3.19):

$$\mathbf{C_{tot}} = \mathbf{C} + \mathbf{C_{ovl}} = \begin{bmatrix} \frac{L_e}{EA} + c_{11} & -c_{12} & -c_{13} \\ -c_{21} & \frac{L_e^3}{3EI} + c_{22} & \frac{L_e^2}{2EI} + c_{23} \\ -c_{31} & \frac{L_e^2}{2EI} + c_{32} & \frac{L_e}{EI} + c_{33} \end{bmatrix} \tag{3.19}$$

The elements of the overall flexibility matrix c_{ij} are calculated from:

$$c_{ij} = \int_{A_c} \frac{\partial^2 \mathcal{G}}{\partial P_i P_j} dA; \quad \text{i,j=1,2,3.} \tag{3.20}$$

$$\mathcal{G} = \frac{1}{E} \left[\left(K_{I1} + K_{I2} + K_{I3} \right)^2 + K_{II2}^2 \right] \tag{3.21}$$

where K_{I1}, K_{I2}, K_{I3} and K_{II2} are the Stress Intensity Factors (SIFs) of the uniform cross section of the beam for the I and II fundamental modes of fracture caused by the forces P_1, P_2 and P_3; A_c is the section area in the location of the crack, and P_i and P_j are the forces on the right side of the cracked element as shown in Figure 3.3.

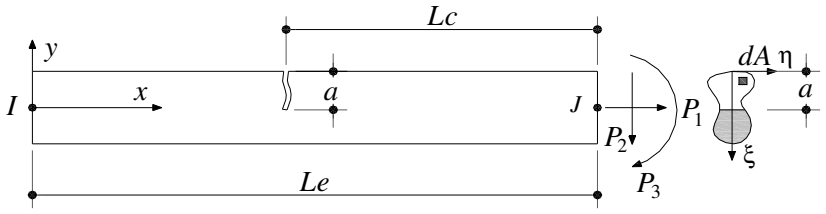

Figure 3.3. Cracked element and adopting forces for the Zheng method.

The SIFs required for this method can be determined for several shapes of cross sections using the method proposed by Ricci and Viola (2006). This procedure determines the SIFs based on the connections between the energy released upon extension of the crack by Δ_a and the release upon widening of the crack by Δ_w (Kienzler and Herrmann 1986),

$$-t_h \mathcal{G} = \frac{\partial U}{\partial a} = 2\beta_s \frac{\partial U}{\partial w} \tag{3.22}$$

where t_h is the thickness of the beam at the crack location. To determine the SIFs it is necessary to calculate $\partial U / \partial w$ and to estimate the non-dimensional parameter β_s.

Kienzler and Herrmann (1986) showed that the corresponding change in energy of the beam can be calculated by:

$$\frac{\partial U}{\partial w} = \begin{cases} -\dfrac{P_1^2}{2EA}\left(\dfrac{A}{A_c}-1\right) & \text{for axial force} \\ -\chi\dfrac{P_2^2}{2GA}\left(\dfrac{A}{A_c}-1\right) & \text{for shear force} \\ -\dfrac{P_3^2}{2EI}\left(\dfrac{I}{I_c}-1\right) & \text{for bending moment} \end{cases} \tag{3.23}$$

where *G* is the shear modulus, and χ is the shearing factor.

Substituting Equations (3.23) and (3.21) into to Equation (3.22) the SIFs are determined as follows:

$$K_{I1} = P_1\sqrt{\frac{\beta_{sP_1}}{bA}\left(\frac{A}{A_c}-1\right)}, \qquad \beta_{sP_1} = \beta_s\frac{H^*}{E} \tag{3.24}$$

$$K_{I2} = P_2\sqrt{\frac{\beta_{sP_2}}{bI}\left(\frac{I}{I_c}-1\right)}, \qquad \beta_{sP_2} = \beta_s\frac{H^*}{E} \tag{3.25}$$

$$K_{I3} = P_3\sqrt{\frac{\beta_{sP_2}}{bI}\left(\frac{I}{I_c}-1\right)}, \tag{3.26}$$

$$K_{II2} = P_2\sqrt{\frac{\chi\beta_{sP_2}2\left(1+\upsilon\right)}{bA}\left(\frac{A}{A_c}-1\right)}, \qquad \beta_{sP_2} = \beta_s\frac{H^*}{E} \tag{3.27}$$

where $H^* = E$ for plane stress and $H^* = E/\left(1-\upsilon^2\right)$ for plane strain conditions and υ is the Poisson ratio.

The slope factor β_s can be determined by two procedures: with detailed Finite Element Models (FEMs) of the cracked zone and with experimental specimens representing the crack. Both procedures are time consuming and fall out the scope of this thesis. Fortunately, Kienzler and Herrmann (1986) obtained good results, in several applications, by assuming $\beta_s = 1$. Nobile (2000) determined SIFs for a simply supported beam with rectangular cross section. The SIFs were in reasonable agreement with those determined by Ricci and Viola (2006) when $\beta_s = 1$ and SIFs determined by experimental results. Furthermore, Dunn *et al.* (1997) obtained the slope factor β_s from a detailed finite element modelling of steel I beams subjected to pure bending moment. They determined that β_s is function of the crack depth ratio $\delta = a/h$ as indicated in Equation (3.28),

$$\beta_s = 1.16\delta_1^{-0.374} \tag{3.28}$$

Afterwards the SIFs are calculated and therefore the overall flexibility matrix, the stiffness matrix of the cracked element $\mathbf{K_c}$ is obtained as follows:

$$\mathbf{K_c} = \mathbf{L}\mathbf{C_{tot}^{-1}}\mathbf{L^T};\ \ \mathbf{L^T} = \begin{bmatrix} -1 & 0 & 0 & 1 & 0 & 0 \\ 0 & -1 & -L_e & 0 & 1 & 0 \\ 0 & 0 & -1 & 0 & 0 & 1 \end{bmatrix} \tag{3.29}$$

where superscript T denotes transpose of the matrix.

The natural frequencies of the beam were obtained using a conventional eigenvalue procedure which required a mass matrix of the beam directly determined from the numerical model. To calculate the corresponding mode shapes, Zheng and Kessissoglou proposed new interpolation functions that satisfy the local flexibility conditions at the locations of the cracks.

3.3 Adopted conditions for the evaluation of the methods

The selected methods for calculating the dynamic behaviour of cracked beam structures were evaluated with a beam structure of rectangular cross section with dimensions set to have a frequency range between 2 to 10 Hz. In this range most of the bridge structures with spans less than 100 m are included. Steel and concrete materials with Young's modulus of 2.5 x 10^7 kN/m^2 and 2.1 x 10^8 kN/m^2 respectively were chosen for the evaluation of a 10 m long beams with two different support conditions, namely simply supported and doubly clamped. The damping ratio for the undamaged beam was set to 2%.

Two damage cases were evaluated for each type of material (steel and concrete). In the first, a concrete beam with a single crack at the mid-span with a depth of one quarter of the total depth of the cross section; and for the steel beam, a crack with one half of the total depth of the cross section. In the second case, four additional cracks were considered placed equidistant one another 0.5 m along the mid-span of the beam and with a depth of one seventh of the total thickness for the concrete cross sections and two sevenths for the steel cross sections. The geometrical properties of the beams, the crack locations along their length and their boundary conditions considered for this example are shown in Figure 3.4 and summarized in Table 3.1.

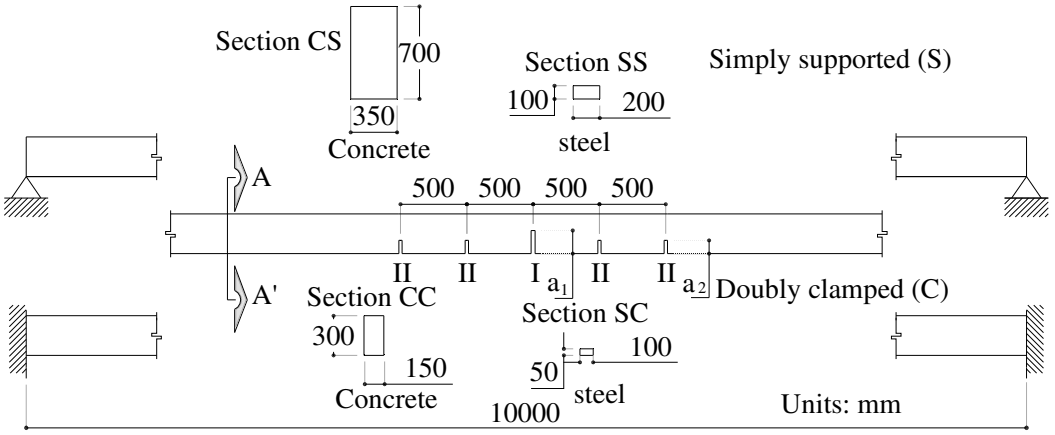

Figure 3.4. Geometrical properties of the beams taken as example.

Table 3.1. Crack depths for the beams adopted as example.

Geometrical properties (mm)	Steel				Concrete			
	I (1 crack)		II (5 cracks)		I (1 crack)		II (5 cracks)	
	SS	SC	SS	SC	CS	CC	CS	CC
Dimensions (b x h)	200 x 100	100 x 50	200 x 100	100 x 50	350 x 700	150 x 300	350 x 700	150 x 300
Crack depth	50	25	28.6	14.3	175	75	100	42.9
1st frequency (Hz)	2.35	2.66	2.35	2.66	10.24	9.95	10.24	9.95

The dynamic response of the cracked beams was obtained by using the high-order recursive algorithm proposed by Wilson (2002). The sampling frequency and acquisition time were set to be able to detect the first three natural frequencies.

The analyzed beam was divided into 20 elements. The force excitation was considered as a vertical load with magnitude, into a predefined range, and location, along the beam nodes, changing randomly each step of sampling frequency. This procedure tried to simulate the case of ambient vibrations during the dynamic data acquisition *i.e.*, forces were not considered during the modal identification instead, accelerations were the only information related with the dynamic response used in the calculations. For this purpose, the Enhanced Frequency Domain Decomposition Method (EFDD) [Brincker *et al.*, 2001] was applied to the acceleration responses calculated from the cracked beams to obtain the modal parameters as determined in experimental way. In total, 72 dynamic simulations and modal identifications were carried out as combination of all the cases. An example of the calculated dynamic response of the beam is shown in Figure 3.5.

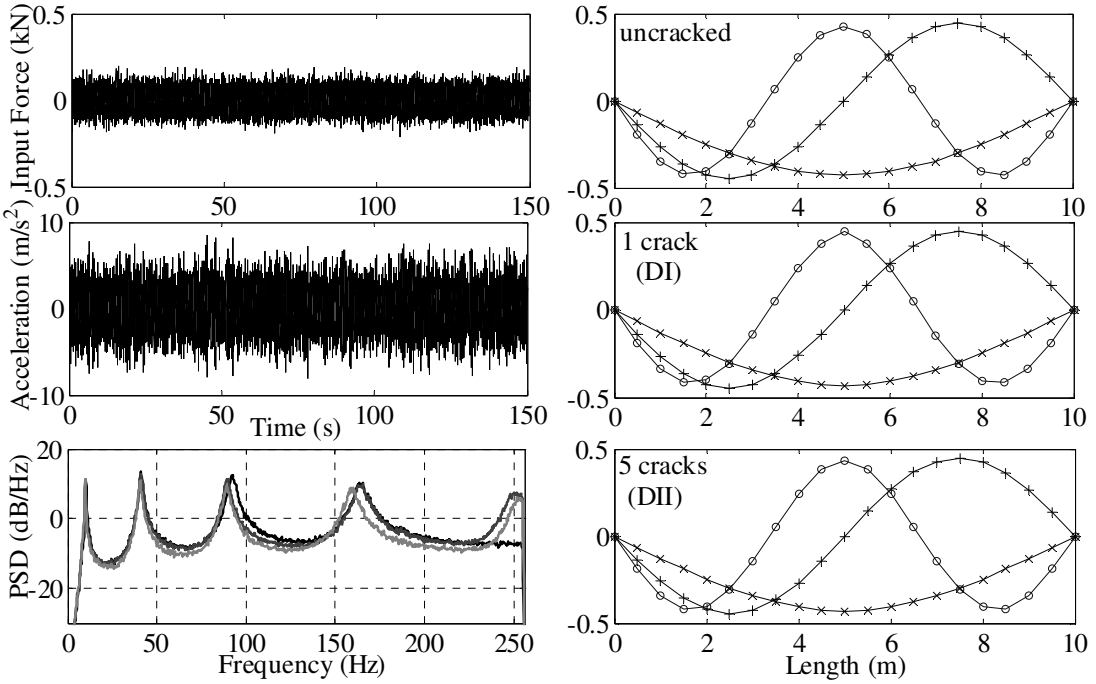

Figure 3.5. Example of the simulated dynamic response of the beam. Keys: (PSD) — uncracked; — DI; — DII; (Modes) —×— mode 1; —+— mode 2; —○— mode 3.

3.4 Comparison of modal parameters calculated from simulated Ambient Vibration Tests (AVTs)

Natural frequencies, mode shapes and damping ratios extracted from the dynamic response of the cracked beams using the EFDD method (Brincker *et al.*, 2001) were compared with their corresponding undamaged modal parameters. First natural frequencies for concrete beams were close to 10 Hz, what simulated a stiff bridge, whereas for steel beams this value was around 2.5 Hz, which is a typical value of flexible bridges. The comparison between these methods was made using the ratio between the undamaged and damaged conditions for the cases related to natural frequency and damping ratio. The comparison of mode shapes was made by using the Normalized Modal Difference (NMD) [Gentile and Gallino, 2008] which is a close estimate of the average difference between the components of two vectors to compare mode shapes for damage detection purposes (see section 2.4.7 of this thesis). The results of the comparison of the previously mentioned parameters are shown in Figure 3.6.

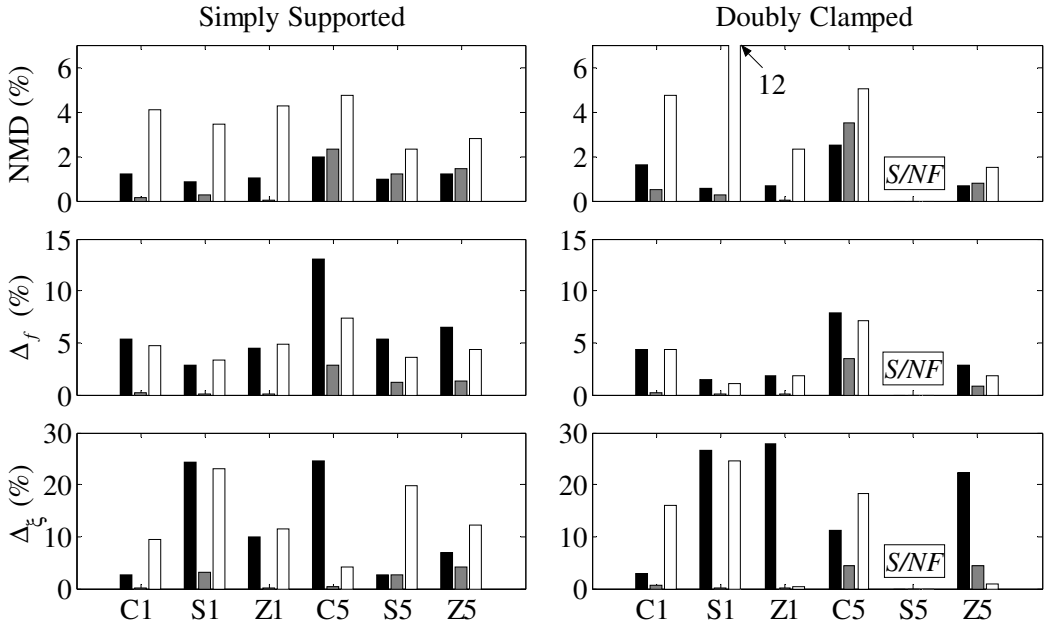

a) Concrete cross sections

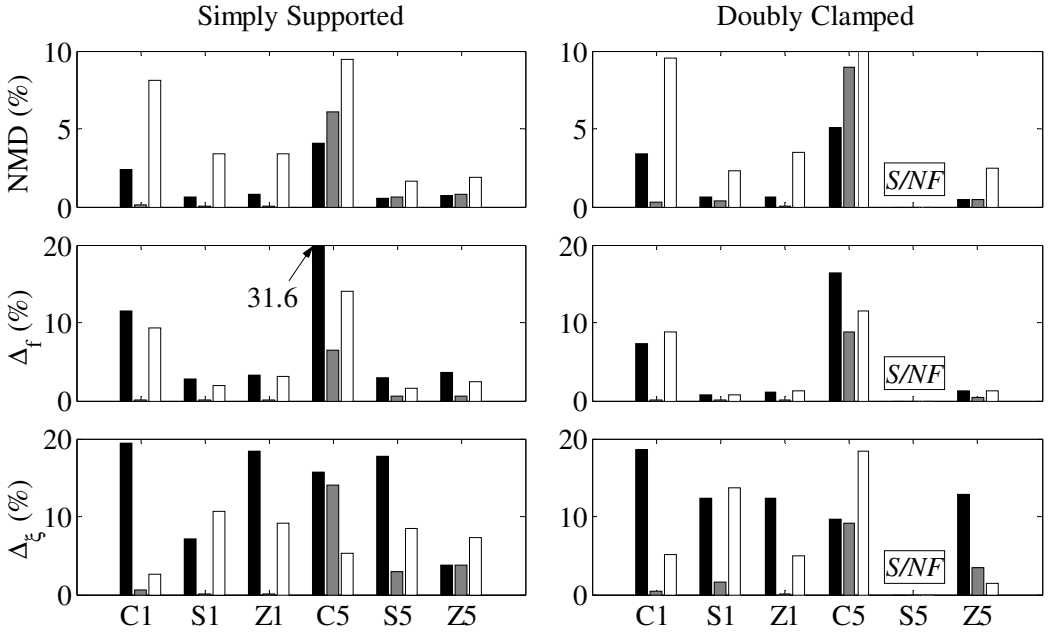

b) Steel cross sections

Figure 3.6.Comparison of the performance of dynamic simulation methods with modal parameters. ■ mode 1; ▒ mode 2 and □ mode 3.

In Figure 3.6 NMD is the Normalized Modal Difference; Δ_f, is the difference between the first three natural frequencies of the undamaged and damaged beam; Δ_ξ, is the difference between the damping ratios of the undamaged and damaged beam; C, S and Z refer to Christides, Shifrin and Zheng methods, respectively, while their

subscripts indicate the number of cracks; *S/NF* indicates that no solution could be found with this method.

From Figure 3.6, for the case of NMD parameter, it is possible to point out that the third mode shape is the most sensitive to damage. In the case of the comparison of frequencies, the second mode shape was the less sensitive to damage. This mode has an inflexion point in the location of damage which leads to small changes in the compared parameters.

For the damping comparison, the first mode shapes gave the largest differences. Regarding the evaluated methods, the Modified Christides and Barr method was the most sensitive to damage, especially when 5 cracks were considered. This method is the easiest to apply, but it is also the less accurate. Its accuracy increases when the number of elements of the beam increases. The dynamic response when 5 cracks were simulated in a doubly clamped beam was not attained with the Shifrin method. The calculation of the roots from Equation (3.17) increases in complexity when the number of involved cracks and degrees of freedom increases. Furthermore, analytical solutions need to be reached for beams of different cross section shapes and boundary conditions. Results obtained with the Zheng method have a similar performance to those obtained with the Shifrin method, with the difference that the solution for determining the dynamic response was found with the Zheng method for all the evaluated cases. Besides, the Zheng method has the advantage to be easily implemented in a computer program for the structural analysis of more complex structures. Moreover, the SIFs required for this method can be obtained for any general cross section using the methodology described here.

3.5 Comparison of modal parameters calculated from the cracked beam methods

Additional to this simulated dynamic analysis, the three selected methods were compared using the frequencies and corresponding mode shapes obtained from their described procedures. At this time, comparison of these modal parameters was carried out from a crack ratio (*a/h*) of 0.0 (undamaged case) to 0.6 represented a severe damage. The results of the frequency and mode shape comparison for the first modal parameters are shown in Figures 3.7 and 3.8 for concrete and steel material, respectively.

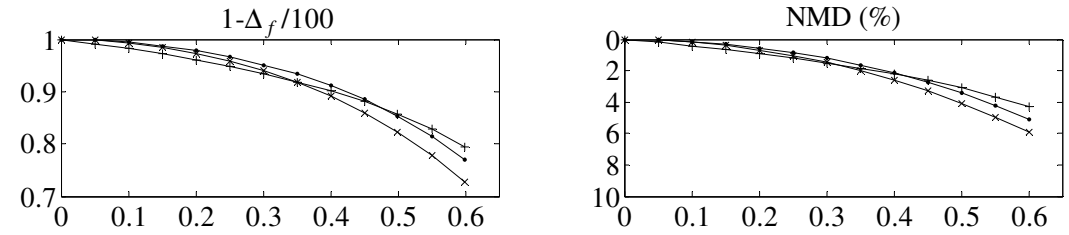

a) Frequency (left) and mode comparison (right); simply supported with 1crack

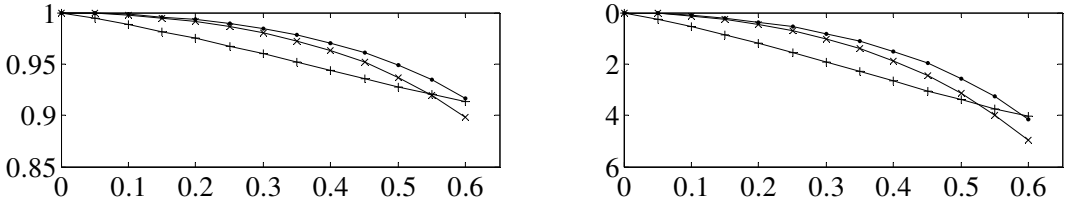

b) Frequency (left) and mode comparison (right); doubly clamped with 1crack

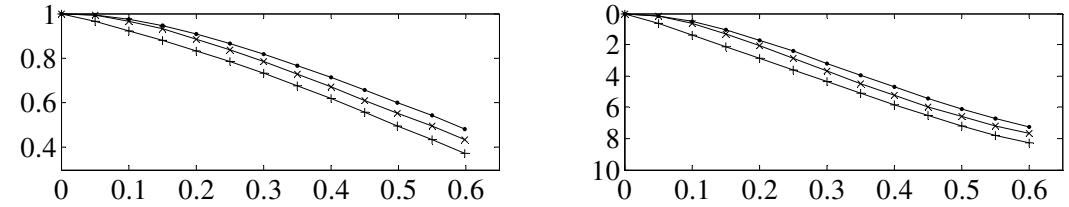

c) Frequency (left) and mode comparison (right); simply supported with 5cracks

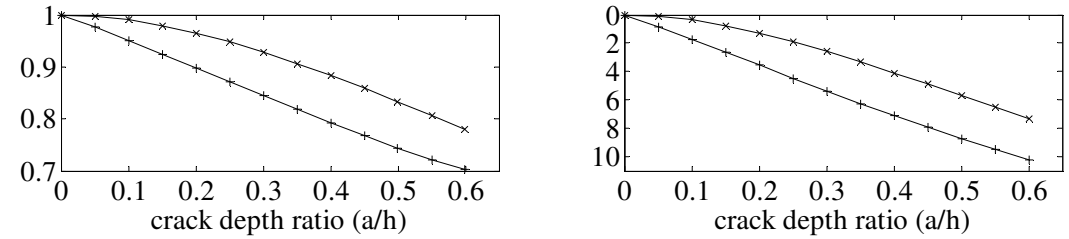

d) Frequency (left) and mode comparison (right); doubly clamped with 5cracks

Figure 3.7. First frequency and mode shape comparison *versus* crack depth ratio (*a/h*) for concrete beams. Keys: —•—Shifrin method; —×—Zheng method and —+— Modified CB method.

For the comparison of concrete beams (Figure 3.7), it was determined that all methods are closely in accordance each other. The Zheng and Shifrin methods presented similar behaviour between them. The modified Christides and Barr methods presented the largest differences compared with the other two methods for the doubly clamped beam. In fact, the experimental exponent α was determined for simply supported beams. Fortunately, these differences for the doubly clamped beam can be considered not significant for the purpose of damage detection. As well as in the analysis of cracked beams with simulated AVTs, the frequency and corresponding mode shapes with the Shifrin method were not found for any cracked

depth ratio when 5 cracks were present in a doubly clamped beam. The numerical procedure written in Matlab (The MathWorks, 2002) was not able to find the roots of the resultant equation product of the determinant of the $U(\lambda)$ matrix of rank 5 x 5 equal to nil.

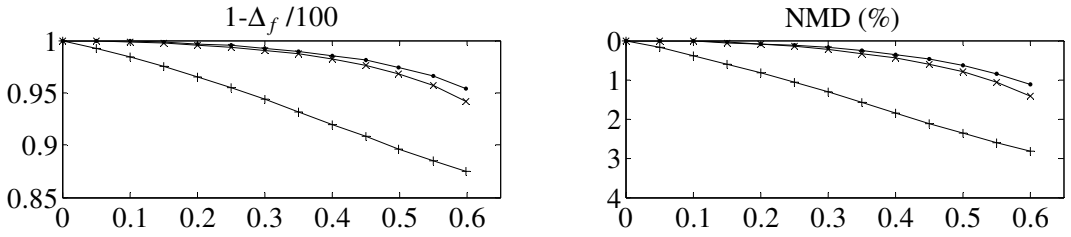

a) Frequency (left) and mode comparison (right); simply supported with 1crack

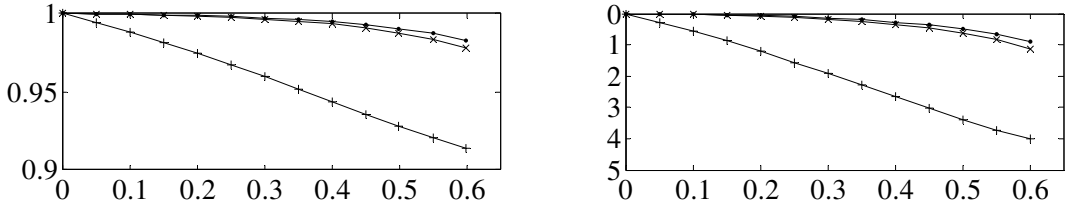

b) Frequency (left) and mode comparison (right); doubly clamped with 1crack

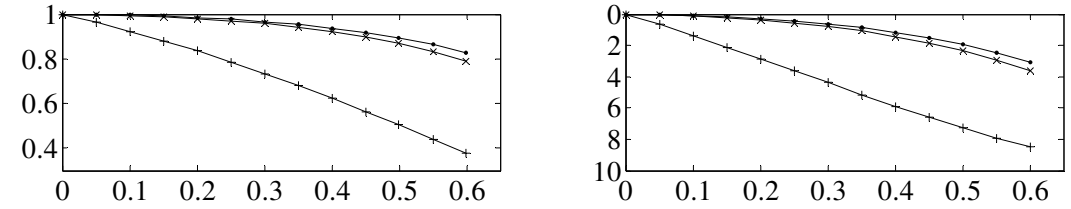

c) Frequency (left) and mode comparison (right); simply supported with 5cracks

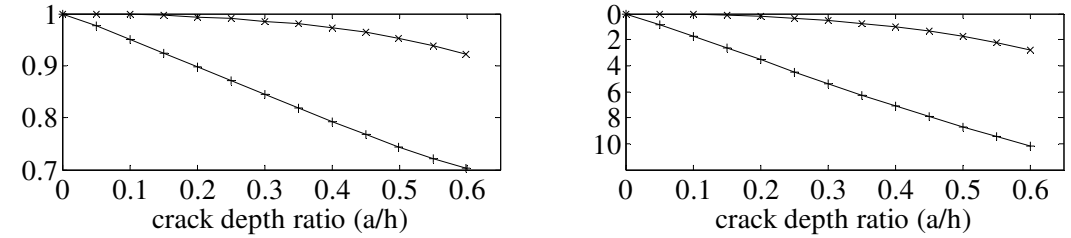

d) Frequency (left) and mode comparison (right); doubly clamped with 5cracks

Figure 3.8. First frequency and mode shape comparison *versus* crack depth ratio (*a/h*) for steel beams. Keys: —•—Shifrin method; —×—Zheng method and —+— Modified CB method.

For the comparison of steel beams (Figure 3.8), the Zheng and Shifrin methods presented close results in frequency and mode shape decay along the crack depth ratios. The modified Christides and Barr method presented results clearly far from the other two methods. This behaviour was caused by the assumption of linear decay of the flexibility of the beam into to the elements. According to Sinha *et al.* (2002)

the presence of a crack causes an important disturbance in the flexibility of the beam on a distance 0.75 times the total depth of the cross section of the beam, in both sides of the crack. For shallow cross sections, as here analyzed for steel beams, the influence length in both sides of the crack is equal to 150 (for 100 mm depth) and 75 mm (for 50 mm depth). Thus, the flexibility variation in the cracked element was not correctly determined.

3.6 Conclusions

In this chapter it was intended to carry out the comparison of three of the existing methods for obtaining the dynamic response of cracked beams. Regarding the procedures followed to obtain the frequencies and mode shapes of cracked beams, the modified Christides and Barr and Zheng methods are approximated procedures while the Shifrin method uses a more consistent solution and therefore was expected to give the most accurate results. However, results showed that the Shifrin method presented difficulties when obtaining the dynamic response of structures with several degrees of freedom and multiple cracks. Complexity for finding the roots of the determinant given in Equation (3.17) grows when increasing the number of cracks, and degrees of freedom. The Modified Christides and Barr method is the simplest, but it is also the less accurate. The precision of this method depends on the number of elements considered in the beam. Since the flexural bending stiffness variation along the element is considered linear, long elements near the crack position introduce big errors in the calculations of the modal parameters. The Zheng method has become a promising alternative for calculating the dynamic response of cracked structures since the SIFs of the general cross section can be obtained with a high degree of accuracy by using the procedure described here. Modal parameters determined through the Zheng method were as accurate as Shifrin method, except that the solution for the dynamic response for all the evaluated cases was only found for Zheng´s method. Moreover, this method can be easily implemented in a computer program for the evaluation of more complex structures. In conclusion, of all three methods evaluated, the Zheng method was considered the best method for obtaining the dynamic response of cracked beams and more complex structures.